UNIONE EUROPEA
Fondo Sociale Europeo

Ministero dell'Istruzione, dell'Università e della Ricerca

PON
RICERCA E INNOVAZIONE
2014 - 2020

Polyurethane foams: novel processing and novel additives for improved thermal insulation properties

Cosimo Brondi

A dissertation submitted for the degree of Doctor of Philosophy in
Industrial Product and Process Engineering (XXXII Cycle)
Department of Chemical, Materials and Production Engineering (DICMaPI)
University of Naples Federico II

PhD Supervisor: Prof. Ernesto Di Maio
PhD Coordinator: Prof. Giuseppe Mensitieri

“I am always doing that which I cannot do, in order that I may learn how to do it”

(Pablo Picasso)

Contents

Chapter 1. Introduction

PART I: Main processes in polyurethane foaming

Chapter 2. Background of the main reactions and foaming processes taking place in polyurethane foams

PART II: Polyurethane foams by high-pressure CO_2

Chapter 3. Effect of CO_2 on the polyurethane curing reaction

Chapter 4. Matching the different timescales: rapid gas depressurization vs. slow curing reaction

PART III: Polyurethane foams by liquid OFAs

Chapter 5. Competing bubble formation mechanisms during the foaming process

Chapter 6. Inhibition of the Ostwald Ripening by liquid-type OFAs

Chapter 7. Conclusions

Appendices

Abstract

Global energy consumption is expected to increase by more than 50% within the next ten years, as a result of the energy efficiency technologies that still do not keep up with the rapid growth of new buildings and the refrigeration sectors. As a consequence of the rising energy demand, environmental issues are becoming more apparent. Moreover, regulations on thermal insulation are becoming ever stricter. For these reasons, there is high industrial interest to design innovative and efficient materials that are capable of lowering the thermal conductivity and then reducing the heat loss in buildings. In this field, polyurethane foams already proved to be one of the most efficient materials in reducing the thermal conductivity. In this dissertation, focus was given to develop new knowledge and gain fundamental understanding about the PU foaming process and the various influencing factors. New strategies were developed in order to obtain rigid polyurethane as well as polyisocyanurate foams with low foam density and reduced cell size that could lead to improved thermal insulation properties. In particular, two main strategies have been followed and defined that can be resumed as follows.

The first approach consisted in the investigation of foaming process of rigid polyurethanes obtained by high-pressure CO_2. High-pressure CO_2 foaming technology proved very effective with thermoplastics. In fact, with the pressure quench method, utmost performances in terms of cell number densities have been reached with numerous thermoplastic polymers: microcellular (cell size in the range 1–10 μm) and, more recently, nanocellular (cell size in the range 1–100 nm) foams have been produced, characterized by improved thermal insulating and mechanical properties as compared to standard cell-sized foams. With regard to thermosetting foams, the same approach used in thermoplastics has been implemented here in this work. To this aim, firstly, (i) the governing factors that affect the curing process of the rigid PU under high-pressure CO_2 were monitored and studied by FT-NIR spectroscopy. (ii) Once that the effect of the CO_2 on the curing process have been clarified, it is necessary to develop a new strategy to cope with the very different timescales of the processes under consideration, namely the rapid depressurization of the sorbed CO_2 and the slow curing reaction. In this way, the polymer does not undergo to excessive stresses due to the depressurization and suitable polyurethane foams can be obtained. In this approach, by pushing on CO_2 bubble nucleation, (iii) microcellular foams by high-pressure CO_2 have been produced.

The second approach consisted in the investigation and monitoring of the foaming process of rigid polyurethane and polyisocyanurate foams obtained by liquid-type organofluorine additives. Liquid-type additives have been extensively used in the last years to reduce the average cell size. Several works have shown the improvement of polyurethane and polyisocyanurate foam

morphologies (and, correspondingly with improved mechanical and thermal properties) as a consequence of the introduction of these additives. However, besides the achievements based on characterization results only, the mechanisms induced by addition of these liquids have not been deeply studied. In our study, it has been found that organofluorine additives are suitable to this purpose, by inhibiting the Ostwald Ripening that affect the late foaming process. With the aim of investigating the effect of these additives, firstly, (i) the competing bubble formation mechanisms and how these are affected by the cell degenerations mechanisms were studied and monitored by in-situ optical observation. (ii) Once that the mechanisms affecting the final morphology are elucidated, it is necessary to develop a new strategy that allows to regulate the aforementioned governing factors. In this approach, by pushing on the depletion of the cell degeneration mechanisms, (iii) polyurethane as well as polyisocyanurate foams by liquid organofluorine additives have been produced.

In conclusion, the developed methodologies allow to control the processing conditions in order to obtain the desired foam morphology.

Chapter 1.

Introduction

In this chapter a brief introduction to the field of polyurethane foams is given. A general context in which this thesis was carried out and its objectives are also described. It is then reported the structure of this thesis.

Chapter 1. Introduction

1.1. Rigid polyurethane foams

Cellular materials, in particular polymeric foams, are two-phase systems in which one phase is a gas that is dispersed in a continuous polymeric matrix. These materials have fascinated scientists for ages. Studying foams is “*like designing materials with air*” as Prof. L. J. Gibson, MIT, Boston, says. These materials can be rigid, flexible or elastomeric and can be produced from a wide range of polymers such as polyurethane (PU), polystyrene (PS), polyisocyanurate (PIR), polyethylene (PE), polypropylene (PP), poly(ethylene-vinyl acetate) (EVA), nitrile rubber (NBR), poly(vinyl chloride) (PVC), or other polyolefins [1,2]. PU are one of the most versatile materials belonging to this category, extremely widespread in several industrial sectors such as automotive, construction, furniture, packaging, medical, sports equipment, etc [3]. As a matter of fact, polyurethane foams (PUFs) dominate the world foam production (being more than 50% of the global volume in polymeric foam market), followed by PS and PVC foams [1,2,4]. Besides their excellent properties, the high demand of these materials is also due to simplicity of the foaming technology used to obtain the foams and the possibility of tailoring the final properties by adequately changing the type and the amount of material such as isocyanate, polyol, surfactants, catalysts and blowing agents (BAs). According to their microstructure classification, these materials can be classified in closed-cell (rigid) and open-cell (flexible) PUFs, as also shown in Figure 1. The polymeric structure presents flat faces and straight edges that are defined by struts and windows, characterized by compartments that can be isolated from each other (closed-cell) or void spaces where air can pass freely (open-cell).

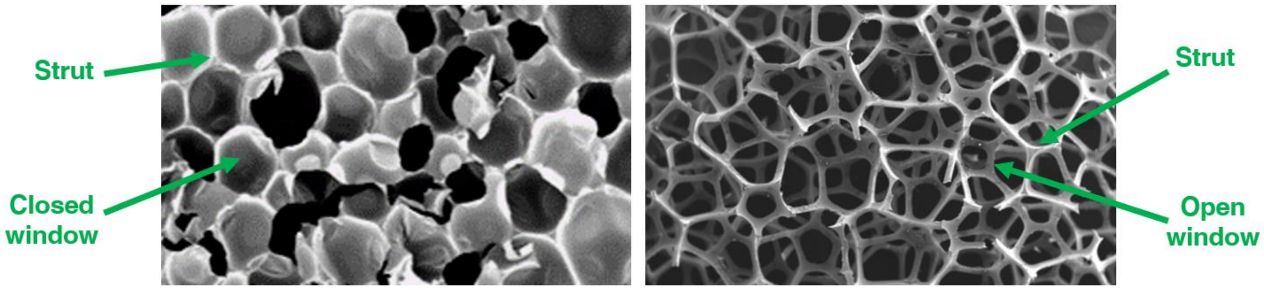

Figure 1. SEM micrographs of (a) a closed-cell rigid PUF and (b) of an open-cell flexible PUF.

Rigid PUFs are characterized by a closed-cell morphology with excellent thermal insulating properties, mainly used in the form of insulation boards or blocks, or in combination with various rigid facings for appliances as a construction and domestic material [5-10]. In addition to the low thermal conductivity, PUFs are stable and durable, which is an important feature to guarantee the stability of the insulating properties. In fact, in building applications, these materials must work for as long as the building stands and should have a useful life beyond 50 years [11]. The inherent chemistry involved in the formation of PUFs, the relative foaming processes and the additive used for their manufacture will be deeply described in the next chapters of this thesis.

1.2. Framework and objectives of the thesis

Although the universities and the companies are different in the values leading their main activity, there is surely space for cooperation that mutually benefits both sides. Universities are mainly focused on education and new knowledge spreading this latter with the public, while the companies are focused on the profit helping transform new breakthroughs into things that people can actually use. Nowadays, with the increasing competition for knowledge, it is crucial for both the sides to collaborate each other to successfully bring new research findings into competitive markets. To this aim, it is also important to understand which are the goals of the research lead by the academic side and how these results may be used by the corporate side. The innovative industrial doctorate [12] takes place in view of a collaboration between university and company.

In the field of PUFs, there is a large interest to improve their thermal insulation properties in order to reduce the energy consumption in appliances as building and domestic households. Currently, typical PUFs are characterized by cell size higher than 100 µm, thermal conductivity around 18 $mW.m^{-1}.K^{-1}$ at 10°C and density in the range 100-200 kg/m^3 [13]. In this context, the **foamlab** research group at the University of Naples Federico II and **Dow Italia**, leader in the field of rigid PUFs, worked together in order **to develop new knowledge and gain fundamental understanding about the PU foaming process and the various influencing factors**. In order to fulfill these requirements, **by developing new know-how that can therefore match the needs of a company to develop new products that are competitive on the market**, two main strategies have been followed and defined that can be resumed with the following points:

- ✓ **Production of microcellular PUFs by high-pressure CO_2:**

1) A tool was developed in order to monitor and understand the governing factors that affect the curing process of the rigid PU under high-pressure.

2) Once that the effects of the CO_2 on the curing process have been clarified, it is necessary to develop a new strategy to cope with the very different timescales of the processes under consideration, namely the rapid depressurization of the sorbed CO_2 and the slow curing reaction. In this way, the polymer does not undergo to excessive stresses due to the depressurization and suitable PUFs can be obtained.

3) In this approach, by pushing on CO_2 bubble nucleation, microcellular foams by high-pressure CO_2 have been produced.

- ✓ **Production of PU and PIR foams by liquid organofluorine additives (OFAs)**:

1) A tool was developed in order to monitor and understand the competing bubble formation mechanisms and how these are affected by the cell degenerations mechanisms.

2) Once that the mechanisms affecting the final morphology are elucidated, it is necessary to develop a new strategy that allows to regulate the aforementioned governing factors. Liquid-type additives have been extensively used in the last years to reduce the average cell size. Several works have shown the improvement of PU and PIR foam morphologies (and, correspondingly with improved mechanical and thermal properties) as a consequence of the introduction of these additives. However, besides the achievements based on characterization results only, the mechanisms induced by addition of these liquids have not been deeply studied. In our study, it has been found that OFAs are suitable to this purpose, by inhibition of the Ostwald Ripening that affects the late foaming process.

3) In this approach, by pushing on the depletion of the cell degeneration mechanisms, PU as well as PIR foams (PIRFs) by liquid OFAs have been produced.

1.3. Structure of the thesis

The present dissertation is divided into an introduction part and three main parts reflecting the tracks on which the research activity has been carried out (see Figure 2). In Part I it is reported an overview on the main chemistry and the foaming processes typical of PUFs in order to introduce the reader to this field. Part II and Part III enclose the two main strategies that have been developed in this work to obtain PUFs with reduced cell size. With regard to Part II and III, each chapter is basically self-consistent: at the beginning, a preliminary introduction to the central topic of the section is provided together with a brief overview of the state of the art, then the results of the investigations are presented and discussed.

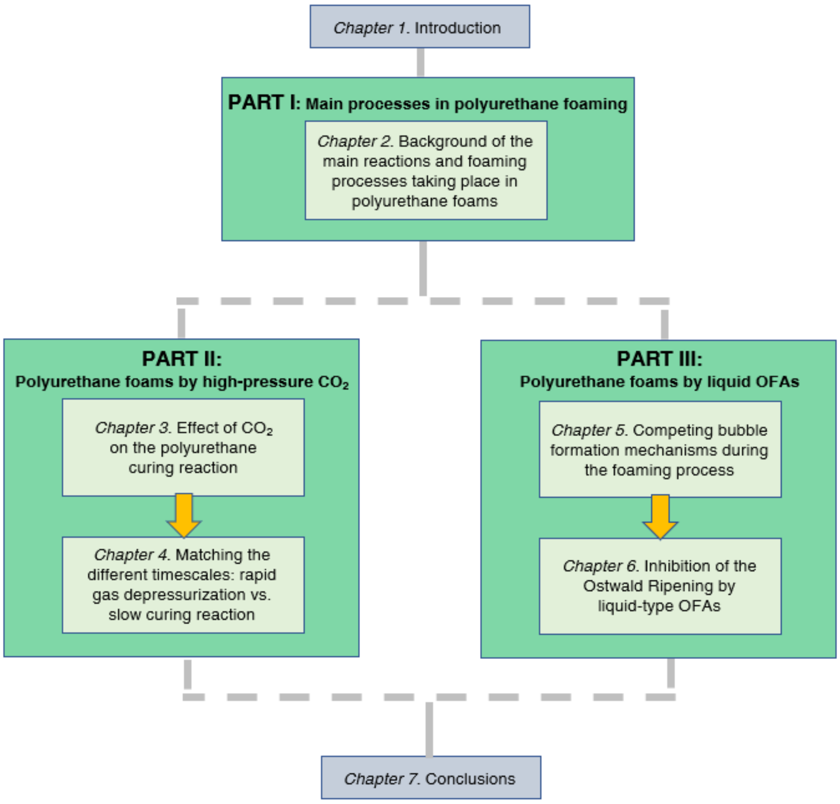

Figure 2. Overview of the chapters of this thesis.

Each chapter includes the following information:

Chapter 1. Introduction: it introduces the framework of this research, the aims and the structure of the thesis

Chapter 2. Background of the main reactions and foaming processes taking place in polyurethane foams: the first part of this chapter summarizes the basic concepts related to the PUFs. In particular, basic chemistry, common raw materials, foaming process, nucleation and cell degeneration mechanisms, properties and applications are reviewed.

Chapter 3. Effect of CO_2 on the polyurethane curing reaction: it is described the methodology developed to monitor the curing process of rigid PU under high-pressure. This methodology is based on the use of FT-NIR spectroscopy.

Chapter 4. Matching the different timescales: rapid gas depressurization vs. slow curing reaction: data gathered in *Chapter 3* were used to develop a new processing procedure that allows to cope with the very different timescales of the rapid gas depressurization and the relatively slow PU curing reaction. Microcellular PUFs were successfully obtained. The aforementioned approach was used to obtain PUFs with other physical blowing agents (PBAs) as well. Experimental results here reported further prove the viability of the this method.

Chapter 5. Competing bubble formation mechanisms during the foaming process: it is reported the investigation on the competing bubble formation mechanisms that take place in conventional PU and PIR foaming process. These mechanisms were observed by developing a tool (optical camera) that allows to in-situ monitor the foaming process.

Chapter 6. Inhibition of the Ostwald Ripening by liquid-type OFAs: it has been observed that these additives act like a cell coarsening inhibitor and foams with an appreciable cell size reduction can be obtained. Starting from PUFs, this strategy was successful applied to PIRFs as well.

Chapter 7. Conclusions: It summarizes the final conclusions obtained during the whole thesis and also possible future works.

1.4. References

[1] W. V. Titow, PVC Technology, Rapra Technology Ltd., Shawbury, UK, 2001.

[2] D. Eaves, Handbook of Polymer Foams, Rapra Technology Limited, Shawbury, Shrewsbury, Shropshire, UK, 2004.

[3] M. Szycher, Szycher’s Handbook of Polyurethanes, CRC press, 2012.

[4] Polymer Foams Market Expected to Consume 25.3 Million Tonnes by 2019. http://www.smithersrapra.com/news/2014/may/polymer-foam-market-to-consume-25-3-million-tonnes, 2014

[5] J. T. Kim, B. K. Kim, E. Y. Kim, H. C. Park, H. M. Jeong, Synthesis and shape memory performance of polyurethane/graphene nanocomposites, React. Funct. Polym. 74 (2014) 16-21.

[6] Qipeng Guo, Thermosets Structure, Properties, and Applications, Amsterdam, Netherlands, 2017.

[7] M. Modesti, A. Lorenzetti, An experimental method for evaluating isocyanate conversion and trimer formation in polyisocyanate-polyurethane foams, Eur. Polym. J. 37 (2001) 949-954.

[8] M. Thirumal, D. Khastgir, N. K. Singha, B. S. Manjunath, Y. P. Naik, Effect of Foam Density on the Properties of Water Blown Rigid Polyurethane Foam, J. Appl. Polym. Sci. 108 (2008) 1810-1817.

[9] W. J. Seo, J. H. Park, Y. T. Sung, D. H. Hwang, W. N. Kim, H. S. Lee, Properties of water-blown rigid polyurethane foams with reactivity of raw materials, J. Appl. Polym. Sci. 93 (2004) 2334-2342.

[10] S. X. Wang, H. B. Zhao, W. H. Rao, S. Huang, T. Wang, W. Liao, Y. Wan, Inherently flame-retardant rigid polyurethane foams with excellent thermal insulation and mechanical properties, Polymer 153 (2018) 616-625.

[11] D. Randall, S. Lee. The Polyurethanes Book, J. Wiley, New York, 2002

[12] Dottorati di ricerca innovativi con caratterizzazione industriale. http://www.ponricerca.gov.it/opportunita/dottorati-innovativi-ciclo-32/

[13] K. H. Choe, D. S. Lee, W. J. Seo, W.N. Kim, Properties of rigid polyurethane foams with blowing agents and catalysts, Polymer J. 36 (2004) 368.

PART I:
Main processes in polyurethane foaming

Chapter 2.

Background of the main reactions and foaming processes taking place in polyurethane foams

This chapter summarizes the basic concepts related to the PUFs that will be used in the next chapters as well. In particular, basic chemistry, common raw materials, foaming process, nucleation and cell degeneration mechanisms, properties and applications are reviewed.

Chapter 2. Background and state of the art

2.1. Basic chemistry

The chemistry involved in the synthesis of PUs is complex because more simultaneous reactions are involved. The simultaneity of several reactions is due to the extreme reactivity of the isocyanate group (-N=C=O) towards the hydrogen active compounds, such as those containing the -OH and -NH functional groups [1]. However, among all the reactions taking place during the foaming process, two reactions are the main processes leading to the formation of a PU foam. On one hand, the polymerization reaction (also known as gelling) occurring between isocyanate and polyol (Figure 1) leads to the formation of the urethane group [1-5].

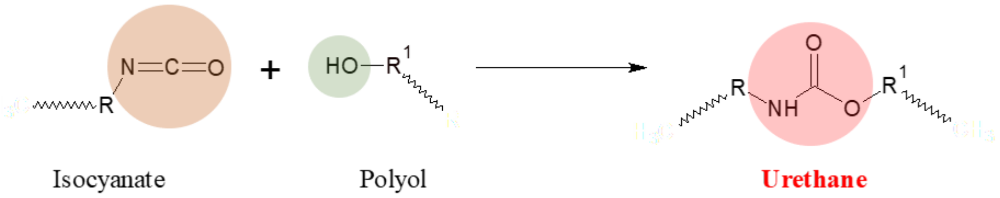

Figure 1. Polymerization reaction: the polyol and the isocyanate react to generate the urethane group.

The second main reaction, simultaneous to the PU formation and, thus, the gelling reaction, is the *blowing reaction*. This process occurs by generation of gas from a chemical blowing agent (CBA). CBAs are used when gases are produced by a chemical reaction. In case of water-blown PU, the isocyanate reacts with water to give an unstable carbamic acid, which spontaneously decomposes into CO_2 and the corresponding amine (Figure 2). Therefore, the generated gas provides the foam expansion [1-5]. The amine may further reacts with another isocyanate molecule to give urea.

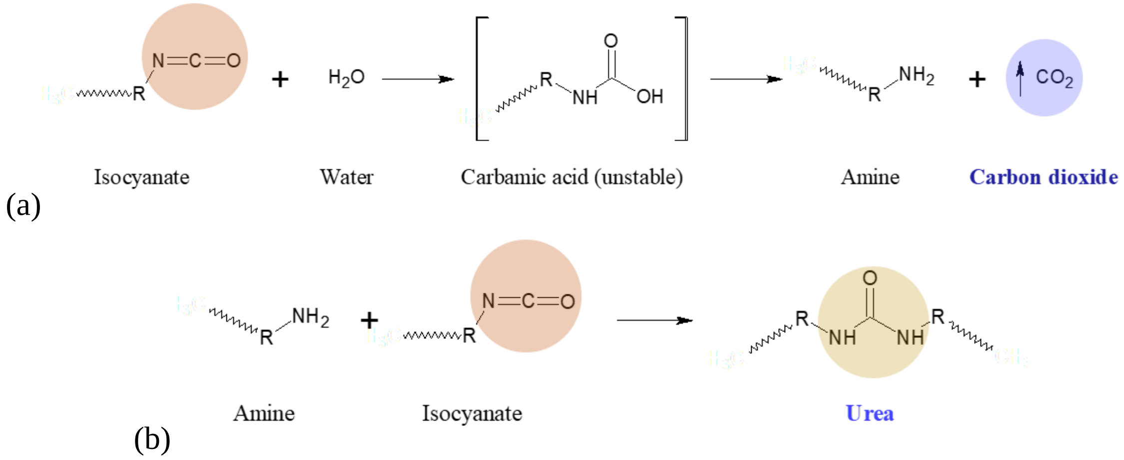

Figure 2. Blowing reaction: (a) the isocyanate and the water react to generate carbamic acid that gives amine and carbon dioxide; (b) the amine and still isocyanate react to generate the urea.

In addition, side reactions may occur in a chemical system where the isocyanate is contained in excess. These reactions may be due to the high reactivity of the isocyanate group, to the adiabatic heat buildup in the reacting mass, or to local inhomogeneities in the component concentration [6]. The isocyanate may be involved in other reactions with urethane and urea leading to the formation of an allophanate (Figure 3) and biuret (Figure 4) compounds respectively [1]. While polymerization and blowing reactions generate urethane and urea products at room temperature (up to 50°C), the reactions producing allophanate and biuret products occur at higher temperatures (up to 150°C) [5].

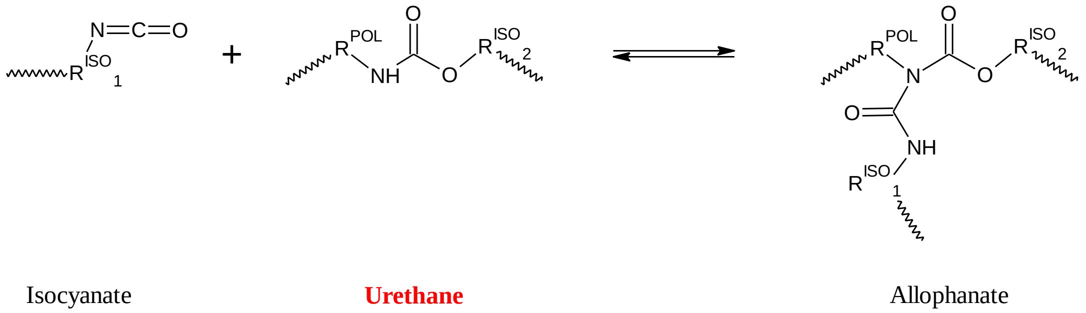

Figure 3.. Isocyanate and urethane react to generate allophanate.

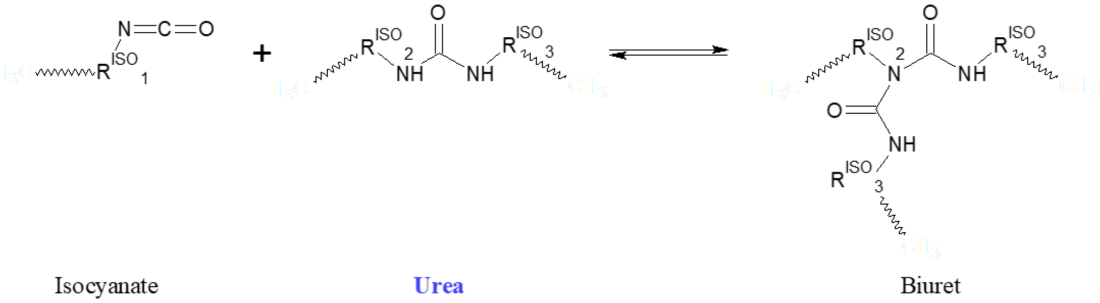

Figure 4. Isocyanate and urea react to generate a biuret.

Isocyanate may also react with other isocyanates molecules to form oligomers (mainly dimers or trimers). In one case, the isocyanate may undergo a dimerization reaction with another isocyanate giving formation to an uretidione ring (Figure 5). This reaction is a reversible process and the dissociation of the ring occurs at relatively low temperatures (80-100°C) [6].

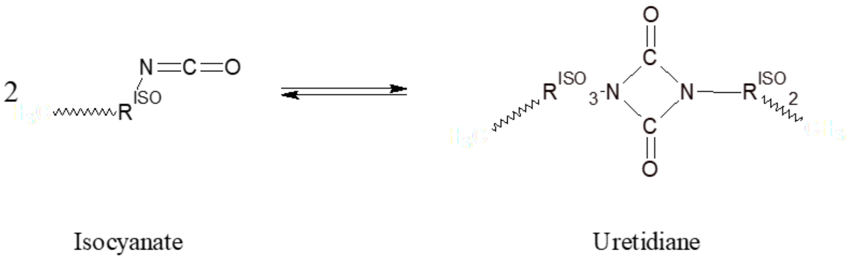

Figure 5. Dimerization reaction: two isocyanates react to give an uretidione ring.

In one case, three isocyanates can react (*cyclotrimerization reaction*) to give an isocyanurate ring (Figure 6). As a result of the high crosslinking of these compounds, PUFs are characterized by an increased thermal stability and flame retardance [1,7]. With the appropriate catalysts, this reactions may also be used to produce polyisocyanurate foams (PIRFs) with isocyanate in large excess at the beginning of the reaction [1,8].

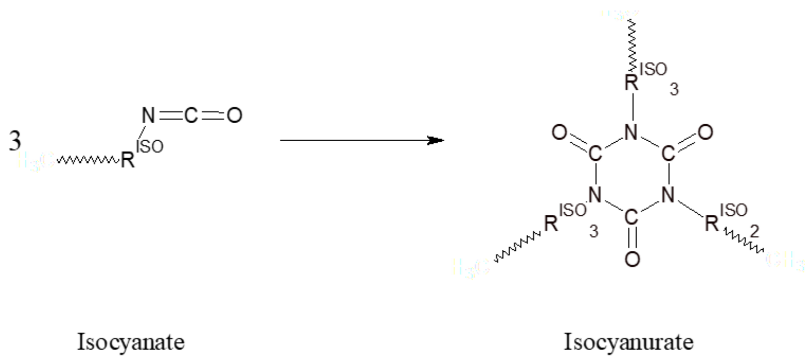

Figure 6. Cyclotrimerization reaction: tree isocyanates react to give an isocyanurate ring.

2.2. Principal polyurethane foam components

Rigid PU foam is a complex structure where several factors play an important role in determining the desired final properties of the foam. The first important key feature in the recipe of PUs is the choice of adequate polyol and isocyanate reactants due to their phase incompatibility. The polymerization reaction is relatively slow at room temperature and a relatively non-polar and denser isocyanate phase has to react with a more polar and less-dense polyol phase [9]. The blowing reaction undergoes the same aforementioned issue of the polymerization reaction. For these reasons, it is necessary to select appropriate catalysts capable of enhancing and regulating the polymerization and the blowing reactions. Moreover, it is essential to select a surfactant that can improve the phase compatibilization and regulate the cell coalescence. Last but not least, it is important also the choice of the BA contributing to the foaming process of the polymer. All the additives and the reactant needed to obtain the PUFs are discussed in the next sections.

2.2.1. Polyols

Polyols are a source of hydroxyl (OH) functional groups that are available for reacting with the reactive isocyanate groups giving formation to urethane (Figure 1). Depending on the desired final properties, polyether or polyester polyols may be used for the production of the rigid PUFs [10]. Polyether polyols are produced by the addition of an alkylene oxide with an initiator in the presence of an acid or a base acting as a catalyst. While alkylene oxide commonly used can be ethylene oxide (EO), propylene oxide (PO), mixtures of EO and PO, or tetrahydrofuran (THF), typical initiators are ethylene glycol (EG), propylene glycol, glycerin, pentaerythritol, trimethylolpropane, sucrose or sorbitol. This category of polyols is used for producing foams that are resistant to hydrolysis [11]. Moreover, they present lower cost production and lower viscosities in comparison with their polyester counterpart. However, foams prepared with these polyols present lower resistance to oxidation. Polyester polyols are generally produced by the polycondensation reaction of multifunctional carboxylic acids and polyalcohols. Typical carboxylic acids used to produce polyester polyols are adipic acid or azelaic acid, while glycerine, trimethylolpropane (TMP), EG or diethyleneglycol (DEG) are used as polyalcohols. PUFs prepared with these polyols are characterized by strong cohesive strength and adhesion, and thus high strength and wear resistance.

When designing PUFs based on their final properties, there is need to consider important parameters related to the polyol characteristics. These features are hydroxyl number, functionality, molecular weight, acid value, moisture, viscosity, density and color. Three polyol features can be considered important characteristics essential to design the PUF properties: 1) The hydroxyl number (or index) represents the amount of hydroxyl groups available for the reaction with isocyanates. It is expressed as milligrams of potassium hydroxide by gram of sample (mg KOH/g). (2) The functionality is defined as the number of hydroxyl groups per each molecule of polyol. (3) The molecular weight of the polyol is the third main parameter in determining the behavior of the final foam. In general, rigid PUFs are prepared with polyols with high hydroxyl number, high functionality and low molecular weight, while flexible PUFs are obtained from polyols with low hydroxyl number, low functionality and high molecular weight. Besides these parameters, it is also important to consider the other polyol features in order to design the appropriate formulation.

2.2.2. Isocyanates

The isocyanate component provides the NCO functional groups to react with the polyol (Figure 1) and the water (Figure 2) and other components in the formulation. Typical isocyanates used to obtain the PUFs are the toluene diisocyanate (TDI) or the diphenyl methane diisocyanate (MDI) [1]. The phosgenation of amines represents the most commercially viable method of producing isocyanates. Isocyanate is obtained by the reaction of gaseous phosgene with amines or amine salt precursors [1]. TDI is the most common isocyanate used for flexible foams. Modified TDI can be used for preparing rigid foams and semirigid foams. However, TDI is not suitable for PIRFs. Pure MDI is used for elastomers and coatings. Polymeric MDI is widely used to obtain rigid and semirigid foams, as well as PIRFs. Currently, TDI is being substituted by polymeric MDI in order to obtain flexible foams, due to the higher toxicity levels of TDI [1]. Also in this case, these reactants are characterized by several features such as the NCO content, functionality, viscosity and acidity (HCl percent). The NCO content represents the weight percent of an isocyanate comprised of NCO groups, generally given in percentage by weight of NCO. In case of isocyanates, the functionality is defined as the number of NCO groups per molecule of isocyanate. Acidity is a measure of the acid content derived from the synthesis of isocyanate that can influence its reactivity [1].

Typically, the total number of isocyanate groups must be higher than, or equal to, the sum of the active hydrogen-containing groups in the reacting system (hydroxyl groups of polyols plus water in water-blown PUFs). This concept is expressed by the isocyanate index or the isocyanate/hydroxyl equivalent ratio, or as expressed in Equation 1 [12]:

$$Isocyanate\ Index = \frac{Actual\ amount\ of\ iscoyanate\ used}{Theoretical\ amount\ of\ isocyanate\ required}\ x\ 100 \qquad (1)$$

Depending on the foam system to be manufactured (for example, rigid or flexible), the isocyanate index is fixed, and thus the amount of isocyanate required to react with the polyol and with any other reactant in the formulation must be calculated in terms of theoretically stoichiometric equivalents. The isocyanate index usually ranges from 90 to 110 for flexible foams [13], from 105 to 120 for rigid foams [5] and up to 300 in case of PIRFs to form the isocyanurate ring [14].

2.2.3. Catalysts

The catalysts used in the PU recipe are necessary to accelerate the reactions and balance the polymerization and the blowing reaction rates. It is crucial that the polymer and the gas formation rates are balanced so that the gas can be entrapped efficiently and the gelling polymer may develop sufficient strength to maintain its structure without collapse or shrinkage [1]. Catalysts suitable to this purpose are amine and organometallic compounds. Common amine catalysts are tertiary amines such as dimethylcyclohexylamine (DMCHA), dimethylethanolamine (DMEA) and triethylenediamine [15]. Both the catalysts induce an enhancement in the reactivity of the PU system by increasing the polarization of either the isocyanate and/or the polyol [6]. Certain tertiary amines affect both the polymerization and the blowing reaction as well as different side reactions, depending on isocyanate excess, catalyst concentration, temperature, etc [6]. Some others catalysts like dibutyltin dilaurate promote primarily the polymerization reaction and chain propagation [1]. Common organometallics catalysts are stannous octoate, dibutyltindilaurate, and tin mercaptides [5]. With respect to tertiary amines, these catalysts are preferred due to their lower volatility, facilitating their maintenance in the foam without causing odors which is an important issue in automotive applications [5]. Both amine and organometallic catalysts can be used either alone or in combination depending on the desired final properties of the foam.

2.2.4. Surfactants

The primary function of the surfactants (or foam stabilizers) is to stabilize the PU foaming process. These additives are constituted by block copolymers of either polydimethylsiloxane-polyoxyalkylene, nonylphenol ethoxylates, silicone oils or some other organic compounds being the polydimethylsiloxane-polyoxyalkylene copolymers the most used surfactants for PUFs [15]. These copolymers can be linear or branched. In case of silicone surfactants, the structural parameters to be considered are the balance of hydrophobic PDMS and hydrophilic oxyalkylene chains that significantly affect their functions [11]. The surfactants perform several functions such as lower surface tension of PU-air interface (thus promoting the stabilization of air bubbles, introduced by mixing step of the PU reactants, which evolve into the foam cells), emulsification of incompatible formulation ingredients (then enhancing the reaction rate as more reactant is available for the polymerization reaction), stabilization of the rising foam by reducing stress concentrations in thinning cell-wall (thus preventing the collapse) [5,6,15]. Among these functions, stabilization of the cell-walls is the most important as this requirement can influence the use of the surfactant for different (specific) applications such as rigid of flexible foam. In case of rigid foams, it is essential that surfactants prevent the coalescence of rapidly growing cells until those cells have attained sufficient strength through polymerization to become self-supporting. Without this effect, continuing cell coalescence would lead to total foam collapse [1]. In the case of flexible foams, surfactants may also regulate the degree of cell-opening. The process of cell opening consists of draining the walls towards the struts during the foaming process in order to promote the cell opening [1].

2.2.5. Blowing agents

The role of the BAs is to provide gas for the polymer expansion. According to the way in which the gas is provided, the BAs can be classified in chemical blowing agents (CBA) or physical blowing agents (PBA). PU foam expansion may occur in presence of a CBA, a PBA or a combination of both. CBAs are compounds which release gas during the foam formation, due to either a thermal decomposition or to a chemical reaction. This is the role of water, which is the most common CBA in PU formation (Figure 2) [1].PBAs are not involved in chemical reactions and are mostly liquids with low boiling points, e.g. chlorofluorocarbons (CFCs), hydrochlorofluorocarbons (HCFCs), hydrofluorocarbon (HCFs) and hydrocarbons (HCs) (e.g. cyclopentane). Their evaporation is due to the heat deriving from the exothermic polymerization and blowing reactions [1]. CFCs and HCFCs were firstly used as PBAs until they were banned for their role in damaging the ozone layer [1]. For this reason, more environmentally friendly BAs, such as cyclopentane (CP), hydrofluoroolefins (HFOs) or water, are currently being used in most of the industrial applications. BAs play a crucial role in determining the final morphology and then the thermal insulating properties of PUFs. Firstly, it is important to carefully choose the amount of BA in order to obtain low foam densities and avoid polymer expansions too violent. In the field of the thermal insulating applications, the thermal conductivity is certainly the most important parameter to be considered. Therefore, it is also important to select a BA that possess a low thermal conductivity [13]. In this context, for example, it takes much longer for CP to diffuse outside the cell, in comparison with CO_2 that diffuse out in less than one month [16].

2.3. Foaming process

Typically the PU reactants (formulated polyol and isocyanate) are mixed at room temperature in a plastic cup or a mold and several characteristic times are measured in order to quantify the reactivity of the PU mixture. The characteristic time intervals are [1]: the cream time (the time elapsed for the foam mixture to start increasing in volume), the gel time (the foam has developed enough gel strength due to the polymerization reaction and corresponds to time when strings of polymer can be withdrawn by dipping a pointer into the foam mixture), the rise time (time elapsed for the foam mixture for the end of increase in volume), the tack-free time (the surface of the foam is not adhesive anymore) and the curing time (the foaming process is complete and the product is completely solidified). The foaming process can be considered mainly composed of four stages [10], namely the gas dissolution stage, the nucleation stage, the bubble growth stage and the bubble stabilization stage.

2.3.1. Gas dissolution stage

The very first stage of a foaming process is the formation of a gas/polymer solution (with the former provided by a CBA, PBA or combination of both the BAs, see *section 2.2.5.*). An essential parameter that characterizes these solutions is the solubility of the gas into the polymer, namely the maximum amount of gas that is necessary to saturate the polymer. This parameter is essentially dependent on the saturation pressure, the saturation temperature and the type of polymer. Furthermore, it is also necessary to take into account the rate of gas dissolution (namely how fast it dissolves into the polymer) that is an entirely different property from solubility [10]. In case of CBAs, as already described, the gas is provided by chemical reaction and its molecules stay dissolved into the polymer until they reach the gas solubility for the specific system. In case of PBAs, a further distinction may be done for low boiling liquids and gases. For low boiling liquids (e.g. CP), also here already described in blowing agents section, the gas molecules are provided by the evaporation of the liquid due to the heat of reaction. Also in this case, the gas stay dissolved into the polymer until it exceeds its solubility. In case of gases (e.g. N_2 and CO_2), these are solubilized into the polymer phase by meaning of high pressures and low temperatures, waiting, in this case, for a time elapsed to the gas to reach its solubility. Typically, the Fick's law is used in the analysis of the gas dissolution process, as expressed by Equation 2:

$$\bar{J} = -\mathrm{D}\,\nabla \mathrm{C} \qquad (2)$$

where $\bar{J}$ denotes the diffusion flux vector, D the diffusion coefficient and C the concentration of the dissolved gas. In scalar form, the distance in the direction of diffusion x, reads:

$$J_x = -\mathrm{D}\,\frac{\partial \mathrm{C}}{\partial \mathrm{x}} \qquad (3)$$

This equation states that the diffusion rate across a given direction is proportional to the concentration gradient. Moreover, from the time derivative of this equation the Fick's second law is derived:

$$\frac{\partial \mathrm{C}}{\partial \mathrm{t}} = \frac{\partial}{\partial \mathrm{x}}\left(\mathrm{D}\,\frac{\partial \mathrm{C}}{\partial \mathrm{x}}\right) \qquad (4)$$

In this way, by simplifying Equation 4 the saturation time t_S of the gas may be estimated:

$$\frac{1}{t_S} = \frac{\mathrm{D}}{x^2} \qquad (5)$$

2.3.2. Nucleation stage

The bubble nucleation stage in induced when the solubility of gas in the polymer is exceeded. As an example, Figure 7 shows a polymer/gas solution: (a) a single phase is reported in which a liquid polymer is saturated with a gas at a certain initial pressure P_0 and initial temperature T_0. When supersaturation is induced (from P_0 to P_s, yet at T_0) new nuclei are formed. In case of a spherical shape, it is allowed the use of simple mathematical expressions based on thermodynamic principles.

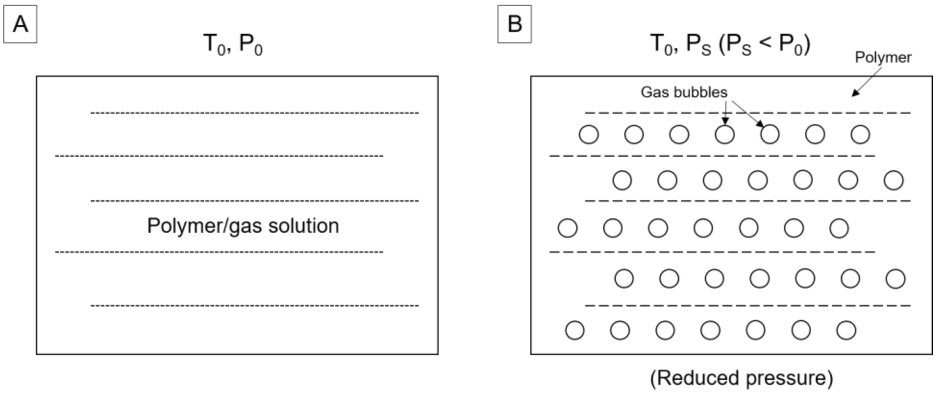

Figure 7. Nucleation process induced by thermodynamic metastability in a polymer/gas solution.

For gases produced by reaction the solubility excess is dictated by the ongoing reaction that continuously gives formation to the gas product. In case of PBAs, the solubility can be exceeded by temperature increase (continuous evaporation of the liquid pre-mixed in the polymer phase) or pressure reduction (gas previously solubilized at high pressure). Therefore, anything that increases the concentration or decreases the solubility of the gas in the liquid will induce a nucleation. In PU and PIR processing, air bubbles are entrapped by initial intensive mixing of the reactants. In fact, in the case of a pre-existing air bubble, there should be no surface energy barrier and the BA evolving from CBA (and PBA) may simply inflate the bubble by diffusion [1]. If the bubbles are formed in an initially homogeneous liquid the process is called *homogeneous nucleation* [17]. If a second phase is initially present and then the bubbles may be readily formed at either a liquid-liquid or solid-liquid interface the process is called *heterogeneous nucleation* [17].

2.3.2.1. Homogeneous nucleation

According to the classical nucleation theory (CNT), nucleation may occur when a sufficient number of dissolved gas molecules form a cluster for a time long enough to obtain a nucleus with a radius greater than the critical radius. Here, the driving force for the nucleation of bubbles is the gain in the volumetric Gibbs energy associated with the transition from the old phase (supersaturated liquid/gas solution) to the new phase (liquid and gas bubbles) [17]. Volumetric free enthalpy gain is counter balanced by the surface free enthalpy required for the formation of the interface between the new phase and the old phase. [17]. Figure 8 shows the Gibbs free energy required for homogeneous nucleation:

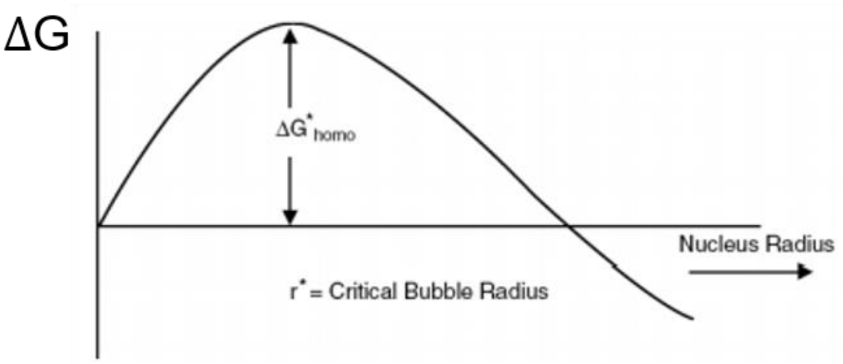

Figure 8. Reduction in the Gibbs energy required to generate a stable nucleus.

Here, the gain in the Gibbs energy for a gas bubble of spherical shape that is forming a liquid medium may be expressed by Equation 6:

$$\Delta G = \sigma A - \left(P_g - P_l\right) V_b + n\,(\mu_g - \mu_l) \tag{6}$$

Where σ is the surface tension, A is the interface area of the bubble, P_g is the pressure of the gas phase, P_l is pressure of the metastable liquid phase, V_b is the volume of the pure gas bubble, n is number of the molecules, μ_g is the chemical potential of the compound contained in the gas phase and μ_l is the chemical potential of the compound contained in the liquid phase. At the equilibrium, the chemical potentials μ_g and μ_l are equal and Equation 6 can be rewritten as follows:

$$\Delta G = \sigma A - \left(P_g - P_l\right) V_b \tag{7}$$

Furthermore, ΔG may be expressed as a function of the bubble radius r by considering the spherical shape of the gas bubble:

$$\Delta G = \sigma\, 4\pi r^2 - \left(P_g - P_l\right) \frac{4}{3} \pi\, r^3 \tag{8}$$

The difference between P_g and P_l represents the level of supersaturation. ΔG reaches the maximum value in correspondence of the critical radius r^*, that is the maximum energy barrier that the system has to overcome in order to let the nucleus become stable. Nuclei whose radius is lower than r^* resorb in the liquid medium, whereas those whose radius is larger than r^* keep growing. It is assumed that the bubble may assume a spherical shape as it represents the shape that requires the minimum resistance to nucleation for a given volume. When $r = r^*$ the free enthalpy derivative tends to zero and the following relations can be derived:

$$\Delta G^*_{hom} = \frac{16\,\pi\,\sigma^3}{3\,\Delta P^2} \tag{9}$$

$$r^* = \frac{2\,\sigma}{\Delta P} \tag{10}$$

Where ΔP is pressure difference. The nucleation rate N_{hom} in polymer/gas system may be then expressed as follows:

$$N_{hom} = f_0\, c_0 \exp\left(\frac{-\Delta G^*_{hom}}{k\,T}\right) \tag{11}$$

Where c_0 is the concentration of gas molecules per unit liquid volume, f_0 is the frequency factor that expresses at which rate the gas molecules reach the critical state, k and T are the Boltzmann constant and absolute temperature, respectively.

2.3.2.2. Heterogeneous nucleation

The heterogeneous nucleation is the process that more commonly takes place in foaming systems where additives are contained. The bubble nucleation efficiency is dependent on several factors such as the type and the shape of nucleating particles and the surface tension of solid and solid-gas interfaces. Blander and Katz derived a simple model of the heterogeneous nucleation in liquids in 1975 [18]:

$$\Delta G^*_{heter} = \sigma_{lg}\, A_{lg} + \left(\sigma_{sg} - \sigma_{sl}\right) A_{sg} - P\, V_b + n\,(\mu_g - \mu_l) \tag{12}$$

Where the subscripts l, g and s stand for liquid, gas and solid phases, respectively. The main effect is due to the external interface that acts as catalyst for the nucleation. The presence of small particles and microcavities reduces the energy required to be reached for a stable nucleus. Figure 9 shows the Gibbs energy reduction required for heterogeneous nucleation:

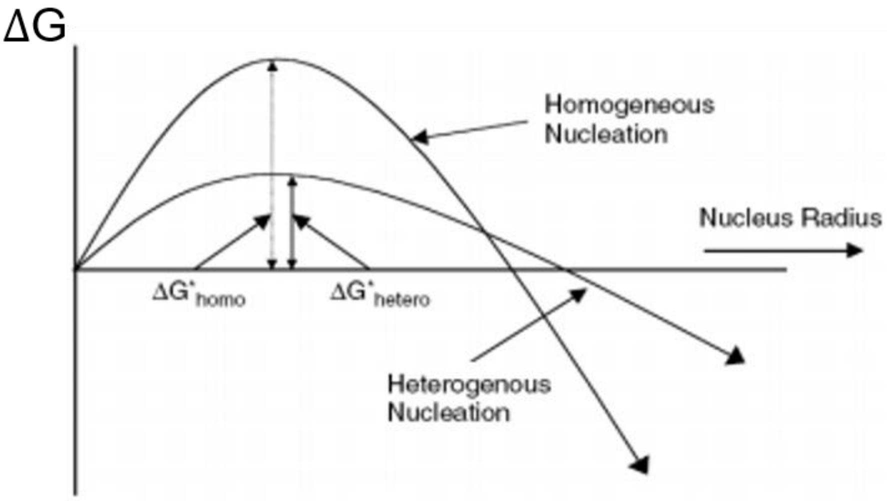

Figure 9. Reduction in the Gibbs energy required to generate a stable nucleus in case of heterogeneous nucleation in comparison with thar required in case of homogeneous nucleation.

The thermodynamics of this process and its mathematical treatment can be derived from Uhlmann and Chalmers [4 rel. primo anno]. A correction factor for the Gibbs energy derived for homogenous nucleation can be used to derive that of heterogeneous nucleation as follows:

$$\Delta G^*_{heter} = \Delta G^*_{hom}\, f(\theta) \tag{13}$$

In this case, the wettability angle θ can be assumed as the angle shown in the following configuration:

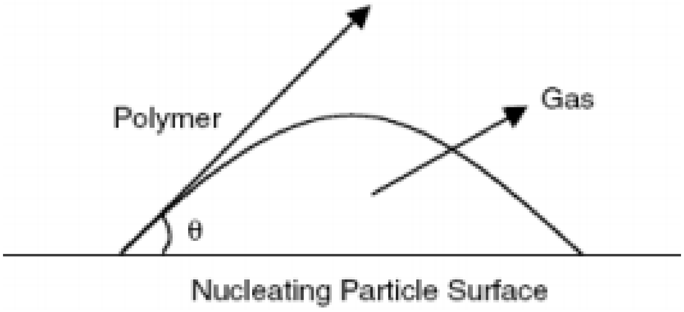

Figure 10. Scheme of the interaction between the surface of a nucleating particle and the polymer/gas system.

Therefore, the correction factor and then the Gibbs energy can be respectively expressed as follows:

$$f(\theta) = \frac{(2+cos\theta)(1-cos\theta)^2}{4} \tag{14}$$

$$\Delta G^*_{heter} = \frac{16\,\pi\,\sigma^3}{3\,\Delta P^2}\, f(\theta) \tag{15}$$

2.3.3. Bubble growth stage

After the nucleation stage, the gas bubbles undergo growth as a consequence of the inflation caused by gas diffusion from the liquid phase into the gas bubble phase. The pressure excess across the curved gas-liquid interface is given by the Laplace equation:

$$\Delta P = \frac{2\sigma}{r} \tag{16}$$

where σ is the surface tension of the liquid and r the radius of the bubble. From this equation, it is evident that the pressure difference across a bubble interface is inversely proportional to the radius of the bubble. In foams there is always a distribution of bubble sizes, hence the pressures in different bubbles will not be the same. This will lead to the diffusion of gas molecules from regions of higher pressure (smaller bubbles) to regions of lower pressure (larger bubbles) (the molecular mechanisms behind this cell degeneration will be more clearly elucidated in the next section). The pressure difference between the gas in a big bubble (a) and that of an adjacent smaller bubble (b) is given by:

$$\Delta P = P_b - P_a = 2\sigma\left(\frac{1}{r_b} - \frac{1}{r_a}\right) \tag{17}$$

Where r_b is the radius of the smaller bubble and r_a is the radius of the larger bubble. Again, σ is the surface tension. The radius of the large bubble, r_a, will be many times greater than the radius of the smaller bubble so that, for a first approximation, the term $1/r_a$ may be neglected. The pressure difference causing gas diffusion is then proportional to the pressure excess in the smaller bubble.

In the context of the PU foaming, the reactive mixture begins to expand when CBA/PBA from the liquid phase diffuses to previously created nuclei. Therefore, the macroscopic expansion is concurrent to the bubbles growth.

2.3.4. Bubble stabilization stage

After the bubble growth stage, single bubbles that were isolated start to touch each other as a consequence of the *impingement*. This so-called wet-dry transition [19] is often characterized by a two-stage process. During the early instants of the foaming process, as aforementioned, the bubble growth is caused by the diffusion of the BA molecules from the polymeric matrix into the bubbles. After this first stage, rounded bubbles isolated in the liquid (wet regime) change their shape into polyhedral cells starting to touch each other (dry regime) [19]. As a consequence, the cells growth rate is reduced. Here, several cell degeneration mechanisms may take place during the foaming process, namely coalescence, coarsening (or Ostwald ripening) and drainage. Coalescence is the process by which two bubbles approach each other (impingement) and, when the film thickness separating them reaches a critical value, it breaks, the bubbles become one [20]. OR consists of a mass transfer mechanism involving two close bubbles of different size: due to the different Laplace pressures, the gas diffuses through the polymer from the smaller bubble to the larger bubbles, deflating the smaller bubble until it disappears [20]. The drainage is caused by capillary forces action that produces transport of the liquid material from the cell walls towards the struts. This mechanism is most frequently found in the case of low viscosity systems such as flexible foams [21].

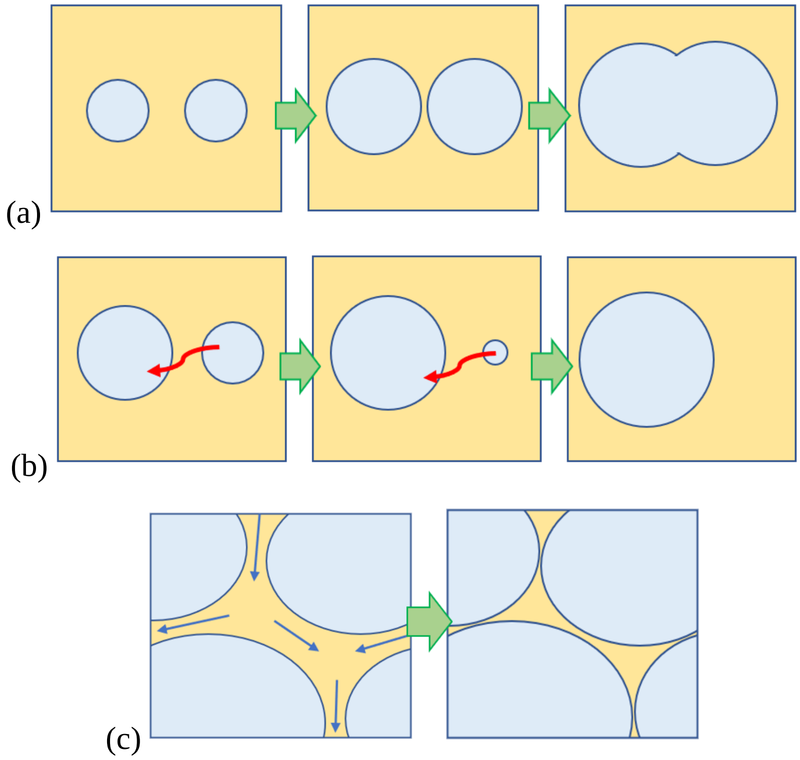

Figure 11. Cell degeneration mechanisms taking place during the foaming process: (a) coalescence, (b) coarsening and (c) drainage.

In this context, it is important that these bubbles are stabilized in order to avoid foams with broader cell size and then non optimal thermal insulating properties. At this stage of the foaming process, the gas is present in the two phases of the system, the bubbles and the polymer/gas solution. With ongoing PU foaming process, the gas contained in the bubbles expand and the gas contained in the solution (supersaturated) diffuses into the existing bubbles. As a result of the bubble expansion, the concentration of gas solubilized is reduced. This concentration may be restored by one of two processes: the surface layer can flow from areas at low surface tension to those at higher surface tension (Marangoni effect) and then the film elasticity is enhanced [22]. In the second case, the surfactant in the interior of the liquid can diffuse to the surface (Gibbs effect) by restoring the surfactant concentration at the surface, but nor the liquid to the film [22]. An increase in temperature may also reduce both viscosity and surface tension, making the thinning of membranes easier, and potentially leading to the rupture of membranes (cell walls) that are too thin to withstand existing stress [22]. The concurrent foam expansion and urethane formation continues until the foam rise to a maximum. At this moment, the cells are filled by the CBA/PBA gas and the equilibrium between the expansion forces and the external polymeric forces is reached. As the foam cools, the pressure inside the cell drops. Rigid foams are strong enough to withstand this gas diffusion outside the polymer and a closed-packed structure without shrinkage is formed. While in case of a flexible foam, the structure will shrink when it cools the low stiffness of the polymer is reached [13].

2.4. Thermal insulation

In consideration of the medium in which the heat transfer is taking place, different mechanisms may occur during the process. In particular, the heat transfer taking please in fluids may be characterized by a *molecular energy transport* (motion of the constituent molecules) and/or a *convective energy transport* (bulk motion of the fluid). Another mechanism, called *diffusive energy transport*, occurs in mixtures that are diffusing into each other. In addition, energy can be transmitted by means of a *radiative energy transport* as well, not requiring a material medium [23]. Here, the heat transfer by molecular transport may be reduced with engineered processes as well as materials with specific shapes and properties [23]. The characteristic parameter is the thermal conductivity, used to measure the ability of a material to conduct heat. Of course, the insulating capability is measured as the inverse of this parameter. Therefore, a low thermal conductivity means a high insulating performance [23]. In the overall applications of thermal insulation, the thermal conductivity is defined by Fourier's law:

$$\bar{q} = -\lambda\, \nabla \mathrm{T} \tag{18}$$

where q is the thermal flux (amount of heat passing through a unitary surface in a unitary time interval), λ is the thermal conductivity T is the temperature [23]. Equation 18 may be expressed in its scalar form (x direction in which the temperature gradient is present):

$$q_x = -\lambda\, \frac{\partial \mathrm{T}}{\partial \mathrm{x}} \tag{19}$$

In this simple case, the equation states that the thermal flux is directly proportional to the temperature gradient and the thermal conductivity is the constant of proportionality [23]. When it comes to cellular materials, we need to account for a more complex behavior of λ [24]. The thermal conductivity of a foam is given by four mechanisms [24]:

$$\lambda_{TOT} = \lambda_{conv} + \lambda_{rad} + \lambda_{sol} + \lambda_{gas} \tag{20}$$

Where λ_{conv}, λ_{rad}, λ_{sol} and λ_{gas} respectively correspond to: i) convection within the cells, ii) radiation, iii) conduction through the solid phase iv) conduction through the gas-filled cell.

2.4.1. Convection contribution to the thermal conductivity

Convection within the cells is related to the gas rising due the density changes caused by temperature. The typical parameter used to quantify this occurrence is the Grashof number (Gr). This dimensionless number is used fluid dynamics and heat transfer to study the natural convection. It approximates the ratio of the buoyancy to viscous forces acting on a fluid:

$$Gr = \frac{g\ \beta\ \Delta T_C\ l^3\ \rho_g^2}{\mu_g^2} \tag{21}$$

Where g is the gravitational acceleration, β is the thermal expansion coefficient of the gas, ΔT_C is the temperature difference within the cell, l is the cell dimension, ρ_g is the gas density and μ_g is the dynamic viscosity of the gas. Typically, a value of 1000 is used for in order to define the minimum l for convection. This is relevant only when the cell dimension is greater than 10 mm, most PUFs have closed cells about one order of magnitude smaller than this value and, therefore, heat transfer due to convection can be considered negligible [24].

2.4.2. Radiation contribution to the thermal conductivity

The radiation contribution is related to the heat flux passing by radiation from a surface at high temperature to a surface at lower temperature. The heat flux is expressed by the Stefan–Boltzmann law:

$$q_{rad} = \varepsilon\ \sigma\ (T_1^4 - T_0^4) \tag{22}$$

Where ε is the emissivity of the surfaces (<1) and σ is the Stefan–Boltzmann constant. The radiation contribution depends on the cell dimensions and the wall thickness: foams composed of many small cells transfer less heat by radiation than foams with few big cells [24].

2.4.3. Solid phase contribution to the thermal conductivity

The contribution of the solid phase, λ_s, may be due to two mechanisms, namely the lattice vibrations and the translation of free conduction electrons. While the lattice vibration contribution is predominant in dielectric solids, the free-electron contribution is predominant energy transport involved in metals. For a polymeric foam the solid phase contribution to the thermal conductivity can be calculated by:

$$\lambda_{sol} = \lambda_{sol}^{*} \varphi \frac{\rho^{*}}{\rho_{sol}} \tag{23}$$

Where λ_{sol}^{*} is the thermal conductivity of the bulk polymer, φ is the efficiency factor taking into account the shape of the cell walls, ρ^{*} is the foam density and ρ_{sol} is the density of the bulk polymer. The contribution of the solid phase to the overall thermal conductivity is low, ca. 10% for PU due to intrinsically low value of the material (0.25 W.m^{-1}.k^{-1} for PU) and the small fraction occupied by the polymeric matrix of the total volume of the foam [24].

2.4.4. Gas phase contribution to the thermal conductivity

This contribution is related to the conduction in the cell gas mixture and can be calculated as follows:

$$\lambda_{gas} = \lambda_{mixt} \left(1 - \frac{\rho^{*}}{\rho_{sol}}\right) \tag{24}$$

Where λ_{mixt} is the thermal conductivity of the gas mixture, ρ^{*} is the foam density and ρ_{sol} is the density of the bulk polymer. Conduction in the cell gas mixture represents the main part of the thermal conductivity of a foam [24]. The conductivity may be further decreased by decreasing the pore size of the material. This is the so-called Knudsen effect, in which is involved that the scale length of the cell is comparable to or smaller than the mean free path of the gas molecules within the cells. The collisions between the gas molecules and the solid are elastic which transfer small amounts of energy compared to the collisions between gas molecules. Smaller cells lead to a higher probability of collisions with pore walls instead of other gas molecules.

2.5. References

[1] David Randall, Steve Lee, The polyurethanes book, New Jersey, 2003.

[2] U. Meier-Westhues, Polyurethanes: Coatings, Adhesives and Sealants, Vincentz Network, Hannover, 2007.

[3] J. T. Kim, B. K. Kim, E. Y. Kim, H. C. Park, H. M. Jeong, Synthesis and shape memory performance of polyurethane/graphene nanocomposites, React. Funct. Polym. 74 (2014) 16-21.

[4] Qipeng Guo, Thermosets Structure, Properties, and Applications, Amsterdam, Netherlands, 2017.

[5] M. Szycher, Szycher's Handbook of Polyurethanes, CRC press, 2012.

[6] M.F. Sonnenschein, Polyurethanes: Science, Technology, Markets, and Trends, 2015.

[7] H. Singh, A. K. Jain, Ignition, Combustion, Toxicity, and Fire Retardancy of Polyurethane Foams: A Comprehensive Review, J. Appl. Polym. Sci. 111 (2009) 1115-1143.

[8] M. Modesti, A. Lorenzetti, An experimental method for evaluating isocyanate conversion and trimer formation in polyisocyanate-polyurethane foams, Eur. Polym. J. 37 (2001) 949-954.

[9] P. Cognard, Handbook of Adhesives and Sealants: Basic Concepts and High Tech Bonding, Elsevier Science, 2005.

[10] D. Klempner, V. Sendijarevic. Polymeric Foams and Foam Technology, Hanser Publishers, 2004.

[11] K. Ashida, Polyurethane and related foams: Chemistry and Technology, CRC Press, 2007.

[12] S. T. Lee, N. S. Ramesh, Polymeric foams: mechanisms and materials, Boca Raton, Florida, USA, 2004.

[13] D. Eaves, Handbook of Polymer Foams, Rapra Technology Limited, Shawbury, Shrewsbury, Shropshire, UK, 2004.

[14] H. Ulrich, Kirk-Othmer Encyclopedia of Chemical Technology, 2000.

[15] J. O. Akindoyo, M. D. H. Beg, S. Ghazali, M. R. Islam, N. Jeyaratnam, A. R. Yuvaraj, Polyurethane types, synthesis and applications – a review, RSC Advances, 6 (2016) 114453-114482.

[16] S. Estravís, J. Tirado-Mediavilla, M. Santiago-Calvo, J. L. Ruiz-Herrero, F. Villafañe, M.A. Rodríguez-Pérez, Rigid polyurethane foams with infused nanoclays: Relationship between cellular structure and thermal conductivity, Eur. Polym. J. 80 (2016) 1–15.

[17] D. Kashchiev, Nucleation Basic Theory with Applications, Elsevier, Amsterdam, 2000.

[18] M. Blander, J. L. Katz, Bubble Nucleation in Liquids, AIChE J. 21 (1975) 833–848.

[19] Y. Furuta, N. Oikawa, R. Kurita, Close relationship between a dry-wet transition and a bubble a bubble rearrangement in two-dimensional foam, Sci. Rep. 6 (2016) 37506.

[20] P. Walstra, Fundamentals of Interface and Colloid Science, Elsevier, 2005.

[21] I. Cantat, S. Cohen-Addad, F. Elias, F. Graner, R. Höhler, O. Pitois, F. Rouyer, A. Saint-Jalmes, S. Cox, Foams: Structure and Dynamics, Oxford University Press, 2013.

[22] N. K. Adam. The Physics and Chemistry of Surfaces. Oxford University Press, 1941.

[23] R. B. Bird, W. E. Stewart, E. N. Lightfoot, Transport Phenomena, John Wiley & Sons, 2006.

[24] L. J. Gibson, M. F. Ashby, Cellular Solids, Structure and Properties, Pergamon Press, 1988.

PART II:

Polyurethane foams by high-pressure CO_2

Chapter 3.

Effect of CO_2 on the polyurethane curing reaction

In this chapter, it is reported the experimental study of the effect of CO_2 on the polyurethane synthesis between a polyol and an isocyanate. Near infrared spectroscopy in reflection mode was used to monitor both CO_2 sorption in the polyol and in the isocyanate and the polyurethane synthesis under pressure. Results revealed a significant slowing down effect by the sorbed CO_2, apparently due to two concurrent mechanisms, namely catalyst deactivation and dilution.

Chapter 3. Effect of CO_2 on the polyurethane curing reaction

3.1. Introduction

In order to use CO_2 as a PBA (to be solubilized at high-pressure in the polyol and/or isocyanate) in PU foaming, it is fundamental to understand the behavior of the reacting system in the presence of CO_2. In particular, CO_2 may play a critical role in the different reactions involved in the PU synthesis. The effect of the CO_2 presence (in particular, in supercritical conditions) in a reacting system has been largely reported in the literature, resulting an additional parameter to manipulate reaction kinetics. For instance, Stassin et al. [1] reported the effect of CO_2 in supercritical conditions on the kinetics of ring-opening polymerization of ε-caprolactone. Authors observed a slowing down of the polymerization reaction, ascribed to the occurrence, in presence of CO_2, of a carbonation reaction responsible for a positive volume of activation and a higher energy of activation as compared to polymerization in a regular hydrocarbon solvent. In particular, the tin alkoxide initiator responsible for the growth of the polycaprolactone chains was carbonated by compressed CO_2, as verified by infrared spectroscopy. Tiltscher et al. [2] showed that catalyst deactivation occurred during a gas-phase reaction, when hexene oligomers with low volatilities deposited on the catalytically active surface. Performing the reaction at the same temperature, but above the critical pressure prevented the deposition of these oligomers and the ensuing catalyst deactivation. The readiness of CO_2 to interact chemically with proton-containing nucleophiles, such as water, alcohols and primary, secondary and tertiary amines was used to develop switchable systems [3,4]. The reversible binding between CO_2 and primary, secondary and tertiary amines is well known in literature, for example in CO_2 capture processes [5-7] and it has been shown of potential interest in other areas such as in catalytic processes, where CO_2 is simultaneously used as solvent and as a protecting group for amines. Examples include the ring closing metathesis and the hydroaminomethylation of secondary amines [8,9].

3.2. Materials and methods

In the attempt to use high pressure CO_2 as a PBA in PU foaming, a throughout and scientifically grounded study has been performed during the previous PhD project carried out by Dr. Maria Rosaria Di Caprio and it has been continued in the context of this PhD work. The sorption thermodynamics and mass transport properties of the CO_2 with both the polyol and the isocyanate have already been studied by using an equipment based on the coupled gravimetry-Axisymmetric Drop Shape Analysis (ADSA) [10,11]. An instrumented pressure vessel [12], recently introduced by our group purposely, was adopted in order to perform the experiments and monitor the PU foaming by high-pressure CO_2,

3.2.1. Materials

A polyether polyol (Table 1) and polymeric methylene diphenyl diisocyanate (PMDI) (Table 2) were supplied by Dow Italia S.r.l. (Correggio, RE, Italy) and used “as received”. In particular, tertiary amine-based catalysts were used within the polyol formulation (e.g. Pentamethyldiethylenetriamine and Dimethylcyclohexylamine). High purity grade CO_2 (99.95% pure) was supplied by SOL (Naples, Italy).

Table 1. Composition of the polyether polyol.

Components	Molecular weight (Mw) (Da)	Functionality (f)	Parts (%)
Glycerin initiated polyether polyol	1000	Low	95
Amine initiated polyether polyol	500	High	
Sorbitol initiated polyether polyol	700	High	
Sucrose/glycerin initiated polyether polyol	500	High	
Catalysts	/		3
Surfactant	/		2

polyol contains 0.2% water and polydispersity index (PDI) is 1-1.5; viscosity = 15150 mPa.s (25°C); data from the supplier

Table 2. Properties of the PMDI.

Component	Equivalent weight	NCO content (%)	Functionality	Viscosity mPa.s (25°C)	Acidity as %HCl
PMDI	135	31.1	2.7	190	0.02

data from the supplier

3.2.2. Experimental setup

In situ FT-NIR spectroscopic investigation of CO_2 sorption and PU curing were conducted by using Frontier™ NIR spectrometer (Perkin Elmer Inc., Waltham, MA, USA) equipped with a tungsten halogen source, a CaF2 beam splitter, a FlexIR™ NIR Fiber Optic reflectance probe (PIKE Technologies, Inc., Madison, WI, USA) and an InGaAs detector. The probe was housed beneath a high-pressure-tight sapphire window (Precision Sapphire Technologies, Vilnius, Lithuania) placed on the bottom plate of a 1 L pressure vessel (Figure 1a and b). The sapphire window was in contact with an optical glass cylindrical sample holder, placed inside the pressure vessel, containing the polyol or the PMDI, kept separate by a rubbery impeller, during the CO_2 sorption test. The rubbery impeller, after sorption, is allowed to mix the two reactants by a lab mixer connected to the impeller via a high-pressure bearing, to study curing under pressure.

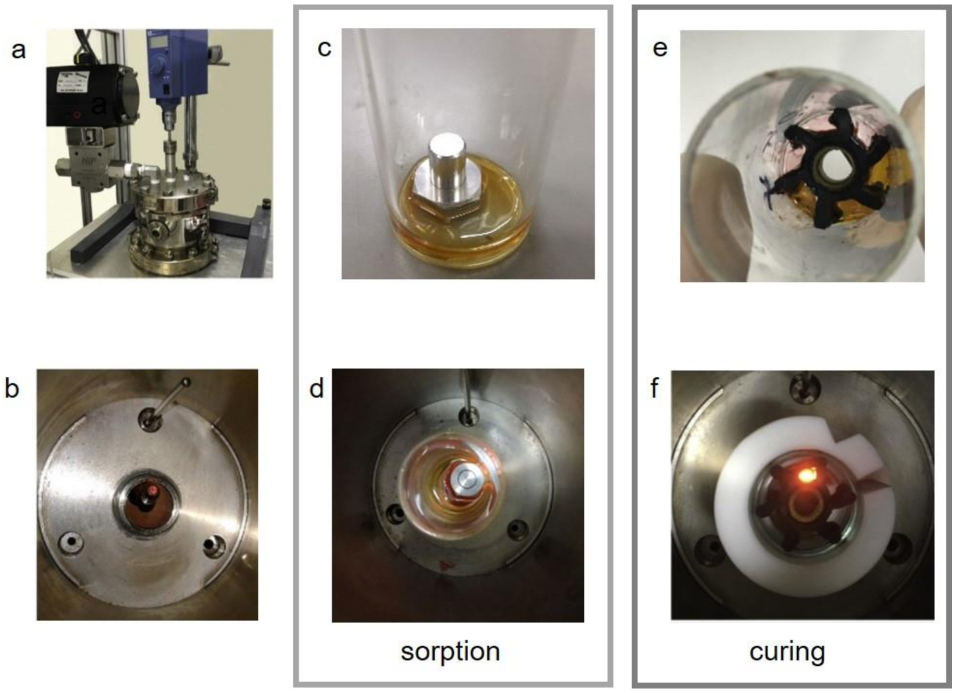

Figure 1. Pictures of the adopted instrumentation. a) Assembly of the high-pressure PU foaming equipment, showing the mixing head and the gas evacuation system; b) detail of the probe and the sapphire windows placed at the bottom plate of the pressure vessel (top view). c) and d) set up for the sorption tests (light gray box): c) sample holder with the polymer (PMDI in this image) and the reflector and d) positioning of said sample holder inside of the pressure vessel. e) and f) set up for the curing tests (dark gray box): e) sample holder with the rubbery impeller that keeps separate the two reactants for sorption and f) details of the Teflon coupling of the sample holder with the sapphire window; the light comes from the NIR probe. See [12] for details.

3.2.3. Sorption

During the sorption tests, the polyol (or the PMDI) was poured in the glass cylindrical sample holder, and a metal reflector (with a path length of approximately 0.5 mm) was placed on top of the sample (Fig.1c). The two reactants are lightly colored transparent viscous liquids and the reflector is necessary in order to return the near-infrared light to the collecting probe (transflectance sampling). The sample holder is then placed in the pressure vessel onto the sapphire window (Figure 1d) and then the pressure vessel is closed. After reaching the testing temperature, in this case 35 °C, CO_2 pressure is increased up to the saturation pressure (in the range from 0 to 4 MPa) and kept for a sufficient amount of time, until equilibrium is reached.

FT-NIR spectra were recorded automatically at regular time interval of 5 min using Perkin Elmer TimeBase software, in the spectral range 4000-10000 cm^{-1} with a resolution of 4 cm^{-1} and 32 scans. It is worth of note, here, that sorption monitoring by infrared spectroscopy has been already reported [13] and requires, for a quantitative analysis, calibration by known concentrations. In this case, sorption was measured by a coupled gravimetry-axisymmetric drop shape analysis on the two reactants, as reported in [10,11]. The FT-NIR acquisitions allowed us to detect the combination bands as due to CO_2 sorption. The area under the monitored peaks was integrated and directly correlated to the amount of CO_2 sorbed in the polymer according to Beer-Lambert Law through univariate analysis by using Perkin Elmer TimeBase software. Subtraction of the spectrum of the initial reactant (polyol or PMDI), with no dissolved CO_2, from all of the spectra allowed to remove the contribution of other bands that overlap with the combination band of CO_2. Moreover, this procedure allowed to remove the contribution of the bands of CO_2 not dissolved within the polymer (CO_2 between the glass window and the sample holder). Further details on the calibration method for quantitative evaluation are reported in section 3.3.1.

3.2.4. Curing

In order to monitor the PU curing, polyol and PMDI (1:1.15 by weight) were gently cast in the sections of a glass cylindrical sample holder formed by the sample holder itself and the blades of a rubber impeller, which prevents the premature mixing of the two reactants (Figure 1e). The sample holder was then placed in the pressure vessel onto the sapphire window and secured by the Teflon coupling (Figure 1f). The pressure vessel is then pressurized and sorption is conducted for a defined period. After sorption, the two reactants are mixed for the reaction to occur by operating the impeller with a mixing shaft connected to a lab mixer by a high-pressure bearing [12]. The curing reaction was conducted, still under pressure, for a suitable amount of time, until completion.

The curing reaction, at several CO_2 pressures and 35°C, was monitored by collecting spectra automatically at regular time interval of 20 seconds with a resolution of 4 cm^{-1} and 8 scans, after mixing at 250 rpm for 10 seconds until the end of the curing. When PU synthesis is monitored by FT-NIR spectroscopy, it is possible to detect, among others, the NCO band decrease and the NH band (of the urethane group) formation and increase, which allows for a quantitative analysis of the curing process [14].

In order to meter a known CO_2 amount in the two PU formulation components, sorption time as well as CO_2 pressures were varied. The total CO_2 amount sorbed within the two phases (PMDI and polyol, separate by the rubbery impeller, see Figure 1e) at a certain CO_2 pressure after a given sorption time was calculated by assuming: i) a Fickian behavior for the two phases, ii) constant thickness and gas diffusivities (PMDI/CO_2 and polyol/CO_2 mutual diffusivities) and iii) one-dimensional transport problem (sorption occurs by diffusion through the top surface, while no flux is assumed to occur at bottom and lateral surfaces) [15]. Solubility and diffusivity data were gathered, for the two compounds, in [10,11]. With these assumptions, the well-known error function describes the CO_2 concentration profiles as a function of time elapsed after instantaneous pressurization. The average CO_2 fraction at each sorption time, for each phase, can be calculated after integration of said profiles. When mixing the two CO_2-laden fluids (a polyol/CO_2 solution and a PMDI/CO_2 solution), the PU synthesis reaction is allowed to start. Due to the different timescales of sorption O(10h) and of reaction O(10min), we assumed the sorption that may occur after mixing negligible. Furthermore, immiscibility of the components excludes the possibility of CO_2 exclusion upon mixing [16]. Hence, the average CO_2 weight fraction in the reacting mixture, $\overline{w}_{CO_2}$, was calculated by weight-averaging the CO_2 fractions sorbed within the two phases before mixing [15].

3.3. Results and discussion

3.3.1. Sorption

FT-NIR spectra of polyol and PMDI before and after exposure for three days at 4 MPa of CO_2 and 35°C are reported in Figure 2a and b respectively. Sorption time was selected, based on diffusivity data [10,11] and on the sample amount, to attain equilibrium. According to previous studies [17], FT-NIR spectra of pure CO_2 show combination bands due to the coupled Fermi resonance. In Figure 2, spectra of samples exposed to CO_2 reveal combination bands at 4950 cm^{-1} ($\nu_1 + 2\,\nu_2 + \nu_3$) and 5070 cm^{-1} ($2\,\nu_1 + \nu_3$) [17]. In the following, the combination band at 4950 cm^{-1} is selected to estimate, via the Beer-Lambert law and by using gravimetric data retrieved in [10] and [11], the amount of CO_2 sorbed in the polymeric phases [13].

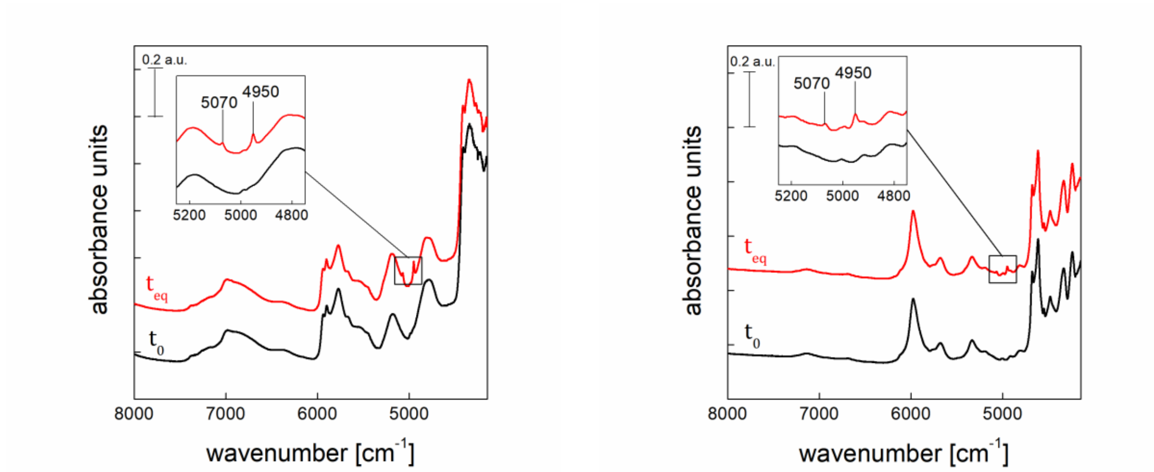

(a) (b)

Figure 2. FT-NIR spectra of (a) polyol and (b) PMDI before (black line) and after (red line) exposure for 3 days at CO_2 at 4 MPa and 35°C. The inset shows a detailed view of the two CO_2 combination bands at 4950 and 5070 cm^{-1}. Spectra are shifted vertically for clarity.

The detailed time-evolution of FT-NIR spectra of CO_2 sorption monitoring in the polyol, at 4 MPa and 35°C, and the difference spectra are reported in Figure 3a and b. Figure 3a reports the evolution of the integrated area under the combination band of CO_2 (A_{CO2}) at 4950 cm^{-1}. A_{CO2} attains equilibrium after ca. three sorption days and the equilibrium value, A_{CO2}^{eq}, can be evaluated as the average value of the final plateau. Assuming a linear dependence (Beer-Lambert law) between A_{CO2} and weight fractions of the CO_2 [18] and the sample thickness, L, constant, FT-NIR kinetics data can be utilized to calculate the mutual polyol/CO_2 diffusivity, D, by fitting data with the first term approximation of the Fickian model [19]:

$$\ln\left(1-\frac{A_{CO2}}{A_{CO2}^{eq}}\right)=\ln\left(\frac{8}{\pi^2}\right)-\frac{D\,\pi^2 t}{L^2} \qquad (1)$$

The evaluation of the limiting slope of $\ln\left(1-\frac{A_{CO2}}{A_{CO2}^{eq}}\right)$ vs. t for the different tests conducted on both the polyol and PMDI at different pressures and at 35°C allowed to measure D of $1.01\cdot10^{-6}$ cm^2/s for the polyol/CO_2 system and of $2.3\cdot10^{-6}$ cm^2/s for PMDI/CO_2 at 4 MPa, in agreement with those retrieved with coupled gravimetry – ADSA [10,11]. It is worth of note, here, that evaluation of diffusivity by the above method does not require any calibration with actual weight fraction data (just the assumption of validity of the Beer-Lambert law).

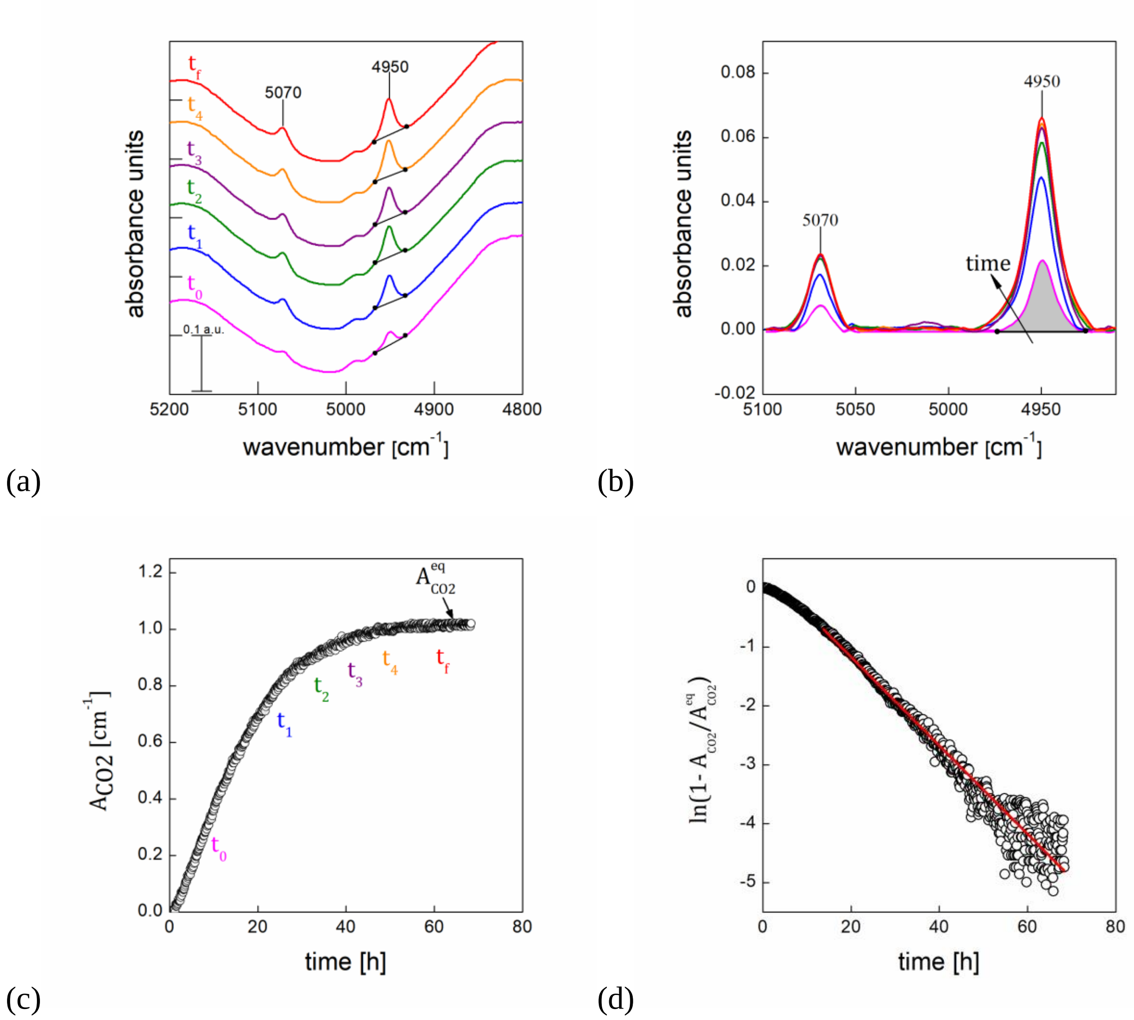

Figure 3. CO_2 sorption monitoring in polyol at 4 MPa and 35°C: (a) time-evolution of FT-NIR spectra, (b) difference spectra, (c) integrated absorbance area A_{CO2} under the CO_2 combination band at 4950 cm^{-1} as a function of sorption time and (d) fit procedure to evaluate D by eq. (1). The monitored A_{CO2} area is indicated in grey in (b) and the spectral acquisition time were: t_0=10h; t_1=25h; t_2=38h; t_3=45h; t_4= 52h; t_f=60h. In (a), spectra are shifted vertically for clarity.

To use spectral information as a quantitative tool for CO_2 sorption, a calibration was performed based on data gathered with coupled gravimetry – ADSA [14,15]. The procedure is described in Figure 4, where, for both polyol and PMDI, A^{eq}_{CO2} values at 2 and 4 MPa and 35°C are reported as function of CO_2 sorption pressure. Data draw a linear dependence with pressure, which can be described as $A^{eq}_{CO2} = m \cdot P_{CO2}$ where m is equal to $2.68 \cdot 10^{-1}$ cm^{-1}/MPa (polyol) and $1.53 \cdot 10^{-1}$ cm^{-1}/MPa (isocyanate). This result allows us to interpret curing results in a more consistent way, as it will be seen in the following. The inset in Figure 4 shows A^{eq}_{CO2} vs. $\overline{w}_{CO_2}$, collectively for both the polyol and PMDI. Data fit nicely on a single line, proving that molar absorptivity of CO_2 is not affected by the specific polymeric phase. This is an important conclusion, that allows a more rigorous treatment of IR data, as it will be shown in the following.

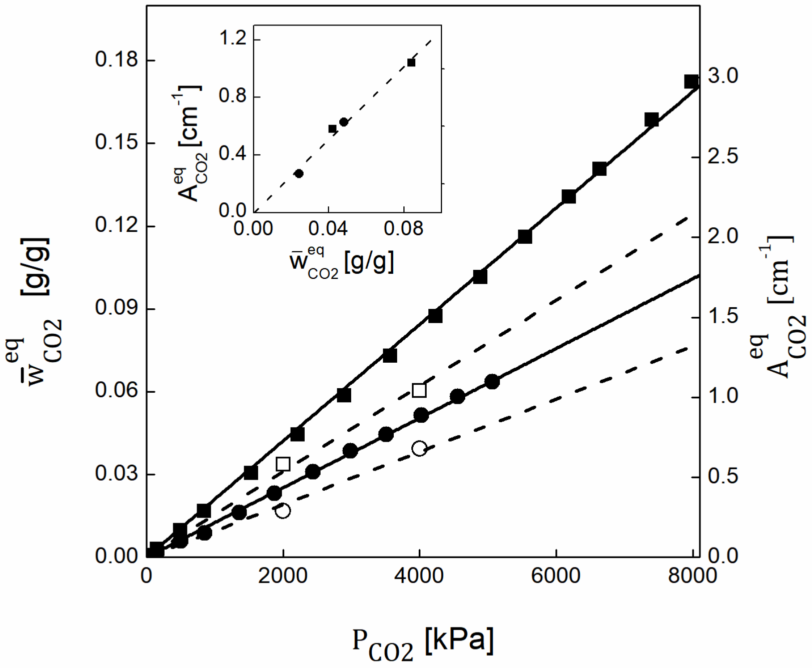

Figure 4. Calibration of FT-NIR sorption in polyol (■) and PMDI (●). A^{eq}_{CO2} vs. P_{CO2} by FT-NIR (this study) (open symbols) and $\overline{w}^{eq}_{CO2}$ vs. P_{CO2} as measured by gravimetry-ADSA [10,11] (closed symbols) (A^{eq}_{CO2} vs. $\overline{w}^{eq}_{CO2}$ as inset). Lines are guide to the eye only.

3.3.2. Curing

The measurement of the effect of the different CO_2 concentrations on the PU curing reaction kinetics is the primary objective of this experimental work, where FT-NIR is utilized to monitor the different isocyanate reactions taking place simultaneously in the standard PU formulations [20]. In particular, in the formulation utilized in the present study the following reactions take place: i) the isocyanate and the hydroxyl group react to give a carbamate ("urethane" in case of high molecular weights) as the desired product; ii) the isocyanate reacts with water to produce a carbamic acid, which breaks down into carbon dioxide and a primary amine that reacts immediately with another isocyanate to form urea. For the sake of clarity, the chemical CO_2 produced by the blowing reaction was considered negligible in comparison with the CO_2 dissolved within the two phases (polyol and isocyanate) during the sorption stage. Hence, the isocyanate, characterized by the NCO group, readily detectable by NIR, is involved in different reactions and may be utilized to describe an overall reaction rate, by following its consumption. Furthermore, the isocyanate and the polyol react together (i) to produce PU which is characterized by the NH(CO)O group where the NH vibration is also readily detectable by NIR [14]. The PU production rate is, hence, quantifiable as well. To this aim, collected spectra can be treated as described by the help of Figure 5, reporting the spectra of the single reactants/CO_2 solutions (a and b), collected before mixing (after 5 hours of sorption time), a spectrum collected right after mixing the two components at 250 rpm for 10 seconds (c) and a spectrum collected at the end of the curing reaction (after 2 hours, d). In this specific case, average CO_2 weight fraction, $\overline{w}_{CO_2} = 0.05$ g/g, was calculated by the procedure described in section 3.2.3. Spectra reported in Figure 5 show that the NCO band at 4680 cm^{-1}, characteristic of the PMDI, does not completely disappear at the end of the cure, proving its excess with respect to the polyol in the adopted formulation.

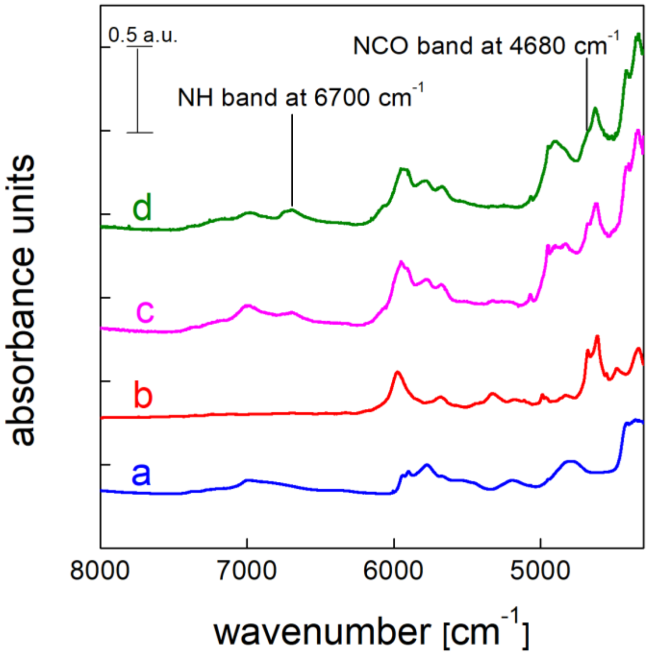

Figure 5. FT-NIR spectra of the single reactants (polyol (a) and isocyanate (b)) collected before mixing (after 5 hours of sorption time), spectra collected right after mixing the two components at 250 rpm for 10 seconds (c) and at the end of the curing reaction (d), at 35°C and at CO_2 concentration of 0.05 g/g. Spectra are shifted vertically for clarity.

In Figure 6 are reported details of the spectral regions of interest in this work and highlights time-evolution of characteristic signals. In particular, Figure 6a shows the wavenumber range 5000-4400 cm^{-1}, where the NCO peak appears at 4680 cm^{-1}, while Figure 6b shows the wavenumber range 8000-5500 cm^{-1}, where the NH peak appears at 6700 cm^{-1}. Correspondingly, Figures 6c and d show in detail the monitored peaks area and Figures 6e and f show the time evolution of A_{NCO} and A_{NH}, respectively.

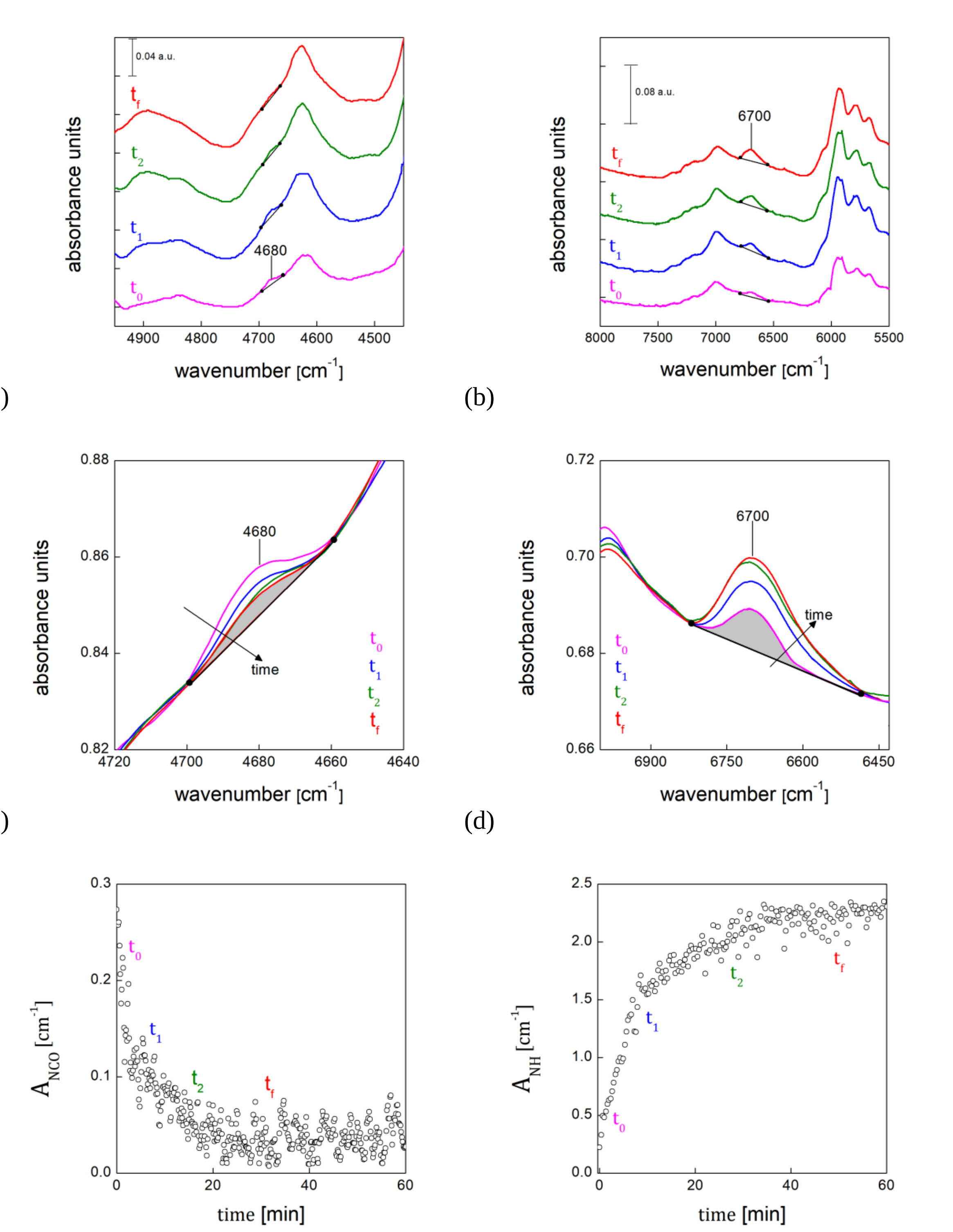

(a) (b)

(c) (d)

(e) (f)

Figure 6. Time-evolution of FT-NIR spectra (a and b), detail of the monitored peaks area (c and d) and integrated absorbance area of NCO (A_{NCO}) and NH (A_{NH}) bands (e and f) at 35°C and at CO_2 concentration of 0.05 g/g. The monitored integrated areas are indicated in grey (c and d). Spectra at t_0 represent the beginning of reaction (after mixing), t_1 and t_2 are intermediate acquisitions (4 and 18 minutes for NCO band, 10 and 30 minutes for NH band), t_f represents the acquisition when the integrated area attains a constant value (ca. 33 and 57 minutes for NCO and NH bands, respectively). In (a) and (b), spectra are shifted vertically for clarity.

The reaction rates can be described by various kinetic models. In particular, as typically done in the case of thermosetting polymers, it was adopted a phenomenological model that describes both homogeneous processes and heterogeneous processes which are governed by phase-boundary reaction mechanisms [21,22], namely:

$$\frac{\mathrm{d}\alpha}{\mathrm{dt}} = \mathrm{k}\,(1-\alpha)^{\mathrm{n}} \tag{2}$$

Where α is the time-dependent relative conversion ($\alpha = 1 - \frac{A_{NCO}}{A_{NCO}^{0}}$, where A_{NCO}^{0} is the initial absorbance area), $k = Ae^{-E_a/RT}$ is the Arrhenius-type kinetic constant and n represents the reaction order. Integration of Equation 2 for $n = 1$ [22] yields:

$$\alpha = \alpha_f(1 - e^{-kt}) \tag{3}$$

Figure 7 shows the results of the fitting of NCO conversion kinetics for selected $\overline{w}_{CO_2}$, evidencing the suitability of the selected simple model for the reaction kinetics, while the results of the fitting procedure (i.e. rate constant, k, and the final conversion α_f) are collectively reported in Table 3 for the whole range of investigated $\overline{w}_{CO_2}$. Kinetics data evidence a strong effect of $\overline{w}_{CO_2}$ on the NCO consumption, with a minor effect on α_f.

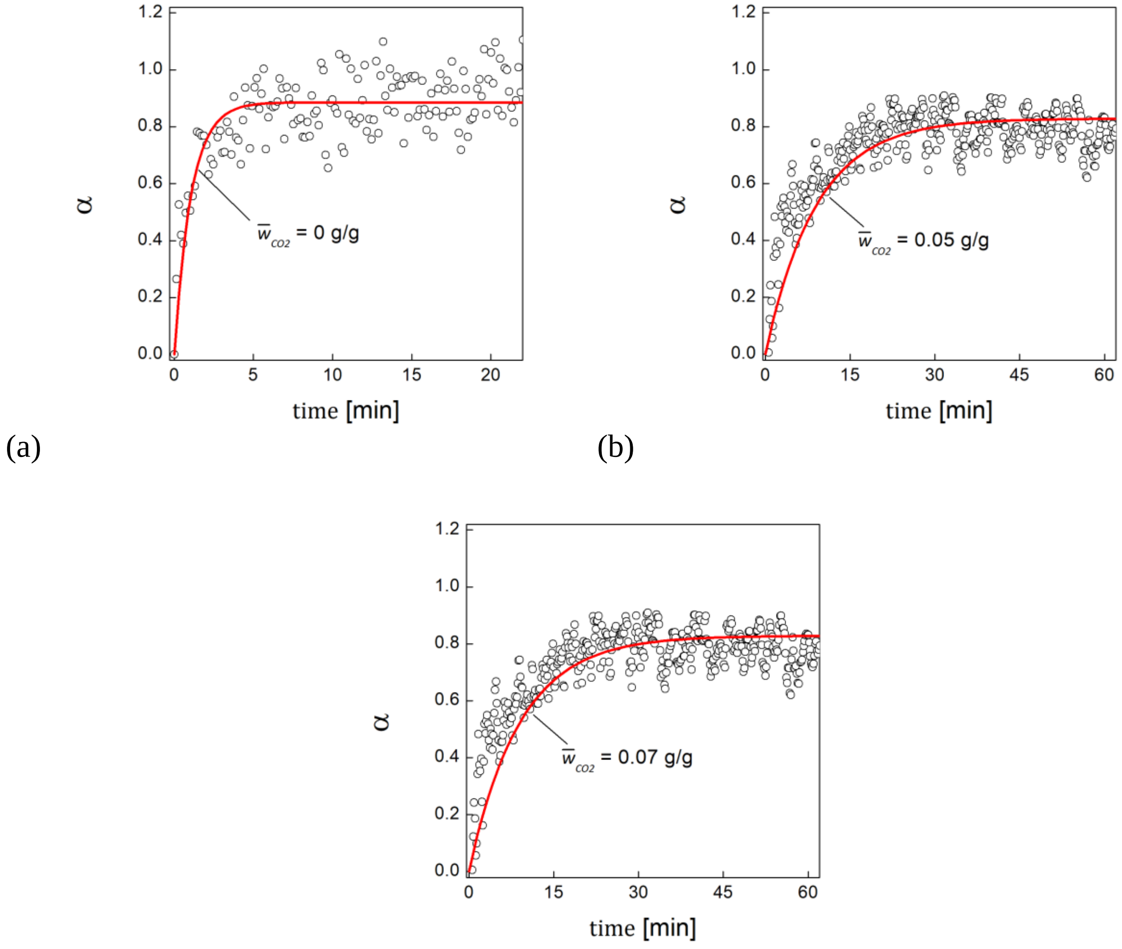

(a) (b)

(c)

Figure 7. NCO relative conversion (α) (at 4680 cm^{-1}) at 35°C and a) $\overline{w}_{CO_2} = 0$ g/g, b) $\overline{w}_{CO_2} = 0.05$ g/g and c) $\overline{w}_{CO_2} = 0.07$ g/g as function of reaction time (abscissa scaled differently). Open symbols are experimental data, lines are the fitting by Equation 3.

Table 3. Effect of CO_2 on NCO conversion: results of the fitting procedure

P_{CO2} [MPa]	CO_2 sorption time [hours]	$\overline{w}_{CO2}$ [g/g]	k [min^{-1}]	α_f	t_{c_NCO} [min]
0	0	0	0.941 ± 0.056*	0.886 ± 0.043	4 ± 1
2	5	0.025	0.126 ± 0.063	0.688 ± 0.13	24 ± 1.5
4	5	0.050	0.110	0.828	45
6	5	0.070	0.075 ± 0.009	0.731 ± 0.036	70 ± 2
7	5	0.085	0.066 ± 0.005	0.771 ± 0.14	80 ± 1
7.5	5	0.090	0.065	0.941	82
8	5	0.100	0.063	0.863	84
10	5	0.120	0.059	0.767	90
12	5	0.140	0.056	0.595	95

* Where reported, standard deviations were evaluated on experiments performed in triplicate

The $\overline{w}_{CO_2}$ effect on the NCO consumption rate can be also evaluated by the conversion time, t_{c_NCO}, as the time needed to reach 0.95·α_f, also reported in Table 3. It is possible to note that t_{c_NCO} increases monotonically with $\overline{w}_{CO_2}$, evidencing the slowing down of the PMDI conversion by CO_2. In particular, Figure 8 shows the effect of $\overline{w}_{CO_2}$ on t_{c_NCO}, highlighting an apparent two-region process, with a decrease of the CO_2 effect above 0.07 g/g. Below this critical value of $\overline{w}_{CO_2}$ the slope of the t_{c_NCO} vs. $\overline{w}_{CO_2}$ curve is 927±69 min.g/g, while at larger $\overline{w}_{CO_2}$ it is equal to 330±40 min.g/g. This occurrence will be more thoughtfully investigated in the following.

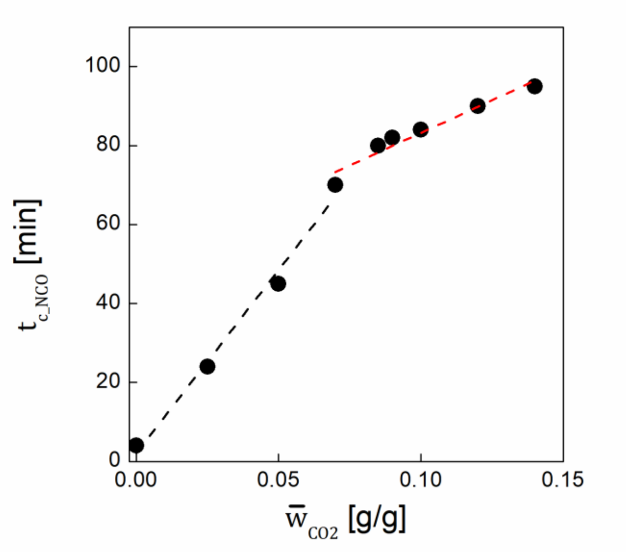

Figure 8. NCO conversion time (t_{c_NCO}) at different $\overline{w}_{CO_2}$. Lines are only guide to the eye.

As described above, the urethane formation, characteristic of the PUFs, is also readily observable by FT-NIR and the rise of the associated peak can be utilized to monitor the curing kinetics. As the urethane formation reaction involves the consumption of species involved in other reactions [20], it is easier to describe its kinetics in terms of the urethane characteristic group (NH) formation, instead of reactants consumption (conversion). The assumptions adopted to derive the simple kinetic model of Equation 2, in this case yield:

$$A_{NH} = A_{NH}^{f}\,(1 - e^{-kt}), \tag{4}$$

where A_{NH} is the integrated absorbance area of the NH peak at time t, and A_{NH}^{f} is the integrated absorbance area final value ($A_{NH}^{0} = 0$, as no urethane is in the system at time $t = 0$) [23]. In this case, it is more appropriate to express the degree of curing by normalizing with respect to the final A_{NH}^{f}, as follows:

$$X(t) = \frac{A_{NH}}{A_{NH_f}} = (1 - e^{-kt}). \tag{5}$$

The experimental data and fitting by Equation 4, for selected $\overline{w}_{CO_2}$ are reported in Figure 9, while the results of the fitting procedure are reported in Table 4.

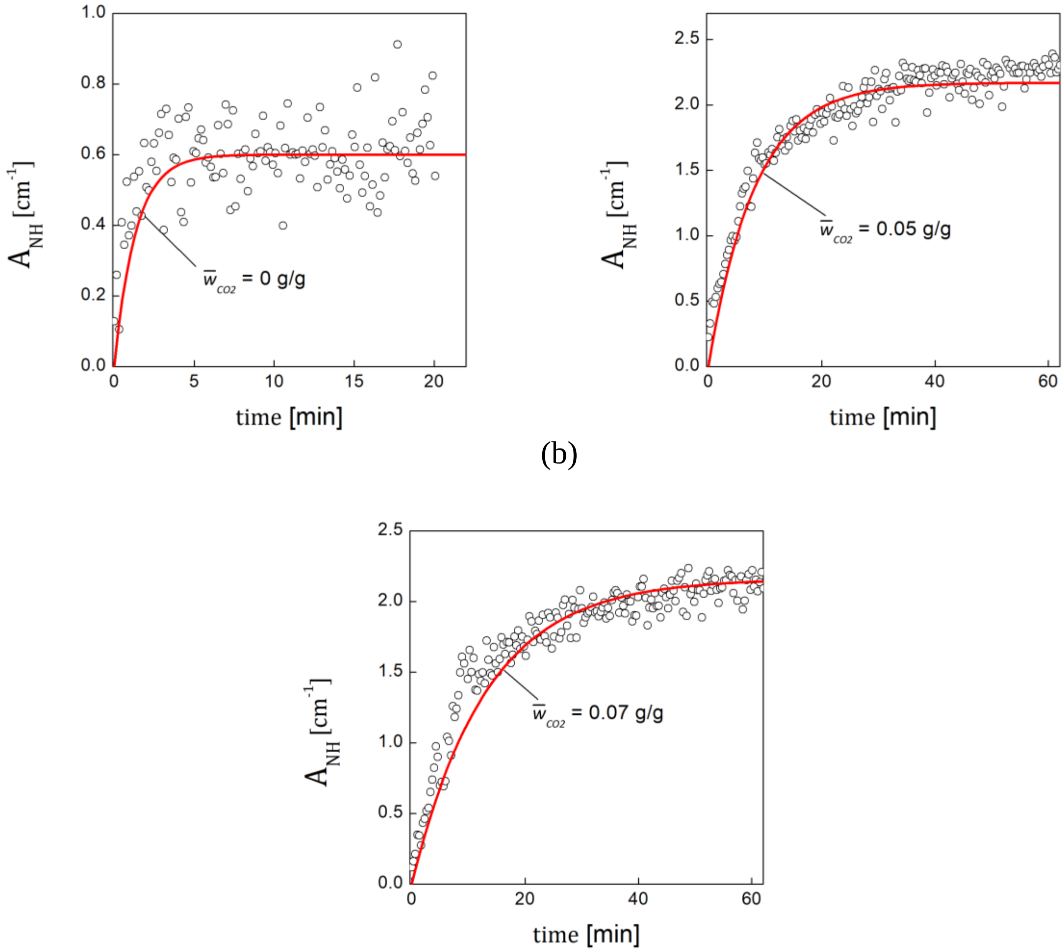

(a) (b)

(c)

Figure 9. NH integrated absorbance area (A_{NH} at 6700 cm^{-1}) at 35°C and a) $\overline{w}_{CO_2}$ = 0 g/g, b) $\overline{w}_{CO_2}$ = 0.05 g/g and c) $\overline{w}_{CO_2}$ = 0.07 g/g as function of reaction time. Open symbols are experimental data, lines are fitting by Equation 4.

Table 4. Effect of CO_2 on NH formation: results of the fitting procedure.

P_{CO2} [MPa]	CO_2 sorption time [hours]	$\overline{w}_{CO2}$ [g/g]	k [min^{-1}]	t_{c_NH} [min]
0	0	0	0.735 ± 0.025*	5.6 ± 0.6
2	5	0.025	0.162 ± 0.001	28.5 ± 3.5
4	5	0.050	0.102	57
6	5	0.070	0.076 ± 0.016	73.5 ± 3.5
6	12	0.079	0.063	77
10	1.5	0.079	0.065	79
7	5	0.085	0.066 ± 0.006	81 ± 2
7.5	5	0.090	0.062	83
8	5	0.100	0.063	87
10	5	0.120	0.056	95
12	5	0.140	0.050	103

* Where reported, standard deviations were evaluated on experiments performed in triplicate

Figure 10 collects all of the reaction kinetics fitting curves at the different $\overline{w}_{CO2}$ highlighting the important slowing down effect by the CO_2 on PU synthesis.

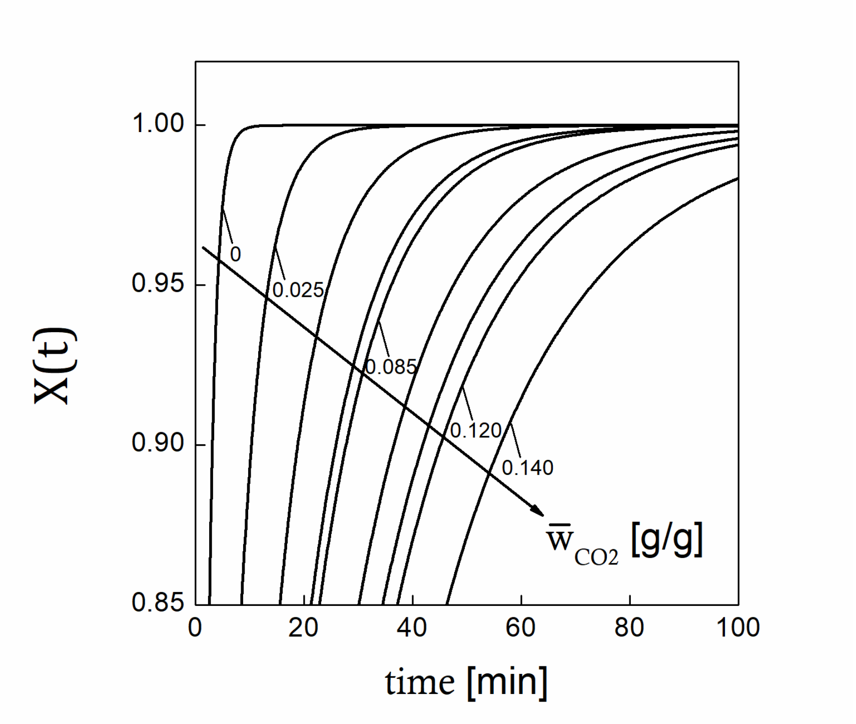

Figure 10. Degree of curing X(t) of PUs reacted at different $\overline{w}_{CO2}$ evaluated as a function of the reaction time. Line represents the fitting of experimental data by Equation 5.

The $\overline{w}_{CO_2}$ effect on the NH formation rate can be also evaluated by the formation time, t_{c_NH}, as the time needed to reach 0.95·X (Figure 11a). It is possible to note that t_{c_NH} increases monotonically with $\overline{w}_{CO_2}$. An interesting question that may arise from these data regards the role of the CO_2 pressure and its supercritical transition. To this aim, we performed additional tests in which the same $\overline{w}_{CO_2}$ is achieved at two different pressures, specifically below and above the critical pressure. Achieving the same $\overline{w}_{CO_2}$ at two different pressures can be easily done by adjusting the sorption time. In particular, Table 4 shows that $\overline{w}_{CO_2}$ = 0.079g/g can be achieved after solubilization at 10 MPa for 1.5 hours or at 6 MPa for 12 hours. Figure 11b and data reported in Table 4 rule out the effect of the supercritical transition and clarifies that, in our case, the controlling variable on the PU synthesis is the $\overline{w}_{CO_2}$, not P_{CO2}, as t_{c_NH} does not change with P_{CO2} (open symbols in Figure 11b), at constant $\overline{w}_{CO_2}$.

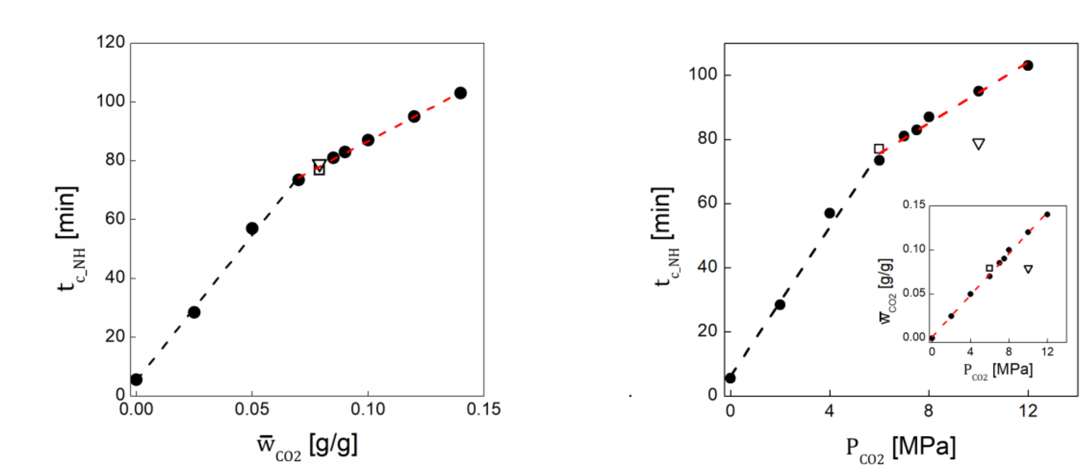

(a) (b)

Figure 11. Effect of CO_2 on t_{c_NH}; data reported as a function of a) $\overline{w}_{CO_2}$ and b) P_{CO2} ($\overline{w}_{CO_2}$ vs. P_{CO2} as inset). Symbols are experimental data, lines are only guide to the eye. Open symbols refer to tests performed at $\overline{w}_{CO_2}$ achieved after sorption conducted at different pressures (by adapting the sorption time): test conducted at 6 MPa and 12 hours of sorption (☐**)**, test conducted at 10 MPa and 1.5 hours of sorption (∇).

As in the case of Figure 8 (for the NCO conversion), Figure 11a confirms the apparent two-stage process, with a decrease of the CO_2 effect above 0.07 g/g. Catalyst deactivation [2,4] as well as dilution effects [24,25] have been reported in the underlying literature. With reference to the former, in the specific case of catalyst deactivation by CO_2, it has been reported, for instance, a reaction between CO_2 and 1,8-diazabicyclo[5.4.0]undec-7-ene (DBU) tertiary amine in 1-hexanol and 1-propanol [7]. The mixture of amidine base and the alcohol reacts with CO_2 to form a high polarity ionic liquid with quaternary ammonium cations and alkylcarbonate anions. In our case, catalyst deactivation can be likewise due to the Lewis acid-base interaction between CO_2, polyol and tertiary amines (the catalytic species in the formulation under study). With reference to the dilution effect, a traditional physical chemistry description of such a reacting system would be of a diffusion-controlled one, where reactant molecules have to jostle their way through the solvent but, when in contact, stay near each other for much longer, in the so-called “cage effect”. In our case, the swelling induced by CO_2 sorption in the two phases (the polyol [10] and PMDI [11]) results in a decrease of reactant concentration and a corresponding decrease of reaction rate [25]. Here, we may speculate that both catalyst deactivation and dilution mechanisms are occurring concurrently, up to a complete saturation of the catalytic sites by CO_2 at 0.07 g/g in this specific case. At higher $\overline{w}_{CO_2}$, the sole diluting effect emerges. At $\overline{w}_{CO_2}$ below 0.07 g/g both mechanisms concur to the effect of $\overline{w}_{CO_2}$ on t_{c_NH}, linearly increasing with a slope of 990±39 min.g/g in the 0-0.07 range, while at larger $\overline{w}_{CO_2}$, catalyst deactivation mechanism fades due to saturation of catalytic sites by CO_2 and only the dilution effect is active, with a corresponding reduced slope of the t_{c_NH} vs. $\overline{w}_{CO_2}$ curve equal to 414±10 min.g/g.

To prove this hypothesis and to separate the catalyst deactivation effect from the dilution effect, further tests were performed on a polyol-PMDI formulation in which no catalyst were included. Obviously, in this case both t_{c_NCO} and t_{c_NH} are expected to increase with respect to the case of the formulation with the catalyst. Here, the effect of CO_2 on reaction kinetics would be solely due to the dilution effect, and should maintain a similar dependence of the high $\overline{w}_{CO_2}$ behavior of the catalyzed formulations. This is indeed the case, as reported in Figure 12, where a comparison is drawn between the catalyzed and non-catalyzed formulations, in terms of the effects of $\overline{w}_{CO_2}$ on t_{c_NCO} and t_{c_NH} (Figures12 a and b, respectively) (Table 5).

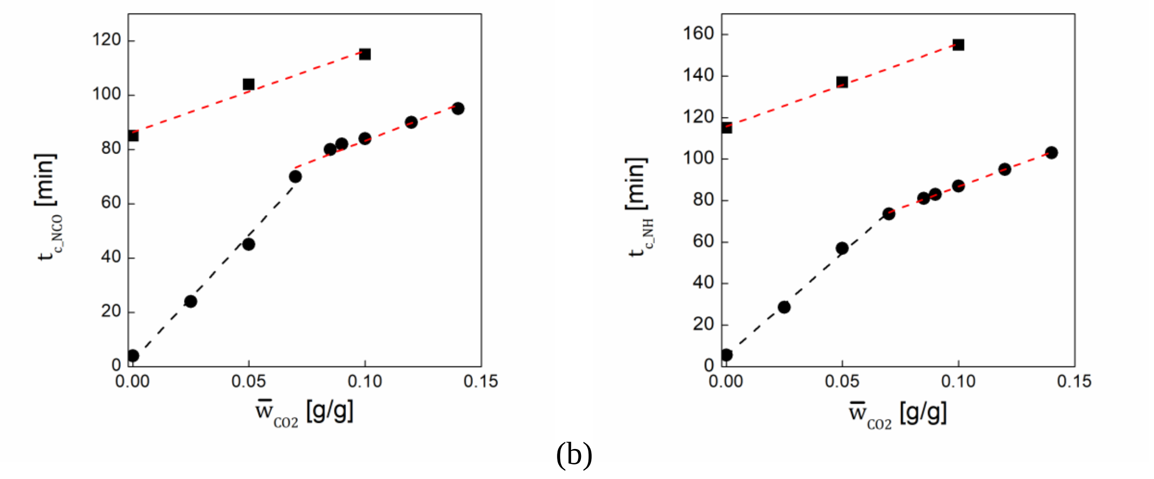

Figure 12. Effect of CO_2 on (a) t_{c_NCO} and (b) t_{c_NH}. Round and square symbols are experimental data for formulations with and no catalyst respectively, lines are only guide to the eye.

Table 5. Effect of CO_2 on t_{c_NCO} and t_{c_NH}: results of the fitting procedure.

P_{CO2} [MPa]	CO_2 sorption time [hours]	$\overline{w}_{CO2}$ [g/g]	t_{c_NCO} [min]	t_{c_NH} [min]
0	0	0	85	115
4	5	0.050	104	137
8	5	0.100	115	155

In the case of the non-catalyzed formulation, the slope of the t_{c_NCO} vs. $\overline{w}_{CO_2}$ curve is 300±46 min.g/g, while for the t_{c_NH} vs. $\overline{w}_{CO_2}$ curve it is 400±23 min.g/g. Of course, as there is no catalyst to deactivate, there is no threshold $\overline{w}_{CO_2}$ value, in this case. Comparison of the slopes of the formulation with catalysts above the catalyst deactivation critical value of $\overline{w}_{CO_2}$, equal to 330±40 and 414±10, respectively for t_{c_NCO} and t_{c_NH} seems a good proof of the proposed two concurring mechanisms. It is worth of note, here, that there was no foaming (by pressure quenching the PBA) during the curing reaction in order to suitably monitor the PU formation under CO_2 pressure. For this reason, after each curing kinetics experiment at several CO_2 pressures and 35°C, the sample was a compact PU product with high density (e.g. 550 kg/m^3).

3.4. References

[1] F. Stassin, R. Jérôme, Effect of pressure and temperature upon tin alkoxide-promoted ring-opening polymerisation of ε-caprolactone in supercritical carbon dioxide, Chem. Commun. (2002) 232-233.

[2] H. Tiltscher, H. Wolf, H. Schelchshorn, Utilization of Supercritical Fluid Solvent-Effects in Heterogeneous Catalysis, Ber. Bunsen Ges. Phys. Chem. 88 (1984) 897-900.

[3] P.G. Jessop, S.M. Mercer, D.J. Heldebrant, CO_2-triggered switchable solvents, surfactants, and other materials, Energy Environ. Sci. 5 (2012) 7240-7253.

[4] P.G. Jessop, D.J. Heldebrant, X. Li, C.A. Eckert, C.L. Liotta, Reversible nonpolar-to-polar solvent, Nature. 436 (2005) 1102.

[5] M.L. Pinto, L. Mafra, J.M. Guil, J. Pires, J. Rocha, Adsorption and Activation of CO_2 by Amine-Modified Nanoporous Materials Studied by Solid-State NMR and $^{13}CO_2$ Adsorption, Chem. Mater. 23 (2011) 1387-1395.

[6] P.N. Sutar, A. Jha, P.D. Vaidya, E.Y. Kenig, Secondary amines for CO_2 capture: A kinetic investigation using N-ethylmonoethanolamine, Chem. Eng. J. 207-208 (2012) 718-724.

[7] Y.G. Ko, S.S. Shin, U.S. Choi, Primary, secondary, and tertiary amines for CO_2 capture: Designing for mesoporous CO_2 adsorbents, J. Colloid Interface Sci. 361 (2011) 594-602.

[8] A. Furstner, G. Seldel, N. Kindler, Macrocycles by Ring-Closing-Metathesis, XI: Syntheses of (R)-(+)-Lasiodiplodin, Zeranol and Truncated Salicylihalamides, Tetrahedron. 55 (1999) 8215-8230.

[9] K. Wittmann, W. Wisniewski, R. Mynott, W. Leitner, C.L. Kranemann, T. Rische, P. Eilbracht, S. Kluwer, J. M. Ernsting, C. J. Elsevier, Supercritical Carbon Dioxide as Solvent and Temporary Protecting Group for Rhodium-Catalyzed Hydroaminomethylation, Chem. Eur. J. 7 (2001) 4584-4589.

[10] M.R. Di Caprio, G. Dal Poggetto, M.G. Pastore Carbone, E. Di Maio, S. Cavalca , V. Parenti, S. Iannace, Polyether polyol/CO_2 solutions: Solubility, mutual diffusivity, specific volume and interfacial tension by coupled gravimetry-Axisymmetric Drop Shape Analysis, Fluid Phase Equilib. 425 (2016) 342-350.

[11] M.R. Di Caprio, B. Immirzi, E. Di Maio, S. Cavalca, V. Parenti, S. Iannace, G. Mensitieri, Mass transport and physical properties of polymeric methylene diphenyl diisocyanate/CO_2 solutions, Fluid Phase Equilib. 456 (2018) 116-123.

[12] M.R. Di Caprio, D. Tammaro, E. Di Maio, S. Cavalca, V. Parenti, A. Fangareggi, S. Iannace, A pressure vessel for studying gas foaming of thermosetting polymers: sorption, synthesis and processing, Polym. Test. 62 (2017) 137-142.

[13] T. Guadagno, S.G. Kazarian, High-Pressure CO_2-Expanded Solvents: Simultaneous Measurement of CO_2 Sorption and Swelling of Liquid Polymers with in-Situ Near-IR Spectroscopy, J. Phys. Chem. 108 (2004) 13995-13999.

[14] J. Dupuy, S. Benali, A. Maazouz, G. Lachenal, D. Bertrand, FT-NIR monitoring of a scattering polyurethane manufactured by reaction injection molding (RIM): univariate and multivariate analysis versus kinetic predictions, Macromol. Symp. 184 (2002) 249-260.

[15] J. Crank, The Mathematics of diffusion, Oxford University Press, Bristol, England, 1975.

[16] C. Wenning, S. Barbe, D. Achten, A.M. Schmidt, M.C. Leimenstoll, Prediction of Initial Miscibility for Ternary Polyurethane Reaction Mixtures on Basis of Solubility Parameters and Flory-Huggins Theory, Macromol. Chem. Phys. 219 (2018) 1700544.

[17] M. Buback, J. Schweer, H. Tups, Near Infrared Absorption of Pure Carbon Dioxide up to 3100 bar and 500 k. I. Wavenumber Range 3200 cm^{-1} to 5600 cm^{-1}, Z. Naturforsch., A: Phys. Sci. 41 (1986) 505-511.

[18] P. La Manna, P. Musto, G. Galli, E. Martinelli, In Situ FT-IR Spectroscopy Investigation of the Water Sorption of Amphiphilic PDMS Crosslinked Networks, Macromol. Chem. Phys. 218 (2017) 1600585.

[19] C. M. Balik, On the Extraction of Diffusion Coefficients from Gravimetric Data for Sorption of Small Molecules by Polymer Thin Films, Macromol. 29 (1996) 3025-3029.

[20] D. Randall, S. Lee, The polyurethanes book, John Wiley & Sons, Inc., New Jersey, 2003.

[21] A.E. Venger, Y.E. Fraiman, F.B. Yurevich, Applicability of one-stage chemical reaction kinetic equation to describe non-isothermal destruction processes, J. Therm. Anal. 27 (1983) 325-331.

[22] G. Carotenuto, L. Nicolais, Kinetic study of phenolic resin cure by IR spectroscopy, J. Appl. Polym. Sci. 74 (1999) 2703-2715.

[23] G. Ragosta, M. Abbate, P. Musto, G. Scarinzi, Spectroscopic, Mechanical and Dynamic-Mechanical Studies on the Photo-Aging of a Tetrafunctional Epoxy Resin, Macromol. Symp. 286 (2009) 34-41.

[24] J.M. DeSimone, W. Tumas, Green chemistry using liquid and supercritical carbon dioxide, Oxford University Press, New York, 2003.

[25] P. Atkins, J. de Paula, Atkins' physical chemistry, eighth edition, Oxford university press, Oxford, England, 2006.

Chapter 4.

Matching the different timescales: rapid gas depressurization vs. slow curing reaction

In this chapter, it is presented a novel method by the gas-foaming technique. In particular, to tackle the inherent difficulties of imposing a rapid pressure quench O(10^{-2} s) to a material whose synthesis timing is much larger O(10^{2} s), a two-stage foaming was utilized. In the first stage, a rapid pressure quench O(10^{-2} s) from the saturation pressure to an intermediate pressure, was imposed to nucleate a large amount of bubbles; in the second stage, the growth of the nucleated bubble is controlled by slowly O(10^{2} s) decreasing the pressure to ambient pressure. In this way, by separating the nucleation from the growth stage and by chasing the synthesis reaction with the pressure to avoid excessive stress to the curing polymer, microcellular polyurethane foams were obtained. Moreover, a further section providing results of PUFs obtained with other physical blowing agents is also reported. This proves the viability of the aforementioned method with also other PU/blowing agent recipes.

Chapter 4. Matching the different timescales: rapid gas depressurization vs. slow curing reaction

4.1. Introduction

High-pressure CO_2 foaming proved very effective with thermoplastics. In this case, the low solubility at ambient pressure is exploited to induce foaming by pressure quenching the polymer/gas solution formed at high pressures. Here, first a suitable PBA (CO_2, but also N_2 and others) concentration is attained at high pressures O(10 MPa) (here. “O” standing for “order of magnitude”) in an extruder or in a pressure vessel, and subsequently a rapid O(10^{-2} s) pressure quench induces bubbles nucleation. The pressure drop rate (*PDR*) is the key to achieve a good morphology, as introduced in the '80s by the MIT group [1], and the number of bubbles nucleated per unit volume exponentially increase with the *PDR* [2]. In fact, with the pressure quench method, utmost performances in terms of cell number densities have been reached with numerous thermoplastic polymers: microcellular (cell size O(1-10 μm)) and, more recently, nanocellular (cell size O(1-100 nm)) foams have been produced, characterized by improved thermal insulating and mechanical properties as compared to standard cell-sized foams [3]. So far, thermosetting foams stay orders of magnitude behind, in terms of cell size, being typically O(100μm).

Because of the environmental concerns and of the encouraging performances in producing microcellular and nanocellular foams with thermoplastic polymers, high-pressure CO_2 foaming of PUs has attracted a growing industrial interest [4]. In this context, in 1972 Dow Chemical [5] introduced a process known as “frothing”, where CO_2 is delivered at moderate pressure yet at the mixing head of the foaming equipment to produce a stable and low-density foam. As CO_2 was delivered right before the mixing head exit, there was no chance to form a solution with the polymeric phases [6]. In this case, CO_2 was separated in a multitude of gas pockets by the mixing system, entrapped within the reacting medium, eventually remaining as bubbles in the solid PU. In this process, bubble size and morphology are dictated by the mixing power/efficiency and the (undesirable) coarsening process, and not by the *PDR* from a polymer/gas solution [7], as in thermoplastics, and not a big improvement in cell size was observed. The frothing process is still in use, after numerous improvements (see, for instance patents by Hennecke GmbH and Bayer AG [8] and Cannon Afros SpA [6]). Micro- and nano-emulsions [9,10] of dense CO_2 (at high pressure) with the polyol, stabilized by surfactants, have also been utilized to avail a fine-phase separated structure which, at pressure quench, brings to fine celled foams. In all of these cases, multi-phases systems with CO_2-rich phases were present. Until only very recently, no method was reported that includes the use of fully solubilized-CO_2 (single phase) in the polyol and/or the isocyanate and the exploitation of pressure quench to induce foaming (the so-called gas foaming method). Despite the opportunity to achieve fine morphologies and improved thermal properties (among others), in fact, two main problems arise in high-pressure gas foaming PU: i) the difficulty of conducting solubilization under pressure on two separate reacting species (that eventually have to get in contact, still, under pressure, for the synthesis) and ii) to impose a rapid pressure quench $O(10^{-2}$ s) on a reacting polymeric system that has been optimized, for decades, to be subjected to a blowing reaction concurrent to the synthesis reaction $O(10^{2}$ s). This mismatch of characteristic times constitutes the most critical difficulty and will be the focus of this chapter.

In this context, in 2019, Yang et al. [11] introduced a method to foam PU by high pressure CO_2 after a solubilization stage in the two reactants. They addressed the aforementioned two points as follows: i) in a batch pressure vessel, the two components of the PU formulation were kept separate by a polyethylene film, which eventually, after sorption, is broken by the mixer blades; ii) pressure quench was conducted after a certain reaction time, tuned to the viscosity of the reacting matter. Authors, in fact, found that a certain viscosity window was suitable for foaming by pressure quenching. As a matter of fact, this viscosity window exists in a region where the viscosity is quickly increasing, which can give repeatability problems and difficulties in scaling up at industrial level. From one hand, the cited study confirms the high scientific interest in this topic; from the other hand, the approach can be considered as a good starting point and a good comparison for the results reported in this chapter, as we moved forward.

4.2. Materials and methods

The method here described, essentially, copes with the two very different timescales of the pressure quench $O(10^{-2}$ s) and the synthesis reaction $O(10^{2}$ s) by separating the nucleation and growth stages in two different processing stages. The method has been successfully applied on an industrial PU formulation.

4.2.1. Materials

A polyether polyol (see Table 1 for details) and a polymeric methylene diphenyl diisocyanate (PMDI) (Table 2) were supplied by Dow Italia S.r.l. (Correggio, RE, Italy) and used “as received”. The catalysts introduced in the formulation were pentamethyldiethylenetriamine (PMDETA) and dimethylcyclohexylamine (DMCHA). High purity grade CO_2 (99.95% pure) was supplied by SOL (Naples, Italy). The formulation here reported is the same formulation described in *chapter 3*.

Table 1. Compositions of the polyether polyol.

Polyol formulation components	Functionality (f)	Molecular weight (Mw) (Da)	Parts (%)
Glycerin initiated	Low	1000	95
Amine initiated	High	500	
Sorbitol initiated	High	700	
Sucrose/glycerin initiated	High	500	
Catalysts	/	/	3
Surfactant	/	/	2

water is 0.2% wt; polydispersity index (PDI) is 1-1.5; viscosity = 15150 mPa.s (25°C); data from the supplier

Table 2. Properties of the PMDI.

Component	Equivalent weight	NCO content (%)	Functionality	Viscosity mPa.s (25°C)	Acidity as %HCl
PMDI	135	31.1	2.7	190	0.02

data from the supplier

4.2.2. Experimental setup

To perform the foaming attempt, the same pressure vessel described in *chapter 3* was utilized. In order to clarify the two different works described in *chapter 3* and *4* respectively, a brief overview of the overall stages taking place in the processing procedure is reported. The equipment is designed to meet the requirements for:

1. allowing PBA sorption at high-pressure and moderate temperature for long time (tens of hours);
2. keeping separate the two reactants for same long time during sorption - O(10^3 s);
3. mixing the two PBA-laden reactants - O(10^1 s);
4. allowing partial curing - O(10^1 - 10^2 s);
5. allowing fast and controlled PBA release for foaming - O(10^{-3} - 10^{-2} s);
6. allowing curing to go to completion - O(10^2 s);
7. NIR-monitoring all (but No. 5) of the above stages.

Figure 1a reports a 3D rendering of the proposed pressure vessel and images of the equipment in two configurations. With respect to the original configuration described in *chapter 3* (see Figure 1b), to apply a partial pressure quench, a gas tank was added to the evacuation system (see Figure 1c).

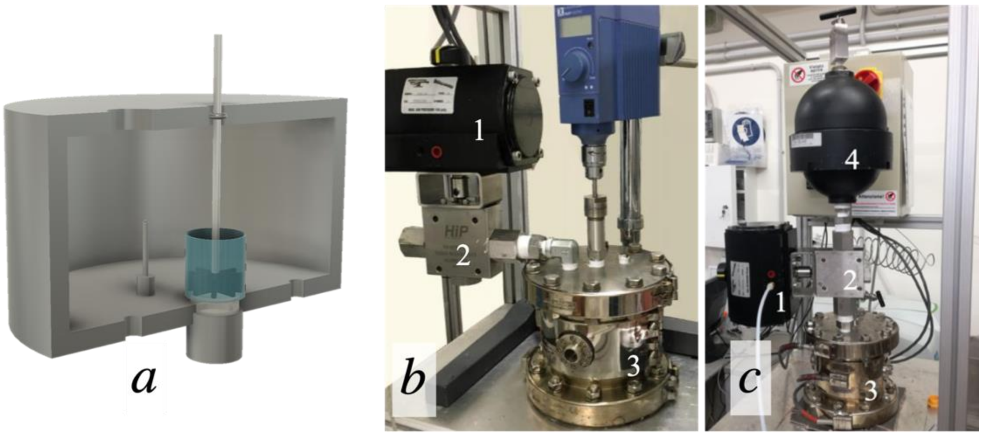

Figure 1. Equipment utilized to perform the foaming tests. (a) 3D scheme showing a cut of the pressure vessel with the sample holder and the mixing shaft. (b) picture of the equipment in the original configuration reported in *chapter 3*: actuator (No. 1 in the image) for the ball-valve (2); pressure vessel (3). (c) upgraded configuration with a gas tank (4), to evacuate the pressure vessel to an intermediate pressure.

In a typical foaming attempt, the two components of the PU formulation, polyol and PMDI are loaded in the cylindrical sample holder (kept separate by the rubbery impeller), and subjected, at 35°C, to a CO_2 pressure ranging from 2.0 to 10.0 MPa. After a defined sorption time, necessary to achieve the desired average CO_2 mass fraction in the total formulation, $\overline{w}_{CO_2}$, as already described also in *chapter 3,* the impeller is put in rotation, and the reactants are allowed to get into intimate contact for the curing reaction to start. Here, it is worth of note that before testing the two-step depressurization method, one-step depressurization method was first utilized, as it will be also described in the next sections. In a different way described in the previous chapter, then, at a certain degree of curing, the actuated ball valve is opened for pressure quench, O(10^{-3} -10^{-2} s) to ambient pressure (one-step depressurization method, configuration in Figure 1b) or to a low, intermediate pressure by evacuating the pressure of the pressure vessel into a known volume tank (two-step depressurization method, configuration in Figure 1c). In the latter case, by using the valve on top of the gas tank, the pressure is eventually brought to ambient (second depressurization) after an additional curing period and at a defined rate, with a characteristic time O(10^2 s). The foamed samples are finally extracted from the sample holder for the characterization.

4.2.3. Foam characterization

Density measurements were performed according to ASTM D792 [12], using an analytical balance (Mettler Toledo, Columbus, OH). The cellular structure of the foams was investigated by using a scanning electron microscope (S440, LEICA). The samples were first sectioned with a razor blade and then coated with gold using a sputter coater. The average cell size (*ACS*) was evaluated according to ASTM D3576-15 standard test method by using an image analysis software (ImageJ). The intersections method has been used in order to evaluate the cell size. Lines in two perpendicular directions (*m* vertical lines of length *h* and *n* horizontal lines of length *l*) are taken in order to make a grid. The grid is overlaid in each micrograph and, for each line, the number of cells intercepted is counted and the line length (*h* or *l*) is divided by the number of cells.

$$ACS = \frac{\sum_{i=1}^{m} ACS_i + \sum_{j=1}^{n} ACS_j}{m + n} \qquad (1)$$

As this chapter deals with a deep insight into the aforementioned method focusing on the cell size reduction of the foams, it is worth of note that no characterization about the thermal conductivity of the obtained PU foams is reported at the current state of this experimental work. Given the actual dimensions of the samples obtained by the aforementioned method (2 cm in diameter and between 2 cm and 3 cm in height), it was not possible to obtain suitable samples that allowed this measurement. However, besides the aims of this chapter, additional foams (with suitable dimensions) will be obtained in a larger pilot plant in order to measure their thermal conductivity.

4.3. Results and Discussion

4.3.1. One-stage foaming

The first attempts to foam the reacting PU formulation were based on the idea that, within the PU curing reaction time O(10^2s), it is in principle possible to guess the *optimal* degree of curing (X - as it is formally defined in the *appendix to chapter 4* by Equation 5, here not reported with the aim of preserving the fluency of the chapter to the reader), and, hence, an optimal polymer viscosity suitable to tolerate the pressure quench, which has to be fast enough to generate a high number of bubbles O(10^{-2}s). At lower X, in fact, the polymer is too weak (low viscosity and low strength) to withstand the large elongational stresses exerted by the polymer confined among the growing bubbles. As a consequence, a pressure quench would induce bubble formation (by the evolution of the BA solubilized under pressure), followed by an intense coalescence and collapse of the structure: an awful, useless foam. From the other side, at higher X the polymer is too rigid and viscous, and, at pressure quench, the gas pressure is not enough to inflate the bubbles, giving a minimal expansion and, again, a useless foam. At intermediate, optimal X, a reasonably low density and fine morphology foam could be expected. A scheme of the one-stage foaming method is reported in Figure 2a. In the scheme, qualitative pressure and curing degree vs. time curves are reported, together with boxes depicting the status of the multi-phase system. The color maps represent the curing degree (pink = low degree of curing, brown = high degree of curing) and the density of the gas contained in the bubbles (blue = high gas density; white = low gas density). In "0", at p_{sat}, the two solutions were just mixed, and the degree of curing is null, the box describes this early stage of curing, with the dense CO_2 solubilized in the polymeric matrix. From "0" to "1" the pressure is maintained at p_{sat} and the reaction proceeds (the boxes color shift to brown, still with dense CO_2 in solution). In "2" the pressure has just been quenched to p_{amb} and the bubbles nucleate and growth, until final curing is attained in "3". In these latter stages ("2" and "3"), gas density is minimal (white color of the bubbles), as the pressure is p_{amb}.

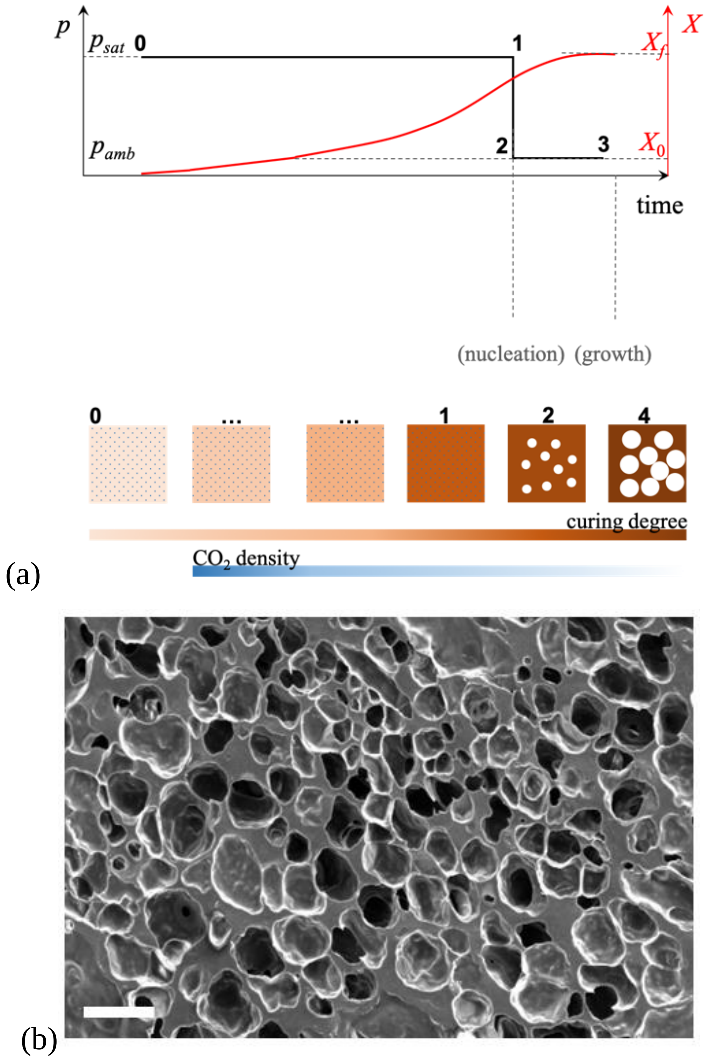

Figure 2. One-stage foaming method: a) scheme of the method; b) SEM micrograph of PU foam. Scale bar is 100 µm.

This one-stage foaming approach of inducing a pressure quench on a sufficiently viscous system was reported in 2019 by Yang et al. [11]. In particular, authors performed in-situ viscosity measurements during the curing process to investigate PU polymerization under high-pressure CO_2. As also described in *chapter 3*, authors observed that the presence of high-pressure CO_2 significantly delayed the viscosity rise characteristic of the PU synthesis. As a consequence, longer times were required for the curing reaction when CO_2 was dissolved within the PU reactants, to attain the same viscosity of the neat formulation. In-situ viscosity measurements allowed to determine suitable foaming windows for the pressure quenching and PUs with good expansion ratios as well as fine cell size were obtained [11].

Likewise, a series of experiments were herein carried out to achieve a suitable degree of curing to sustain the pressure quench. In fact, numerous foaming attempts failed, proving the difficulty to achieve a homogeneous foam morphology with a low-enough density. In this series of experiments, the reactants were kept separate under CO_2 for 3 hours at 35°C and 6 MPa for sorption and then mixed and cured for 3.7 minutes. After the curing stage, the system was pressure quenched to ambient pressure at 40 MPa/s. Figure 2b reports the scanning electron micrographs of a PU porous solid (not even a foam!) achieved by one-stage foaming: non-uniform cell size distributions in the range of 20-80 µm and densities around 600 kg/m^3 were obtained.

The impossibility to achieve a fine celled, low-density foams by one-stage foaming persuaded us to derive a new method. The main issue with one-stage foaming was, to our point of view, the very different timescales between reaction time, $O(10^2 s)$, and pressure quench, $O(10^{-2} s)$, and, more generally, the underlying idea to overturn the decades of development of PU foaming, that has brought to "a chemistry" optimized for the foaming reaction to be concurrent to the curing one, both taking $O(10^2 s)$. The 4-orders of magnitude difference between curing time and pressure quench time and the failed one-stage attempts was the key point to develop a new strategy.

4.3.2. Two-stage foaming

The two needs of i) imposing a fast pressure quench and ii) allowing the relatively slow curing, brought to the introduction of a two-stage foaming. Two-stage foaming was already utilized in thermoplastic foaming, e.g. to achieve bi-modal pore morphologies where the holding stage between two depressurization steps allowed the formation of the bi-modal cell structure development [13]. The main idea under the present two-stage method is to separate bubble nucleation from bubble growth, allow the two phenomena following two different timescales, $O(10^{-2} s)$ and $O(10^2 s)$, and, hence, controlling the bubble growth to be concurrent to viscosity evolution. In particular, in the first stage, bubble nucleation is promoted by fast pressure quenching (as fast as possible, considering the specific equipment) the reacting mixture from the saturation pressure, p_{sat}, to a low, intermediate pressure, p' (higher than ambient pressure, p_{amb}). In this stage, hence, a large number density of bubbles is formed, which partially grow in volume up to a certain limit, as their volume growth is restricted by the pressure. In fact, as p' is higher (O(0.5-1 MPa)) than p_{amb}, the gas contained in the cells has a relatively high density and is "stored" in the bubbles, available for the following growth, when pressure will be afterward brought to ambient. The limited cell growth will prevent cell coalescence, as small bubbles are separated by relatively thick walls. Secondly, pressure is slowly O(10^2s) reduced to p_{amb}. In this stage, bubbles' volume will increase due to the pressure reduction of the gas mass contained within the bubbles. In fact, a small amount of gas is still solubilized in the curing matter at p', and is de-sorbed with the pressure reduction, further contributing to the growth. It is worth of note that, as the CO_2 solubilized in the polymer affects the synthesis reaction kinetics, the external pressure control has an effect on the reaction kinetics, and this effect has to be taken into account to the purpose of accurately designing the foaming process. We may describe this method as "chasing the synthesis reaction with the pressure" (*reactionem pressione urgēre*), intending the use of external gas pressure to control expansion of the gas contained in the bubbles, while the curing reaction is running. This method is schematically shown in Figure 3. Here, as in Figure 2a, qualitative pressure and curing degree vs. time curves are reported, together with boxes depicting the status of the multi-phase system. The color maps represent the curing degree (pink = low degree of curing, brown = high degree of curing) and the density of the gas contained in the bubbles (blue = high gas density; white = low gas density). The initial system is composed by the polyol/CO_2 and the isocyanate/CO_2 solutions, containing an average $\overline{w}_{CO_2}$, at p_{sat}, just mixed to initiate the curing reaction ($X_0 = 0$; "0" in Figure 3, and corresponding pink-colored square with high-pressure - dense-CO_2 in solution). The curing reaction is conducted for a certain period, t_{0-1} (up to "1"), under p_{sat} in the stage I, after which the pressure is quenched at high *PDR* to p' ("2"), to nucleate bubbles. After a certain period (t_{2-3}) at p', where the degree of curing reaches X' ("3"), the pressure is allowed to slowly decrease to p_{amb} (4) and, concurrently, the curing reaction continues to completion ($X = X_f$). To evidence the use of gas density to control the growth, bubbles in the boxes in Figure 3 have colors fading from blue to white, from "3 to "4".

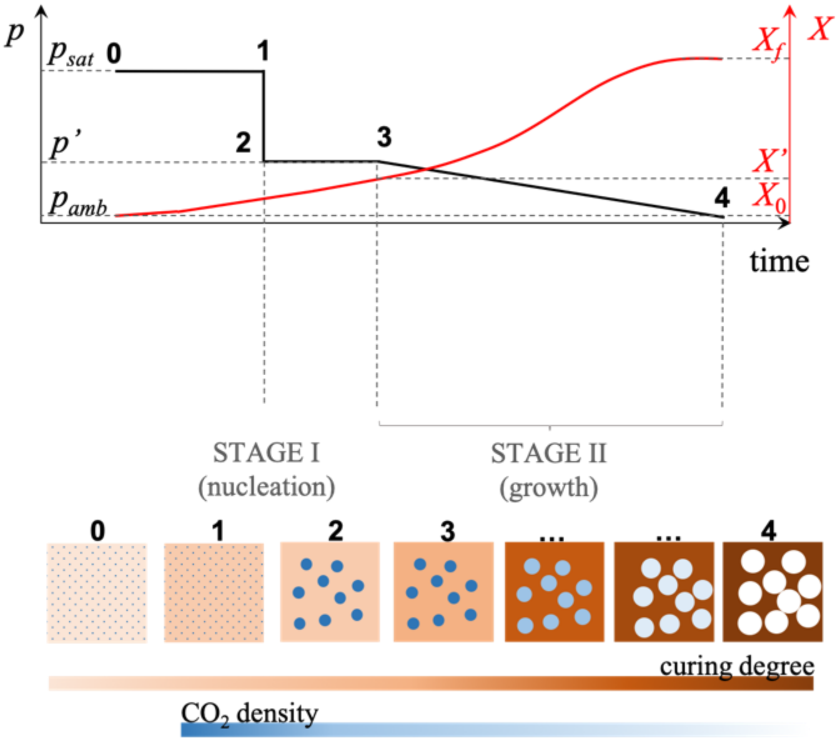

Figure 3. Scheme of the two-stage foaming method.

In fact, it is possible to design the pressure drop history in the stage II (path 3-4 in Figure 3) to attain X_f in the very moment when pressure equals ambient pressure, starting from X' and p'. As a proof of concept, and as it is also simpler to apply to an equipment, we may, for example, linearly decrease pressure (applying a constant pressure drop rate, $\dot{p}$). The evaluation procedure to estimate the value of $\dot{p}$ to be applied, given X', X_f and p' is detailly reported in the appendix to *chapter 4* at the end of this thesis. To include the experimentally observed effect of the $\bar{w}_{CO_2}$ on the curing kinetics, we assumed that, during the slow pressure release, the dissolved CO_2 concentration is spatial uniform and dictated by the phase equilibrium with the gas phase in contact with the liquid reacting mixture and that the following form can be used, at constant temperature (see appendix to chapter 4 for variables definitions):

$$X(t) = 1 - e^{-A\, e^{-(B\bar{w}_{CO_2})}t} \tag{2}$$

In a more general case, the pressure drop rate, $\dot{p}$, that has to be imposed to the system during the second depressurization stage, here, defined as $|\dot{p}|$ (see appendix to *chapter 4* for details on this definition), to achieve the desired X_f when $p = p_f$, reads:

$$|\dot{p}| = \frac{A}{B\ H} \frac{\left(e^{-B\ H\ p_f} - e^{-B\ H\ p'}\right)}{ln\left(\frac{1-X'}{1-X_f}\right)} \tag{3.a}$$

In the case of interest in the work reported in this chapter, since $p_f = 0$ (approximation reasonable in such a case for the ambient CO$_2$, when the pressure vessel is exposed to ambient at valve opening, see appendix to *chapter 4*) the Equation (3.a) collapses to:

$$|\dot{p}| = \frac{A}{B\ H} \frac{\left(1 - e^{-B\ H\ p'}\right)}{ln\left(\frac{1-X'}{1-X_f}\right)} \tag{3.b}$$

Where H is the Henry constant for CO$_2$ in the averaged polymeric matter [17]. In particular, Equation 3.b describes the effect of the reaction rate parameters, A and B in Equation 2, the Henry constant, H, the initial conditions (p', X') and the desired X_f on $\dot{p}$. The parameters A and BH represent the reaction rate without CO$_2$ (at ambient pressure) and the way CO$_2$ slows down the curing reaction, respectively. Equation 3.b shows that $\dot{p}$ is governed by A/BH and BHp', which can be utilized to optimize the aforementioned processing variables to achieve a desired foam. Figure 4 reports the $\dot{p}$ as a function of X' and p', at X_f = 0.90, 0.95 or 0.99.

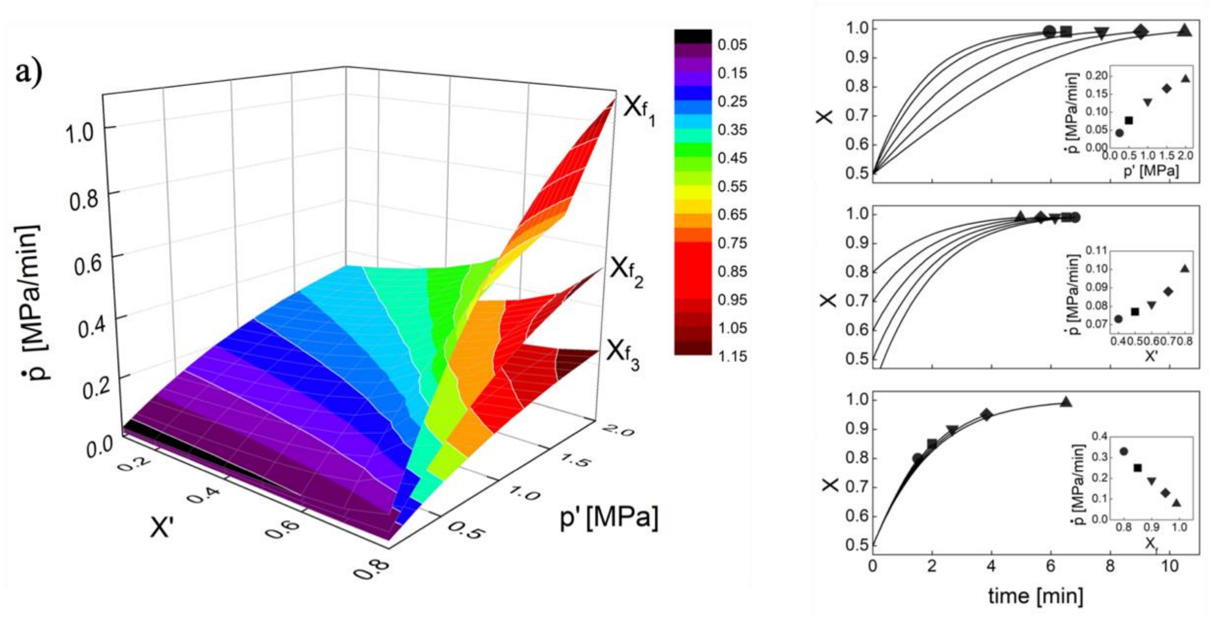

Figure 4. Design criterion of the second foaming stage as by Eq. (3.b). a) ṗ as a function of the initial conditions p' and X' at different $X_{f_1} = 0.90$, $X_{f_2} = 0.95$ and $X_{f_3} = 0.99$; b), c) and d) $X(t)$ as a function of the initial conditions (p' and X') and the final condition, X_f; b) effect of p' ($X' = 0.50$ and $X_f = 0.99$); c) effect of X' ($p' = 0.5\ MPa$ and $X_f = 0.99$); d) effect of X_f ($p' = 0.5\ MPa$ and $X' = 0.50$). Insets report $\dot{p}$ as a function of p', X' and X_f.

As it could be expected, $\dot{p}$ increases with p', as the larger is p', the larger is the distance to p_{amb} . $\dot{p}$ also increases with X', as, starting from the same p', larger X' means a minor distance from the desired X_f, and lower reaction time for this latter stage. Finally, $\dot{p}$ decreases with X_f, as higher final curing degrees are reached more slowly, ceteris paribus. The effect of each variable (X', p', and X_f) on the curing rate (in stage II) is reported in Figures 4b-d.

These calculations allowed us to design the process and conduct the two-stage foaming experimental campaign. Figure 5 reports the SEM images of three foams produced as by the processing program detailed in Table 3. In particular, PUFs were produced after solubilization at 4.0, 5.0 or 6.0 MPa, then pressure quenched after 3.7 minutes from mixing the two high-pressure polyol/CO_2 and isocyanate/CO_2 solutions to 0.35, 0.46 or 0.70 MPa, respectively. The reacting system is kept at said pressure for 3 minutes and finally brought to ambient pressure at a $\dot{p}$ calculated by Equation 2b. The processing steps for the three different procedures brought the system at a X' equal to 0.92, 0.86 and 0.79, respectively. The values of $\dot{p}$ given by Equation 3.b to bring the systems to ambient pressure and X_f were, respectively, 0.10, 0.11 and 0.13 MPa/min (see Figure 5a, b and c, respectively). As it can be observed in Figure 5, uniform cell distributions with *ACSs* in the range 20-50 µm and final foam density in the range 150-240 kg/m^3 were achieved. By comparing results reported in Figure 5 and Table 3, achieved by two-step foaming with those gathered by the use of one-step foaming (see Figure 2) it is possible to appreciate the value of the two-stage method in achieving medium to low-densities foams with uniform morphologies. The available processing parameter, having fixed the polyol/isocyanate system (and, therefore, also *A*, *B* and *H* in Equation 2b, solely dependent on the formulation and the interaction with CO_2), are:

- the average amount of CO_2 in the solutions' mixture;
- the CO_2 pressure (p_{sat});
- the reaction time at high pressure (t_{0-1});
- the intermediate pressure value after pressure quench (p');
- the pressure drop rate (from p_{sat} to p');
- the reaction time at intermediate pressure (t_{2-3}).

In fact, the pressure reduction rate from p' to ambient pressure cannot be considered a processing variable, as it is fixed by former parameters and is calculated by Equation 3.b. Similarly, the degree of curing, X', is a result of the processing history and cannot be considered a processing parameter. Furthermore, use of Equation 3.b may help selecting the most suitable polyol/isocyanate system, as it was shown that $\dot{p}$ is governed by the groups A/BH and BHp'. The numerous processing parameters as well as the features of the polyol/isocyanate system at play in the two-stage method allow for process optimization and for fine tuning the foam performance to the specific application.

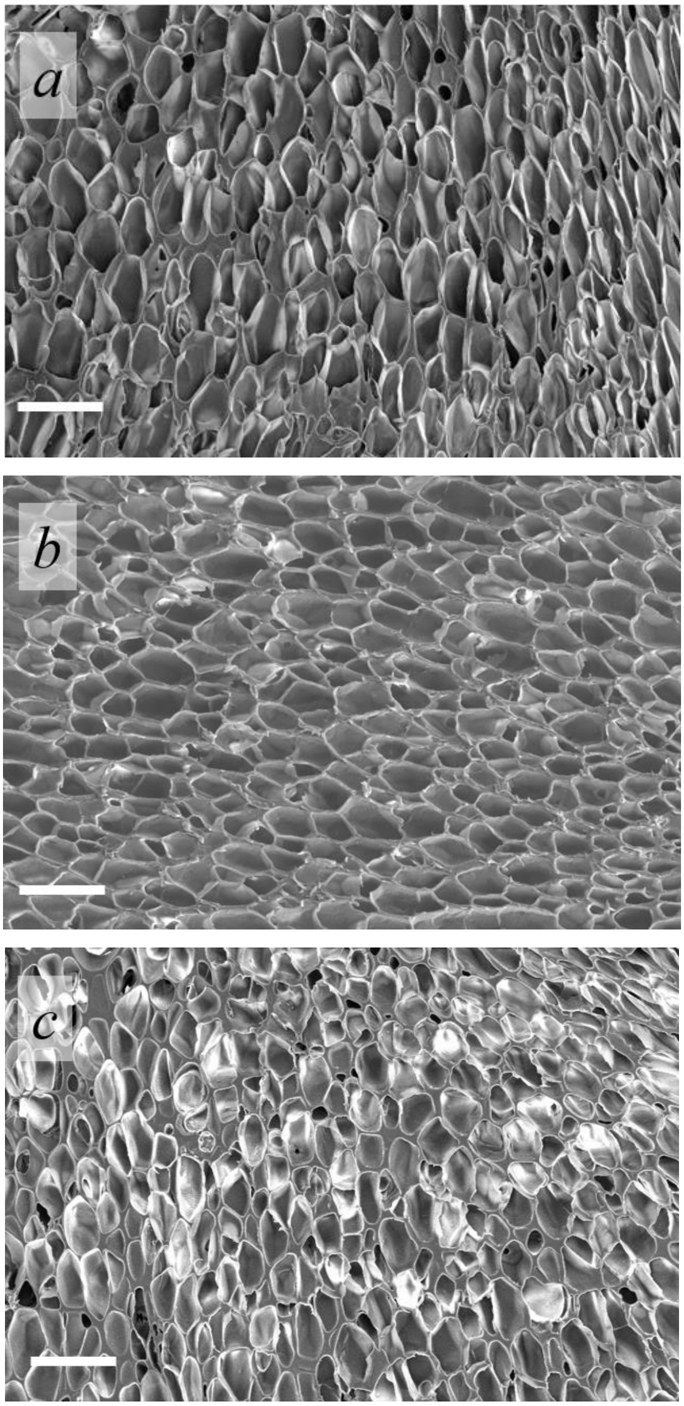

Figure 5. Results of two-stage foaming attempts: SEM micrographs of PU samples. Scale bar is 100 µm.

Table 3. Processing program and features of the achieved foams in one-stage (sample I) and two-stage foaming (samples a, b and c).

	Stage 0-1		Stage 2-3		Stage 3-4				
Sample	p_{sat} [MPa]	t_{0-1} [min]	p' [MPa]	t_{2-3} [min]	X'	X_f	$\dot{p}$ [MPa/min]	ACS [μm]	Density [kg/m^3]
I	6.0	3.7	/	/	/	/	/	20-80	600
a	4.0	3.7	0.35	3	0.92	0.99	0.10	20	150
b	5.0	3.7	0.46	3	0.86	0.99	0.11	43	200
c	6.0	3.7	0.70	3	0.79	0.99	0.13	50	240

4.3.3. Implementing the two-step foaming strategy with other PBAs

In this case, the same two-step pressure quench method was utilized by using N_2 and N_2/CO_2 80-20 vol/vol mixture as well. As reported in the literature [14], an optimization tool for the PBA foaming is represented by the BA recipe. In particular, N_2 is typically utilized to decrease the cell size, with the disadvantage of reduced solubility and, hence, higher densities with respect to CO_2. A proper mixture of the two can be therefore utilized to further tune foaming. Moreover, in order to obtain a suitable comparison with CO_2-blown PUFs, CO_2 as PBA only was used once again with same experimental conditions. Figure 6 reports the SEM images of three foams produced with neat CO_2, neat N_2 and with a N_2/CO_2 80/20 vol/vol mixture, as PBAs. Following the same procedure described in the previous section, in a typical foaming attempt, polyol and PMDI are loaded in a cylindrical sample holder, kept separate by a rubbery impeller to avoid premature curing, and subjected, at 35°C, to a CO_2, N_2 or a N_2/CO_2 80-20 vol/vol mixture saturation pressure, p_{sat}, of 6, 12 or 15 MPa, respectively. After a defined sorption time (3 hours), necessary to achieve the desired PBA sorption level, the impeller is put in rotation, and the reactants are allowed to get into intimate contact for the curing reaction to start. Then, at a certain degree of curing attained after 12 minutes (common to all of the PBAs), an actuated ball valve is opened for the pressure quench with a characteristic time O(10^{-3} -10^{-2} s) to a low, intermediate pressure, p' = 0.67, 1.58 and 1.25 MPa, respectively, by evacuating the pressure of the pressure vessel into a known volume tank (*foaming stage* I). After a certain degree of curing, X', at p' for 3 minutes, the pressure is eventually brought to ambient, p_{amb}, at a rate of = 0.10, 0.20, 0.15 MPa/min, respectively (*foaming stage* II), when the curing has attained completion. The foamed samples are finally extracted from the sample holder for characterization. It is worth of note that, in the previous section, it was reported a model to calculate the pressure drop rate, $|\dot{p}|$ of the second stage to get from p' to p_{amb} exactly when curing attains completion, known the other processing parameters, the solubilities and the (retarding) effect of the PBA on the curing reaction rate. Here, as a first attempt to utilize the two-stage foaming method with other PBAs as well, the same $|\dot{p}|$ calculated from foaming experiments carried out with CO_2 was utilized.

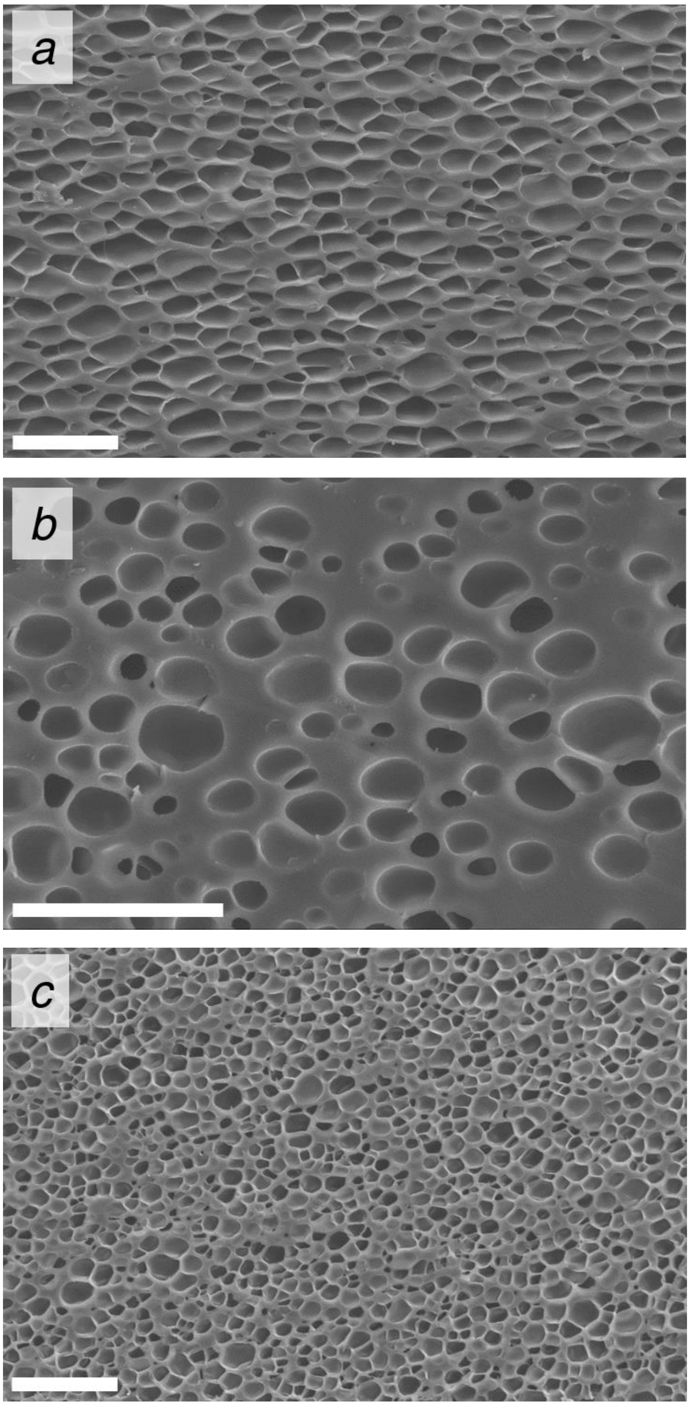

Figure 6. SEM micrographs of foamed samples: a) CO_2, b) N_2 and c) N_2/CO_2 80/20 vol/vol mixture. Scale bars are 20 µm.

As it may be observed from the SEM pictures, extremely fine morphologies were achieved, with the expected effect of the PBA composition. In fact, as depicted in Figure 7 reporting the features of the achieved foams, the PBA mixture behavior is intermediate between CO_2 and N_2. For instance, CO_2, with a relatively high solubility in the two precursors even at moderate pressure of 6 MPa (p_{sat}), gave a low-density foam, with *ACS* of ca. 10 μm.

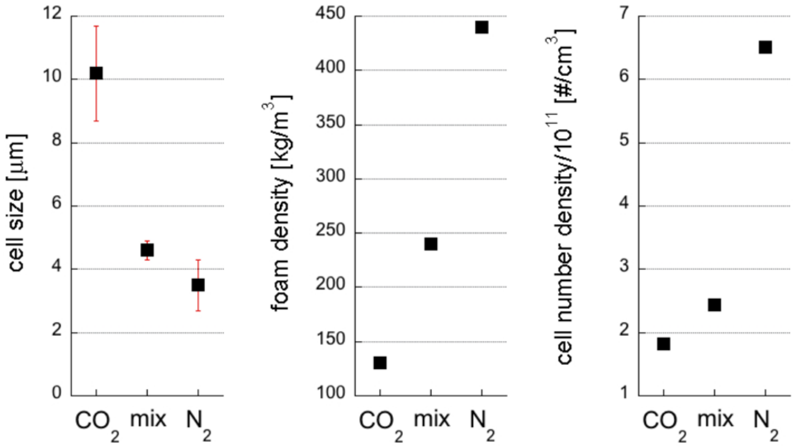

Figure 7. Features of the achieved foams with CO_2, N_2 and N_2/CO_2 80/20 vol/vol mixture.

Use of neat N_2 required the use of much larger p_{sat} to attain reasonable density reduction. However, extremely small average cell size of 3.5 μm was achieved in this case. Finally, the use of a N_2/CO_2 80/20 vol/vol mixture allowed to obtain a compromise between density reduction and cell size reduction. The observed cell number density values $O(10^{11}\ \#/cm^3)$ (Figure 7), in effect, are much larger than those typically observed in PU $O(10^6\ \#/cm^3)$, proving that: i) a large number of cells were successfully nucleated in the first stage of the process; ii) those cells were kept sufficiently small and far apart from each other by p' to hinder premature coalescence and iii) the pressure reduction rate of the second stage is sufficiently fast to allow for proper expansion and sufficiently slow to avoid cell coalescence.

4.4. References

[1] C. B. Park, D. F. Baldwin, N. P. Suh, Effect of the pressure drop rate on cell nucleation in continuous processing of microcellular polymers, Polym. Eng. Sci. 35 (1995) 432-440.

[2] D. Tammaro, A. Astarita, E. Di Maio, S. Iannace, Polystyrene Foaming at High Pressure Drop Rates, Ind. Eng. Chem. Res. 55 (2016) 5696-5701.

[3] S. Costeux, CO_2-Blown Nanocellular Foams, J. Appl. Polym. Sci. 131 (2014) 23.

[4] Dow Italia S.r.l., LIFE 13 ENV/IT/001238 http://ec.europa.eu/environment/life/project/Projects/index.cfm?fuseaction=search.dspPage&n_proj_id=5077.

[5] B. Barron, J. Dunlap , Air frothed polyurethane foams, US Patent US3821130A, 1972.

[6] C. Fiorentini, A. C. M. Griffiths, Froth process for continous manufacture of polyurethane foam slab-stocks, US Patent US5665287A, 1993.

[7] E. Di Maio, E. Kiran, Foaming of polymers with supercritical fluids and perspectives on the current knowledge gaps and challenges, J. Supercrit. Fluids 134 (2018) 157-166.

[8] R. Eiben, W. Ebeling, H. M. Sulzbach, R. Raffel , Method and device for the production of foam using carbon dioxide dissolved under pressure, US Patent US5883143A, 1998.

[9] S. Lindner, W. Friederichs, R. Strey, T. Sottmann, E. Khazova, L. Kramer, V. Dahl, A. Chalbi , Process for producing a polyurethane foam by means of supercritical or near-critical blowing agent. US Patent US9139683B2, 2009.

[10] M. Fricke, M. Schütte, T. M. Staudt, C. Holtze, S. Koch, F. Bartels, Micro-emulsions, WIPO (PCT) Patent WO2013026813A1, 2011.

[11] Z. Yang, T. Liu, D. Hu, Z. Xu, L. Zhao, Foaming window for preparation of microcellular rigid polyurethanes using supercritical carbon dioxide as blowing agent, J. Supercrit. Fluids 147 (2019) 254-262.

[12] ASTM D792: Standard Test Methods for Density and Specific Gravity (Relative Density) of Plastics by Displacement.

[13] J. B. Bao, T. Liu, L. Zhao, G.-H. Hu, A two-step depressurization batch process for the formation of bi-modal cell structure polystyrene foams using $scCO_2$, J. Supercrit. Fluids, 55 (2011) 1104-1114.

[14] E. Di Maio, G. Mensitieri, S. Iannace, L. Nicolais, W. Li, R. W. Flumerfelt, Structure optimization of polycaprolactone foams by using mixtures of CO_2 and N_2 as blowing agents, Polym. Eng. Sci. 45 (2005) 432-441.

PART III:
Polyurethane foams by liquid OFAs

Chapter 5.

Competing bubble formation mechanisms during the foaming process

In this chapter, it is reported the investigation of the influence of air bubbles inclusion on the rigid polyurethane and polyisocyanurate foaming process. It was observed that, when a large number of air bubbles was included in the reacting system during the mixing stage at high stirring velocity, no further bubble nucleation from water and pentane occurred, and foam morphology was dictated by the mixing stage and later bubble coarsening. Instead, when stirring velocity was low and no air bubble formed during mixing, nucleation of new bubbles from water and pentane was observed. Furthermore, both bubble coalescence and Ostwald Ripening were observed as the mechanisms responsible for the foam morphology coarsening, the latter being less effective in the case of polyisocyanurate foams.

Chapter 5. Competing bubble formation mechanisms during the foaming process

5.1. Introduction

PU and PIR properties of interest in the respective application fields are, among others, as thermal conductivity, compression strength, density, acoustic absorption, dimensional stability, fire properties and adhesion. These are tightly related to the foam density and morphology (e.g., the cell size distribution, the open/closed feature and the polymer fraction in the struts and in the walls) and, to the aim of controlling properties, it is key to assess the governing mechanisms in the morphology evolution, both at the early stages, where bubble form and at the later stages, when they grow, impinge and possibly merge into each other, thereby inducing a morphology coarsening. Here, in the context of this chapter, bubble formation mechanisms are *aeration* and *nucleation*.

In aeration, also referred to as mechanical foaming or frothing, the gas, most commonly air, is dispersed into the starting reactants by vigorous agitation, which leaves air bubbles entrapped within the polymeric matrix [1]. This method is popular in food [2], for example it is utilized in cream whipping, but also in polymers, like in the Dunlop process for natural rubber latex foams [3] and, of course, in PUFs. In nucleation, as widely described in *chapter 2* [4], gas bubbles form from a liquid/gas solution when the latter is supersaturated (i.e.: gas concentration is larger than its solubility at same temperature and pressure). Here, the driving force for the nucleation of bubbles is the gain in the volumetric Gibbs energy associated with the transition from the old phase (supersaturated liquid/gas solution) to the new phase (liquid and gas bubbles) [4]. Aeration and nucleation may, here, be considered as competitive mechanisms: if air bubbles are already present in the reacting system, homogeneous CO_2 and PBA nucleation should be hindered, depending also on the amount of available air bubbles.

Once new bubbles formed (by aeration and/or nucleation) followed by their growth, foam morphology degeneration may occur by coalescence and/or Ostwald Ripening (OR). Coalescence is the process by which two bubbles approach each other (impingement) and, when the film thickness separating them reaches a critical value, it breaks, the bubbles become one [5]. OR consists of a mass transfer mechanism involving two close bubbles of different size: due to the different Laplace pressures, the gas diffuses through the polymer from the smaller bubble to the larger bubbles, deflating the smaller bubble until it disappears [5].

In this context, it is very important to avail tools to measure and appreciate the different mechanisms at play, to understand the governing factors, in turn to design efficiently new products and technologies. A few attempts have been performed by microscopic techniques in order to study which mechanisms taking place during the PU foaming process are responsible for final morphology of the PU foam. Baumhäkel [6] in 1972 studied the influence of stirring velocity and air loading on the formation of water-blown flexible PUFs in an open container. It was observed that the agitator speed and, as a consequence, the amount of air bubbles introduced into the system, had a great influence on the production of flexible PU. The authors developed a model suitable to describe the interrelationships between the gas loading and the reaction kinetics of the resulting foams. Finally, it was concluded that the air bubbles introduced into the system by the mixing process accounted for all the cells present in the final foam. However, this study was conducted by meaning of an *ex-situ* technique. Only the final PU samples were characterized without a direct observation of the foaming mechanisms. It is in 2000 with Minogue [7] that the cell structure evolution with time was *in-situ* monitored by meaning of a PC-controlled camera connected to a stereo optical microscope. In this case, the effect of several parameters such as the amount of catalyst, the surfactant and the type of BA on the foaming process were studied. In particular, it was observed that H_2O (CBA) concentration did not affect the amount and the size of bubbles during the foaming process and that increasing the amount of cyclopentane (PBA) led to an increase of the average bubble size. While these results represent an initial study on how the type and the amount of BA may affect the bubbles growth, however, no clarification was given about if these bubbles were air bubbles formed by the mechanical agitation of the PU reactants or bubbles originated by the nucleation of the BA molecules. More recently, in 2012, Pardo-Alonso et al. [8] used high-resolution microfocus X-ray radioscopy to investigate the nanoclays effect on the nucleation and coalescence mechanisms taking place in a small droplet (used to limit the number of cells at 2-3 maximum in the depth direction). Using this technique in combination with image analysis (IA) it has been possible to in-situ monitor the foaming process from the beginning of the PU expansion. The authors observed that the introduction of nanoclays into the PU reacting mixture could induce a strong nucleation at initial foaming stage dominating on the cell coalescence (not even observed). These results give an interesting point on how these additives may influence the foaming mechanisms but, however, the study on the competition between the bubble formation mechanisms such as aeration and nucleation were not explored. It is worth of mention here, the work conducted in 2019, by Reignier et al [9] in which the morphology evolution of rigid PU was followed by cryogenic scanning electron microscopy (cryo-SEM). The authors observed that the presence of sub-micron size cavities within the initial reaction mixture is attributable to liquid isopentane droplets which remain partly dispersed (not solubilized) in the polymeric phase and diffuse into the air bubbles (introduced by mixing step) rather than nucleate and form their own bubbles. This technique provided interesting results that can be considered as a good starting point and a good comparison for the results described in this thesis.

Despite the efforts above reported, in our opinion some more light needs to be shined to the nucleation and bubble growth mechanisms involved in the PU (and in the context of this study, PIR as well) foaming process. The aforementioned processes simultaneously take place during the polymer expansion, so it may be difficult to study nucleation and growth mechanism in a system where the bubble generation and the expansion are in continuous evolution. On account of this, the aim of this study is to investigate on the competing bubble formation mechanisms by a methodical approach that allows to evaluate separately:

Bubble *nucleation* and growth:

I) of pentane in the single reactant phase (liquid BA evaporation induced by externally heating the sample holder);

II) of CO_2 (isocyanate-H_2O blowing reaction) in the PU (and PIR) reacting mixture;

III) of CO_2 (isocyanate-H_2O blowing reaction)-pentane (evaporation induced by the heat of reaction) in the PU (and PIR) reacting mixture;

Air bubbles inclusion (*aeration*) and growth:

IV) in the single reactant phase by pentane diffusion (liquid BA evaporation induced by externally heating the sample holder);

V) in PU (and PIR) reacting mixture by CO_2 (isocyanate-H_2O blowing reaction) diffusion.

VI) in PU (and PIR) reacting mixture by CO_2 (isocyanate-H_2O blowing reaction)-pentane (evaporation induced by the heat of reaction) diffusion.

5.2. Materials and methods

5.2.1. Materials

A formulated mixture of polyether polyols (density = 1.08 g/cm^3, viscosity = 6700 mPa·s), with silicone surfactant and catalysts was utilized with polymeric methylene diphenyl diisocyanate (PMDI) (31.1% NCO, 1.20 g/cm^3, 190 mPa.s) to obtain PUFs. A formulated mixture of aromatic polyester polyol (density = 1.24 g/cm^3, viscosity = 650 mPa.s), with silicone surfactant and catalysts was utilized with PMDI (high functionality, 30.5% NCO, density = 1.24 g/cm^3, viscosity = 600 mPa.s) to obtain PIRFs. All were formulated and supplied by Dow Italia s.r.l. (Correggio, RE, Italy) and used “as received”. Water was always utilized as the CBA and pentane (namely, cyclopentane and a mixture of cyclo/isopentane (70/30), Synthesis S.p.A., Bianconese di Fontevivo, PR, Italy, for PU and PIR, respectively) was used in addition to water in some tests as PBA. Chemical compositions of the formulated polyols are detailed in Table 1. Codes of the different PU and PIR samples and the content of the CBA and PBA, together with the processing data are reported in Table 2.

Table 1. Chemical composition of the formulated polyols.

Chemicals	in PU formulation		in PIR formulation	
	Description	Parts	Description	Parts
Polyol	Mixture of polyether polyols	95.4	Mixture of aromatic polyester polyols	97
Surfactant	Silicone type	2.8	Silicone type	3
Catalysts	Amine type	1.2	Amine type	1.7
	Amine type	0.6	Amine type	0.7
Trimerization catalyst	/	/	Potassium salt	1
Chemical Blowing Agent	Water	0.1	Water	0.1
Physical Blowing Agent	Cyclopentane	14.5	Cyclo/isopentane (70/30)	19.5

Table 2. Foam samples codes and processing details (type and amount of BAs and processing conditions).

Sample	water|C_5H_{12} amount (parts)	Mixing process
PU-CO_2	0.1|0	50 rpm for 20 s
PU-CO_2-C_5H_{12}	0.1|14.5	50 rpm for 20 s
PU-Air-CO_2	0.1|0	1000 rpm for 8 s
PU-Air-CO_2-C_5H_{12}	0.1|14.5	1000 rpm for 8 s
PIR-CO_2	0.1|0	50 rpm for 20 s
PIR-CO_2-C_5H_{12}	0.1|19.5	50 rpm for 20 s
PIR-Air-CO_2	0.1|0	1000 rpm for 8 s
PIR-Air-CO_2-C_5H_{12}	0.1|19.5	1000 rpm for 8 s

5.2.2. Experimental setup

A micro-optical observation system was set-up and nucleation, air bubbles inclusion and growth were observed by computerized digital imaging. The experimental setup is shown in Figure 1. A CMOS camera (model DMK 33UX178) from The Imaging Source (Bremen, Germany) was used for this study. The digital camera has a resolution of 3072×2048 (6.3 MP) and a frame rate of 60 fps. The gain can be varied in the range of 0-48 dB and each pixel has a size of 2.4 µm x 2.4 µm. A bi-telecentric lens (model TC23004, x2 magnification, with a working distance of 56 mm and a field depth of 0.23 mm) from Opto Engineering (Mantova, Italy) was utilized. In case of study of nucleation, air bubbles inclusion and their growth and, therefore, the need to observe the foaming process of a PU (or PIR), the reactants were kept separate by a rubber impeller as shown in Figure 1b and c. The single process is then observed immediately right after the mixing (the mixing conditions for each observed phenomenon will be specified in the experimental section). In the case of bubble nucleation and air bubbles inclusion in the single reactant phase, only the specific reactant is poured in the sample holder. The copper plate, used to keep the sample holder, was also equipped with a heating band (from ESAF s.r.l.) which allows to heat the sample and a thermocouple (PT100 type from ESAF s.r.l.) in order to monitor the temperature. Temperature control is set by a PID controller (ETR-9100 model from ESAF s.r.l.). In a typical heating test, the copper plate is first heated up (heating rate of 5°C/min) to set temperature (90 ° C). Once that the desired temperature is reached, the sample holder is placed inside the copper plate so that the single reactant phase can be heated. In this way, it is possible to observe the eventual bubble nucleation and the inclusion of air bubbles.

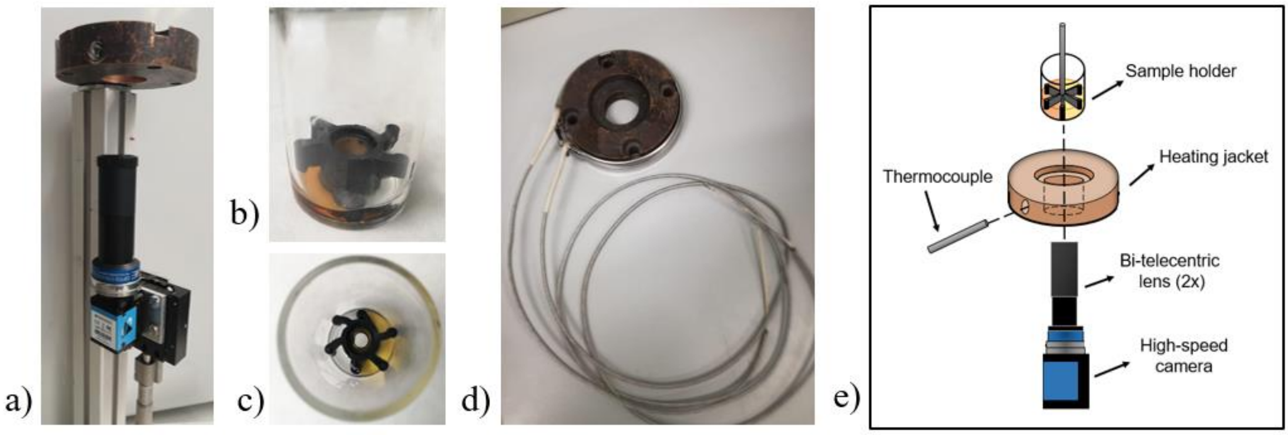

Figure 1. (a) Micro-optical observation system composed by the high-speed camera with a copper plate used to keep the sample holder; (b) sample holder with the rubbery impeller keeping separate the two reactants and (c) its top view; (d) heating jacket used to heat the copper plate; (e) schematic view of the observation system.

5.2.3. Image analysis

The different cellular structures as well as the bubble size distribution were evaluated by a semi-automatic method of IA using ImageJ software (U.S. National Institutes of Health). The region of interest (ROI), consisting of a selection of the area of interest of the image, was defined in order to carry out a more accurate analysis of the dispersed phases. As regards for the foaming results, the average size of the dispersed phases was defined as the diameter of a circle of area equivalent to the projected area of the dispersed phase. The average diameter was then multiplied by a correction factor of 1.273 [10] to calculate the reference three-dimensional cell size. On the other hand, the cell density was evaluated by measuring only the image area (A) and number of the dispersed phases (n), according to Kumar's theoretical approximation [11]. For each formulation, the cell size and the cell density of three samples were measured and averaged. The IA was applied to 36 scans in the foaming process of the two materials covering approximatively the initial 300 s. In the case of foaming test related to the PU (PIR) reacting mixture, images were acquired and processed on the bottom side of the sample holder in order to in-situ monitor the cell size evolution during the foaming process. As for bubble nucleation and air bubbles inclusion tests in the single reactant, the images were acquired and processed at different positions (different fields of view) starting from the bottom side of the sample holder in order to obtain an accurate and continuous monitoring of the bubbles dynamics.

5.2.4. Foam density

Foam densities were also measured according to ASTM D1622/D1622M standard test method [12]. The samples were cut by a razor blade after that the foams were removed from the sample holder. The size of the specimen was 10 mm x 10 mm x 10 mm (width x length x thickness). The densities of three samples were measured and averaged.

5.3. Results and Discussion

5.3.1. Foaming behavior

The foaming mechanisms have been observed in both the PU and the PIR formulations. The formulations under the present study are industrially utilized with pentane isomers (cyclo or iso/cyclo depending from the selected formulation) as PBA. As also the water is contained in polyol formulations, the foaming process was also observed without pentane addition in order to evaluate the effect of air bubbles inclusion with only water (CO_2 generation by blowing reaction) as CBA. PU and PIR foaming were conducted at the same mixing conditions at high (introduction of air bubbles at 1000 rpm for 8 s) and low (no air bubbles at 50 rpm for 20 s) stirring velocities. The foaming behavior was also observed at low stirring velocity in order to give an elucidation about the mechanisms taking place when no air bubbles are introduced in the reacting system. After several attempts, the mixing condition at 50 rpm for 20 s was found to be suitable to our purpose. In this way, it was possible to eventually evaluate the air bubbles inclusion and growth (high stirring velocity) separately from the BA nucleation (in the absence of entrapped air bubbles).

Collected samples used for the video acquisition are shown in Figure 2. From these images we can already observe that the different mixing conditions play a fundamental role in determining the final morphology of the foams. On one hand, for both PU and PIR foaming, foams obtained at 50 rpm have a lower expansion ratio with bigger cells, while, on the other hand, foams obtained at 1000 rpm have a higher expansion ratio and a more uniform and finer cell size distribution. Foams without air bubbles were obtained by a milder mixing that can lead to unsuitable mixing of the reactants. Under these considerations, in the case of low stirring velocity, the higher degree of inhomogeneity and the lower expansion ratio may be attributed to a slowing down of the gelling and blowing reactions due to a more indigent contact of the reactants. The same behavior can be observed when also pentane is added to the mixture which, with its plasticizing effect of the polymer, leads to higher expansion ratios [13] and, in the case of PU at 50 rpm, may result in a collapsed foam when the polymer is not strong enough to withstand the bubbles expansion

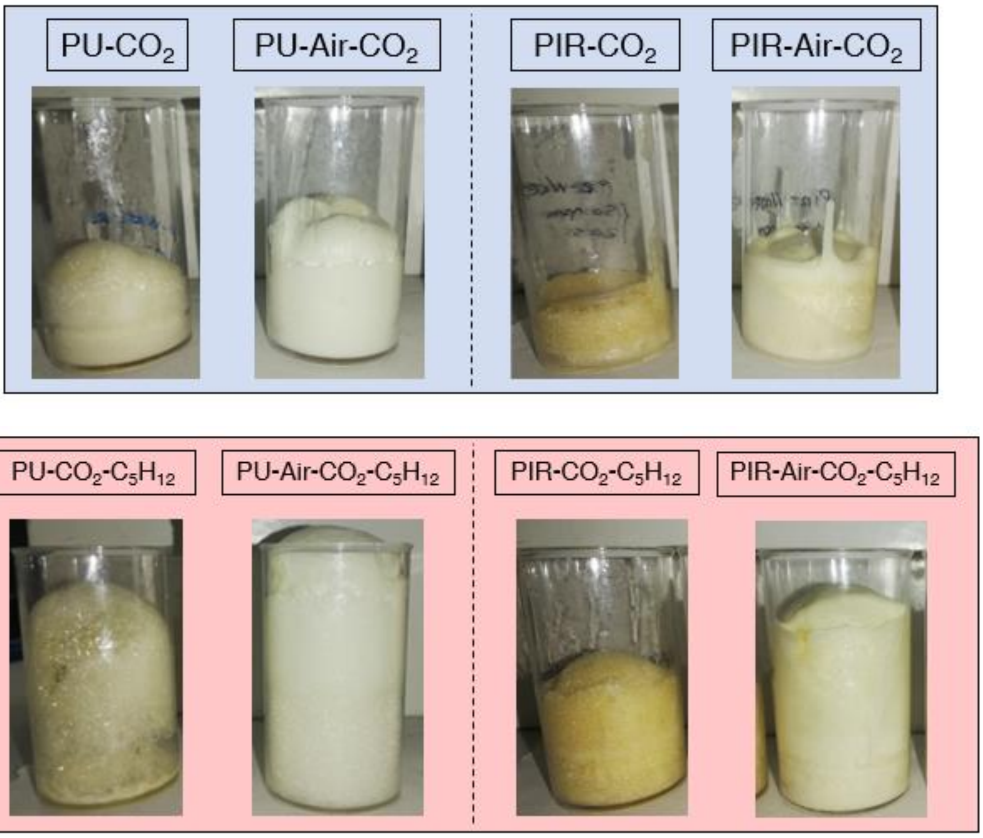

Figure 2. Foaming behavior of PUs and PIRs.

In Table 3 are also reported the foam densities of the observed samples (foams were collected after the video acquisition and were kept for 2 days before density measurement). Foams obtained by low mixing conditions have densities with greater standard deviation with respect to those obtained by faster mixing. As aforementioned, lower mixing conditions did not allow a suitable contact of the reactants and, as a consequence, inhomogeneous foams are obtained. Of course, when pentane is added as PBA, lower densities are obtained for both PU and PIR ranging from a slow and inefficient (in case of water blown only) to a faster and more suitable expansion of the polymer.

Table 3. Foam densities.

Sample	Density [kg/m^3]	Sample	Density [kg/m^3]
PU-CO_2	51.24 ± 6.35	PIR-CO_2	59.87 ± 5.98
PU-CO_2-C_5H_{12}	33.42 ± 4.23	PIR-CO_2-C_5H_{12}	43.56 ± 5.06
PU-Air-CO_2	44.57 ± 0.79	PIR-Air-CO_2	51.44 ± 0.97
PU-Air-CO_2-C_5H_{12}	29.47 ± 0.52	PIR-Air-CO_2-C_5H_{12}	35.63 ± 0.66

5.3.2. Bubble formation mechanisms: nucleation and aeration

Pentane bubble nucleation induced by external heating into the single reactant phase (polyol component) is reported in Figure 3. Bubbles originated from the BA molecules (pentane evaporated from its liquid phase) appear to nucleate approximatively after 3 minutes (the time elapsed for the bubbles to appear in the polymer phase). With regard to the nucleated bubbles size and density, no quantification is reported as it was difficult to distinguish between the simultaneous growth of these bubbles (change in size due to the pentane diffusion in the nucleated bubbles) and their rise upwards (change in size as the bubbles progressively move away from bottom side of the sample holder and then from the field of view of the camera).

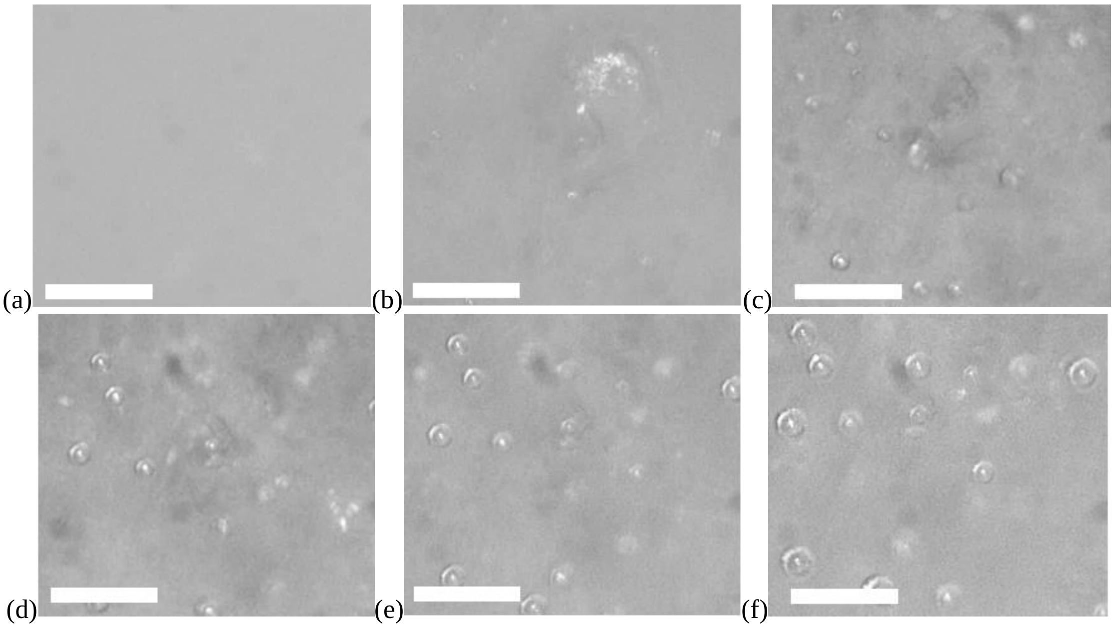

Figure 3. Pentane bubble nucleation induced by temperature control within the polyether polyol at different times: (a) 10 s, (b) 30 s, (c) 180 s, (d) 210 s, (e) 240 s and (f) 300 s. Scale bars are 300 µm.

An example of bubble nucleation and growth (pentane evaporated from its liquid phase and CO_2 formed by the blowing reaction) mechanisms occurring into the reacting mixture are reported in Figure 4. In this case, no dispersed phases were observed by the end of the mixing stage unlike the case of the high stirring velocity (as will be shown below in Figure 6). These bubbles appear to nucleate approximatively after 10 s (the time elapsed for the bubbles to appear in the polymer phase ranged from 10 s to 20 s for the whole set of experiments) and grow until they undergo a strong coalescence.

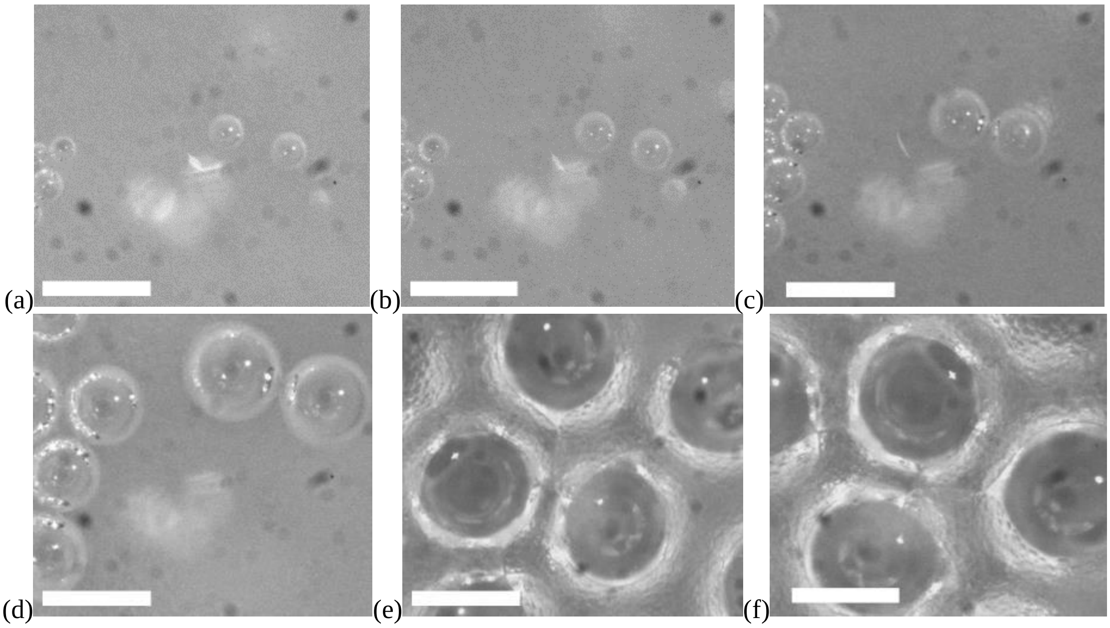

Figure 4. Foaming behavior at low stirring velocity. PBA/CBA bubble nucleation and growth of PU at different curing times: (a) 10 s, (b) 30 s, (c) 40 s, (d) 120 s, (e) 240 s and (f) 300 s. Scale bars are 300 µm.

The air bubbles inclusion in the single reactant phase is shown in Figure 5. The mixing conditions were 1000 rpm for 8 s. In this case, as can be expected, the polymeric phase shows dispersed phases (air bubbles) from the very beginning of the observation (right after the mixing stage). In comparison with the nucleation experiments conducted in absence of air bubbles, it was observed that no nucleation occurred during the process, while the air bubbles underwent to expansion (induced by the pentane diffusion).

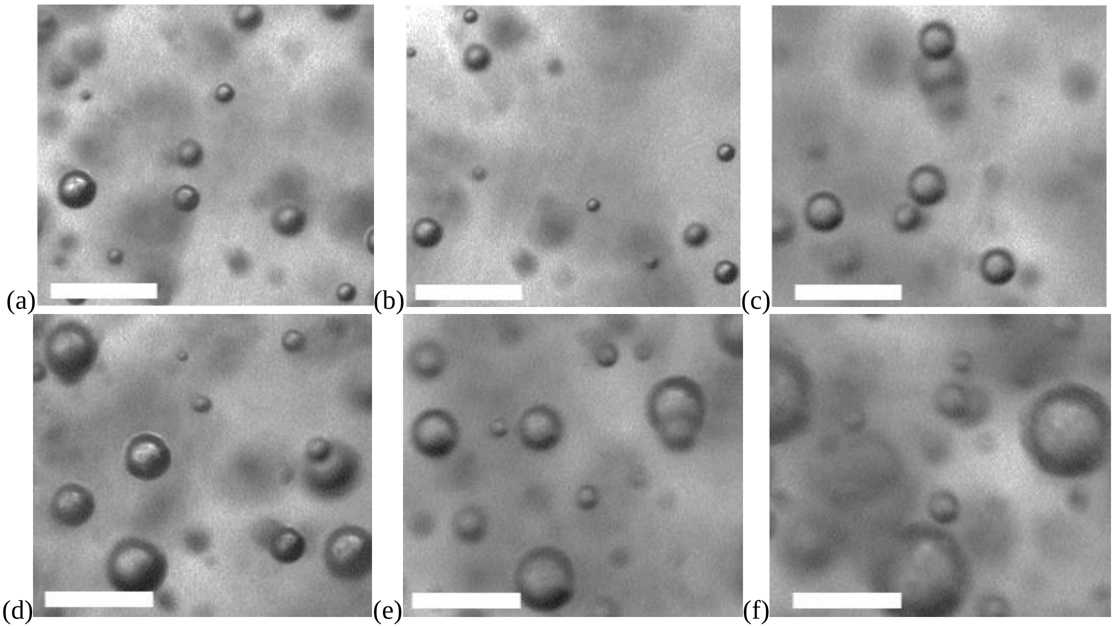

Figure 5. Air bubbles expansion by pentane diffusion (evaporation induced by temperature control) within the polyether polyol at different times: (a) 10 s, (b) 30 s, (c) 40 s, (d) 120 s, (e) 240 s and (f) 300 s. Scale bars are 300 μm.

Figure 6 shows the cell morphology development of the pentane-water blown PU and PIR formulations respectively. As shown, the polymeric matrix appears as a single uniform phase with no other heterogeneous phases within the system, while, air bubbles are introduced during the mixing step (at 1000 rpm for 8s). More importantly, it was possible to observe that the foaming process was characterized by a two-stage cell growth mechanism [14]. During the early instants of the PU foaming process, a combined effect of coalescence and OR was responsible for the cell degeneration, while in the later foaming stage only the OR occurred. In the case of PIR foaming, no coalescence was observed whereas the OR affected less the cell growth in comparison with PU. Also in this case, nucleation did not occur during the foaming process, in agreement with the results observed from the air bubbles inclusion tests on the polyol phase.

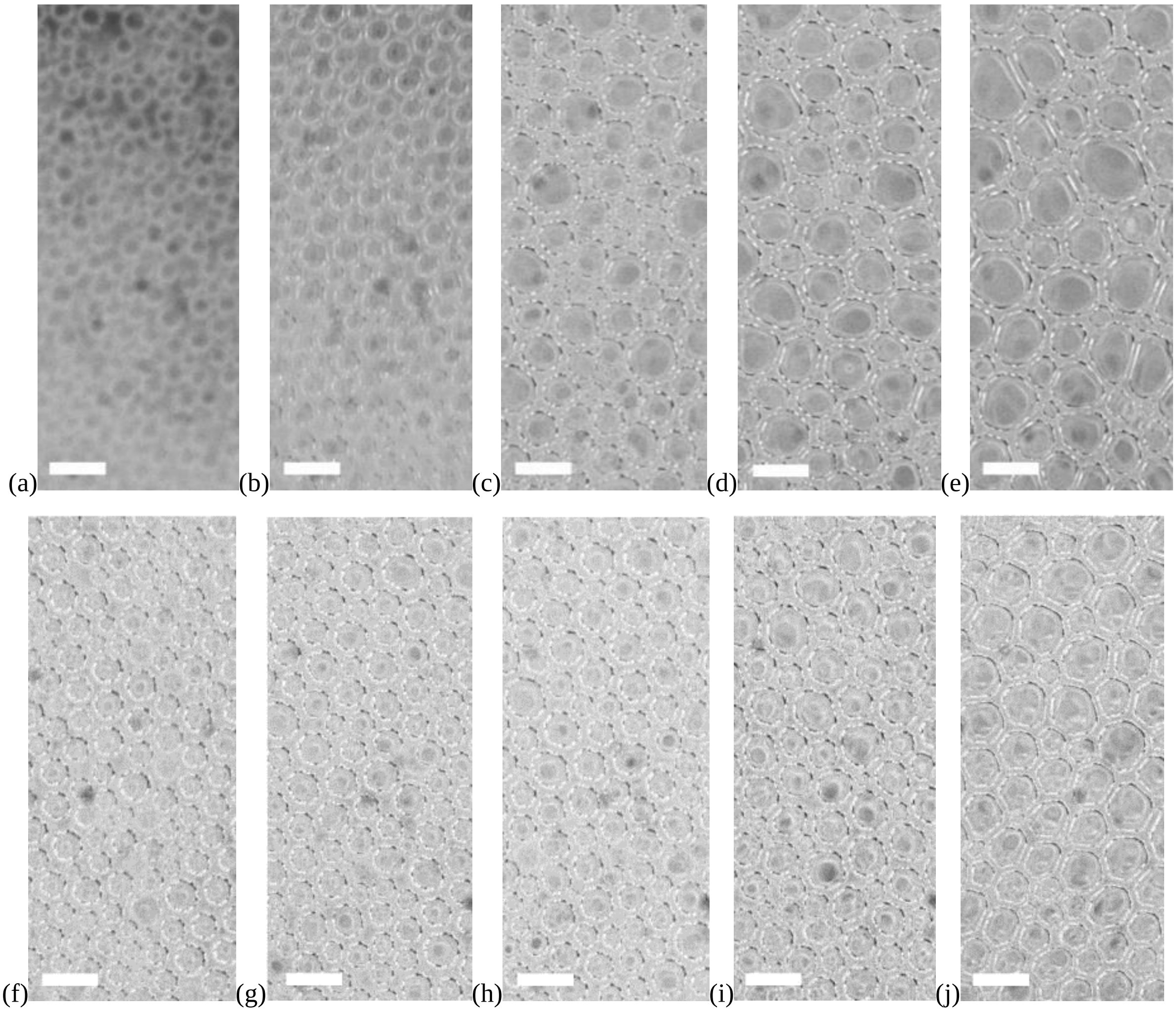

Figure 6. Foaming behavior at high stirring velocity. Air bubbles growth induced by CO_2 and pentane diffusion of PU and PIR at different curing times: (a and f) 10 s, (b and g) 30 s, (c and h) 40 s, (d and i) 120 s and (e and j) 300 s. Scale bars are 200 µm.

With reference to water blown and pentane-water blown PU and PIR, Figure 7 and 8 report the collective results of the whole set of experiments. The foaming behavior is reported in terms of cell density (N) (standard deviation ranged approximatively from $2 \cdot 10^3$ cell/cm^3 to $5 \cdot 10^3$ cell/cm^3 for each experimental point) when the mixing varies with the aforementioned conditions. When air bubbles are introduced, a degeneration of the cells is observed over time without any increase in cell density that could be attributable to bubble nucleation (Figure 8b and d). In the absence of air bubbles, the experimental data seem to confirm that an initial nucleation occurred followed by cell coarsening (Figures 7b and d). Focusing on the cell size (ϕ) evolution (standard deviation ranged approximatively from 5 µm to 10 µm for each experimental point), it is clear that in the case of introduction of air bubbles (Figures 8a and c), the foams are finer than those where nucleation occurred, while in the latter case, the bubbles undergo a strong coalescence (Figures 7a and c). As aforementioned, foams obtained by lower stirring velocity undergo to unsuitable mixing of the reactants. As a consequence, the higher degree of cell degeneration may be attributed to a slowing down of the gelling reaction due to a more indigent contact of the reactants.

As it is true for the all the mechanisms based on the mass transport, the diffusion coefficient Ɗ is a proportionality constant between the molar flux due to molecular diffusion and the gradient in the concentration of the species (or the driving force for diffusion) [15]. Typically, the diffusivity is prescribed for a binary system (given pair of species) and the higher the diffusivity (of one substance with respect to another), the faster they diffuse into each other [15]. In our specific case, as already proposed by several authors in the literature [16-19], we can adopt a model used to describe the bubble growth. This model is developed by assigning a specific amount of liquid to each individual bubble in a liquid medium that contains a large number of gas bubbles. The single bubble is considered spherical and is surrounded by a concentric liquid shell. The gas bubble can be composed of a pure or a mixture of several components, while the liquid in the envelope is a solution which contains the same components at a uniform initial concentration [17]. Based on this assumption, we may define an apparent diffusivity $Ɗ_a$ taking into account the relative diffusion of these components from the polymer matrix to the dispersed phase, namely a global diffusion coefficient referred to the overall solute. Based on the cell size data acquired from the image sequences of the optical acquisition, we may extrapolate the apparent diffusivity $Ɗ_a$, evidencing the reduction of diffusivity provoked by the ongoing curing reaction. This coefficient can be determined by the following equation [18,19]:

$$\phi = 6\left(\frac{3}{4\pi}\right)^{0.33} (Ɗ_a t)^{0.5} \tag{1}$$

The initial growth of spherical bubbles in expanding liquids can be well-described with the square root of time and therefore ϕ is reported as function of $t^{0.5}$ [18,19]. Figure 7 and 8 (a and c respectively) highlight an interesting two-stage cell growth mechanism, for each system, that can be attributed to the so-called wet-dry transition [14]. During the early instants of the foaming process, a first linear trend (I) is shown and can be attributed to the bubble growth caused by the diffusion of the BA molecules from the polymeric matrix into the bubbles. After this first stage, rounded bubbles isolated in the liquid (wet regime) change their shape into polyhedral cells starting to touching each other (dry regime) [14]. As a consequence, the cells growth rate is reduced and a second linear trend (II) can be observed. A reduction in $Ɗ_a$ (results are reported in Table 4) can be noticed when foams are prepared by high stirring velocity (in particular, for the first stage of the bubbles growth, from $3.16\cdot10^{-5}$ cm^2/s and $2.70\cdot10^{-4}$ cm^2/s of the PU-CO_2 and PU-CO_2-C_5H_{12} formulations respectively to

$2.23 \cdot 10^{-6}$ cm^2/s and $2.25 \cdot 10^{-5}$ cm^2/s respectively when air bubbles are introduced into the system). Likewise, also in PIR foaming results a reduction in $\mathcal{D}_a$ is observed, in agreement with those related to PU foaming (in particular, for the first stage of the bubbles growth, from $2.84 \cdot 10^{-6}$ cm^2/s and $1.46 \cdot 10^{-4}$ cm^2/s of the PIR-CO_2 and PIR-CO_2-C_5H_{12} formulations respectively to $1.98 \cdot 10^{-6}$ cm^2/s and $2.38 \cdot 10^{-5}$ cm^2/s respectively when air bubbles are introduced into the system). The linear fitting of the cell density data may also represent an useful tool aimed to a qualitative (see Table 4) evaluation on the cell nucleation (or coarsening in case of air bubble inclusion) rate (dN/dt) [19].

It is interesting to notice that, while the air bubbles growth gives the same results in terms of cell coarsening rate for both pentane-water blown PU and PIR (ranging from -1903 $cell.cm^{-3}.s^{-1}$, of the PU-Air-CO_2-C_5H_{12} formulation, to -2004 $cell.cm^{-3}.s^{-1}$ of the PIR-Air-CO_2-C_5H_{12} formulation), the cell development during the time is completely different in the case of the low stirring velocity. In this latter case, the cell nucleation rate ranged from -5928 $cell.cm^{-3}.s^{-1}$, of the PU-CO_2-C_5H_{12} formulation, to -554 $cell.cm^{-3}.s^{-1}$ of the PIR-CO_2-C_5H_{12} formulation. However, these results may be influenced as the nucleated bubbles undergo a more dramatic coalescence in the PU formulation. This effect may be ascribed to the plasticizing effect of pentane on the reaction mixture which, by lowering the viscosity of the polymer melt [13], causes an even stronger coalescence. On one hand, for PU, it appears that the polymer is not stable enough to withstand the pentane bubble expansion and the cell density immediately collapses with reference to that of water blown only (Figure 7b). On the other hand, in the case of PIR, the polymer structure is strong enough to withstand the pentane bubble expansion leading, therefore, to an enhanced cell density (Figure 7d).

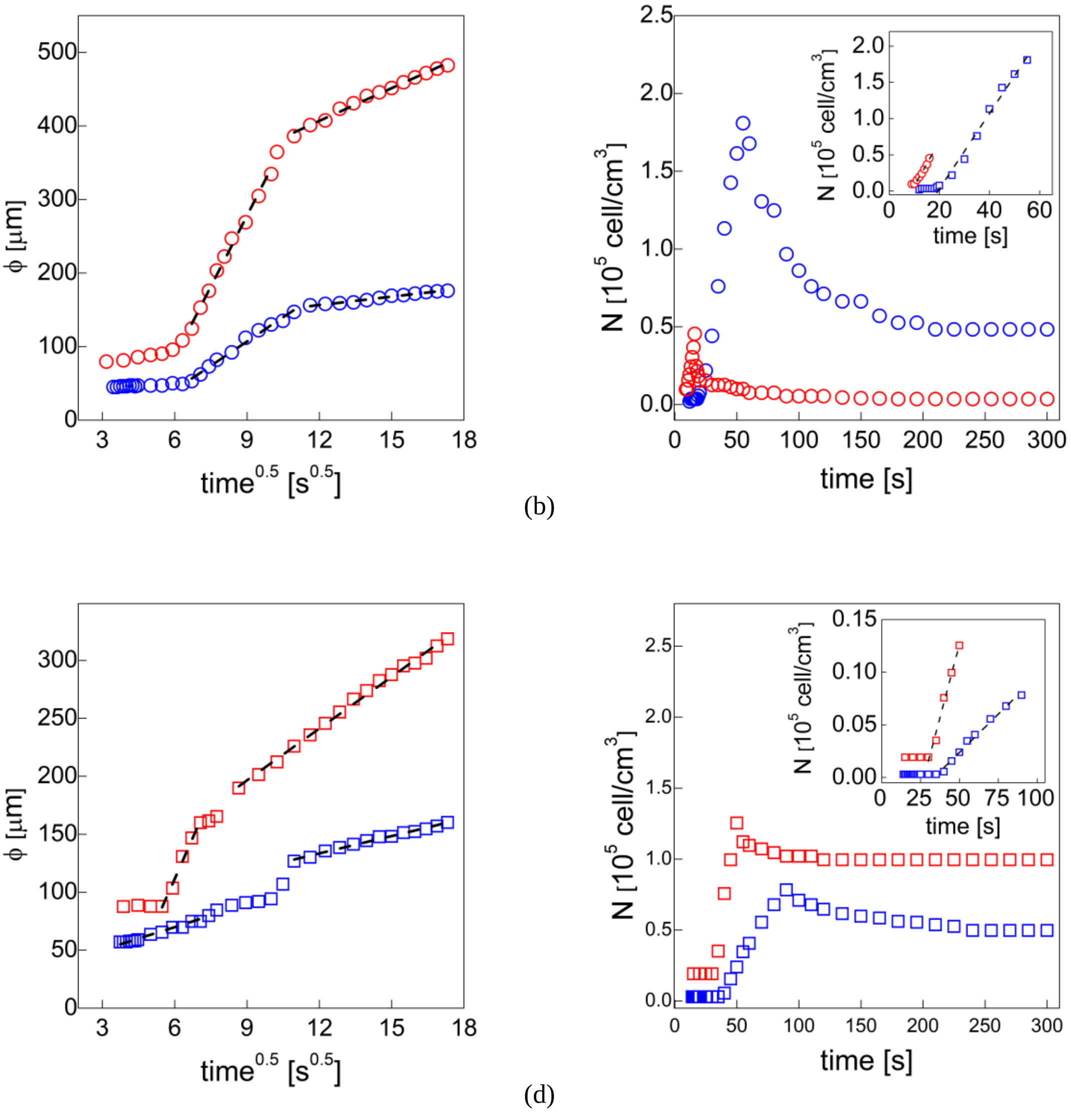

(a) (b)

(c) (d)

Figure 7. Bubble formation and growth: average cell size and cell density evolution of water blown (blue symbols) and water-pentane (red symbols) of PUs (a and b) and PIRs (c and d). Lines represent the linear fitting of the experimental data (by Equation 1 in data related to cell size). Insets detail the bubble formation stage.

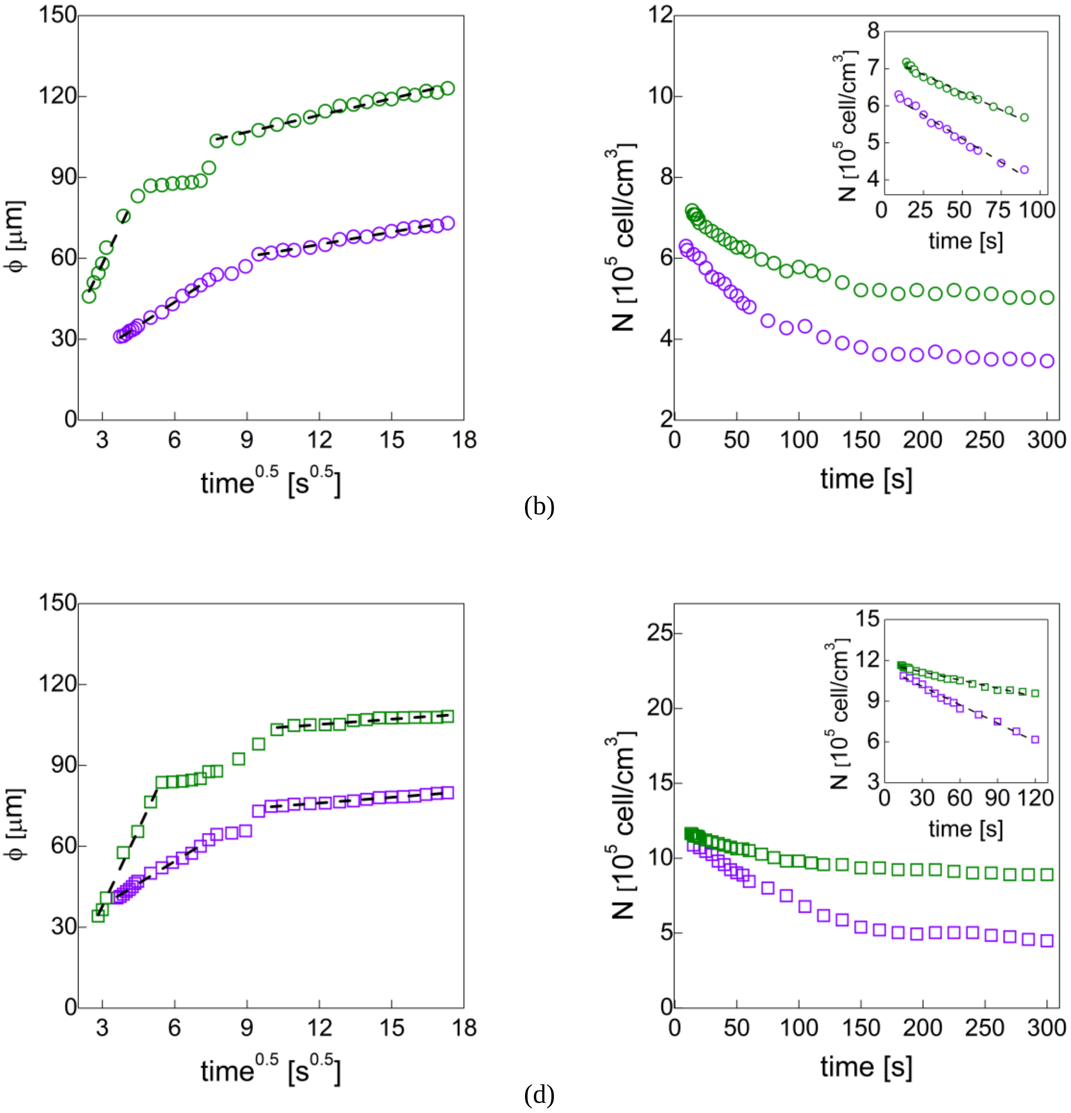

(a) (b)

(c) (d)

Figure 8. Air bubbles growth: average cell size and cell density evolution of water blown (violet symbols) and water-pentane blown (green symbols) PUs (a and b) and PIRs (c and d). Lines represent the linear fitting of the experimental data (by Equation 1 in data related to cell size). Insets detail the first cell coarsening stage.

Table 4. Apparent diffusion coefficients and cell nucleation/coarsening rate of water blown and water-pentane blown PU and PIR.

Sample	$\mathcal{D}_a$ [cm^2/s]		dN/dt [cell.cm^{-3}.s^{-1}]
	I	II	II
PU-CO_2	$3.16\cdot10^{-5}$	$9.51\cdot10^{-7}$	5206
PU-CO_2-C_5H_{12}	$2.70\cdot10^{-4}$	$1.44\cdot10^{-5}$	5928
PU-Air-CO_2	$2.23\cdot10^{-6}$	$1.55\cdot10^{-7}$	-2534
PU-Air-CO_2-C_5H_{12}	$2.25\cdot10^{-5}$	$2.82\cdot10^{-7}$	-1903
PIR-CO_2	$2.84\cdot10^{-6}$	$1.63\cdot10^{-6}$	145
PIR-CO_2-C_5H_{12}	$1.46\cdot10^{-4}$	$1.46\cdot10^{-5}$	554
PIR-Air-CO_2	$1.98\cdot10^{-6}$	$3.16\cdot10^{-8}$	-4503
PIR-Air-CO_2-C_5H_{12}	$2.38\cdot10^{-5}$	$2.79\cdot10^{-8}$	-2004

Another interesting question that may arise regards the cell density results showing that no nucleation occurred when air bubbles are included in the reacting mixture. These results can be explained if one considers the classical nucleation theory and the classification that can be given to the different nucleation mechanisms [20]. Homogeneous (i) and heterogeneous (ii) nucleation mechanisms are processes where the formation of a new gas phase has to overcome a very high energy barrier (radius of the nuclei greater than the critical radius in order to let the bubble spontaneously grow up). On the contrary, the nucleation cannot be accounted by the classical nucleation theory when pre-existing bubbles are contained inside the system. In particular, when the radius of curvature of these pre-existing bubbles is smaller than the critical radius (iii) less nucleation energy barrier is required, while, in case of the radius of curvature greater than the critical radius (iv), the required energy lowers to zero [20]. Due to the presence of air bubbles within the reacting mixture since the very beginning (introduced by mixing step), we may conclude that the BA molecules would rather diffuse toward these pre-existing air bubbles (no energy barrier to overcome, iv) than nucleate in gas bubbles into the PU matrix (i).

5.4. References

[1] X. D. Zhang, C. W. Macosko, H. T. Davis, A. D. Nikolov and D. T. Wasan, Role of Silicone Surfactant in Flexible Polyurethane Foam, J. Colloid Interface Sci. 215 (1999) 270-279.

[2] G. M. Campbell, E. Mougeot, Creation and characterisation of aerated food products, Trends Food Sci. Technol. 10 (1999) 283-296.

[3] D. C. Blackley, Polymer Latices Science and Technology Volume 3: Application of Latices, Chapman & Hall, London, 1997.

[4] D. Kashchiev, Nucleation Basic Theory with Applications, Butterworth-Heinemann, 2000.

[5] P. Walstra, Fundamentals of Interface and Colloid Science, edited by J. Lyklema, Elsevier, 2005.

[6] R. Baumhakel, Influence of stirring velocity and air loading on the formation of flexible urethane foams, J. Cell. Plast. 8 (1972) 304-310.

[7] E. Minogue, An in-situ study of the nucleation process of polyurethane rigid foam formation Ph. D Thesis, Department of Chemical Sciences, Dublin City University, 2000.

[8] S. Pardo-Alonso, E. Solorzano, S. Estravis, M.A. Rodriguez-Perez, J.A. de Saja, In situ evidence of the nanoparticle nucleating effect in polyurethane-nanoclay foamed systems, Soft Matter 8 (2012) 11262-11270.

[9] J. Reignier, P. Alcouffe, F. Méchin, F. Fenouillot, The morphology of rigid polyurethane foam matrix and its evolution with time during foaming – New insight by cryogenic scanning electron microscopy, Journal of Colloid and Interface Science 552 (2019) 153-165.

[10] ASTM D3576-04. Standard Test Method for Cell Size of Rigid Cellular Plastics, ASTM International: Plastics (II).

[11] Kumar V. Process synthesis for manufacturing microcellular thermoplastic parts. PhD Thesis, Massachusetts Institute of Technology, Cambridge, MA, 1988.

[12] ASTM D1622/D1622M: Standard Test Method for Apparent Density of Rigid Cellular Plastics.

[13] T. M Pontiff, Physical Foaming Agents: Structure, Property and Performance, Blowing Agents' 99 Conference proceedings, Paper 13 (1999) 1-5.

[14] Y. Furuta, N. Oikawa, R. Kurita, Close relationship between a dry-wet transition and a bubble a bubble rearrangement in two-dimensional foam, Sci. Rep. 6 (2016) 37506.

[15] R. B. Bird, W. E. Stewart, E. N. Lightfoot, Transport Phenomena, John Wiley & Sons, 2011.

[16] R. D. Patel, Bubble growth in a viscous Newtonian liquid, Chem. Eng. J. 35 (1980) 2352-2356

[17] M. Amon, C. D. Denson, A study of the dynamics of foam growth: Analysis of the growth of closely spaced spherical bubbles, Polym. Eng. Sci. 24 (1984) 1026-1034.

[18] M. Favelukis, R. J. Albalak, Bubble growth in viscous Newtonian and non-Newtonian liquids, Chem. Eng. J. 63 (1996) 149-155.

[19] S.Pérez-Tamarit, E.Solórzano, R.Mokso, M.A.Rodríguez-Pérez, In-situ understanding of pore nucleation and growth in polyurethane foams by using real-time synchrotron X-ray tomography, Polymer 166 (2019) 50-54.

[20] S. F. Jones, G. M. Evans, K. P. Galvin, Bubble nucleation from gas cavities – A review, Adv. Colloid Interface Sci. 80 (1999) 27-50.

Chapter 6.

Inhibition of the Ostwald Ripening by liquid-type OFAs

Chapter 6. Inhibition of the Ostwald Ripening by liquid-type OFAs

3072 × 2048 (6.3 MP) and a frame rate of 60 fps. The gain can be varied in the range of 0-48 dB and each pixel has a size of 2.4 μm × 2.4 μm. A bi-telecentric lens (model TC23004) from Opto Engineering was mounted (×2 magnification) with a working distance of 56 mm and a field depth of 0.25 mm. The micro-optical observation system is shown in Figure 1. In case of study of air bubbles inclusion and their growth, the effect of OFAs on these processes and therefore, the need to observe the foaming process of a PU or PIR, the reactants kept separate by a rubber impeller as shown in Figure 1b and c. The single process is then observed immediately right after the mixing (the mixing conditions for each observed phenomenon will be specified in the experimental section). In the case of air bubble inclusion in the single phase (polyol or isocyanate), only one single reactant is poured in both the locations of the sample holder as already shown in Figure 1b and c (here, the configuration without the heating system described in the previous chapter is used).

Chapter 7.

Conclusions

This section is dedicated to a brief summing-up of the activities conducted during the three years of this PhD project, aiming to highlight the main findings of the performed research. Moreover, additional future activities are proposed as a further improvement of the results obtained so far, or new strategies to be used for other thermosetting materials.

Chapter 7. Conclusions

7.1. Conclusions

In *chapter 3*, carbon dioxide sorption in polyol/PMDI system, under high-pressure, was studied by in situ FT-NIR spectroscopy. A kinetic analysis was performed on the PU reacting system, at 35 °C and still under CO_2 pressure (up to 12 MPa) and characteristic urethane (NH group) and PMDI (NCO group) bands were monitored. Results revealed, in the investigated experimental range, a significant slowing down effect of the sorbed CO_2, apparently with two mechanisms: i) the catalyst deactivation due to a reaction of tertiary amines with CO_2 and the polyol and ii) the dilution effect due to swelling by CO_2 sorption in the two reacting phases. Above a weight fractions of ca. 0.07 g/g, where, apparently, catalytic sites were saturated by CO_2, only the swelling by CO_2 further contributed to the slowing down of the reaction kinetics. This effect has been confirmed by testing a PU formulation without catalysts. Finally, it has been proved that the sorbed CO_2 weight fraction is, in fact, responsible for the observed effects, not the pressure. In particular, apparently, the transition to the supercritical state of the outer CO_2 in contact with the polymeric phases is not relevant to the reactions analyzed in this work.

In *chapter 4*, a two-stage gas foaming method was introduced to cope with the two very different timescales of the pressure quench O(10^{-2} seconds)and the synthesis reaction O(10^2 seconds) by separating the nucleation and growth stages. The method, which may be described as ¨*chasing the synthesis reaction with the pressure*¨ allows a gentle growth of nucleated bubbles by a controlled pressure reduction following a first fast pressure reduction from the saturation pressure to an intermediate (higher than ambient) pressure. The derived model and resulting equation allowed clarifying the number of independent variables and groups at play, for proper material selection and processing optimization. Microcellular thermosetting PUFs by high-pressure CO_2 were achieved with average cell diameter of 20 µm and foam density of 150 kg/m^3. Excellent preliminary results were also obtained by using other PBAs as well, namely N_2 and an 80/20 vol/vol mixture of N_2 and CO_2, with an intermediate behavior between neat N_2 and neat CO_2. Average cell size below 4 µm, with foam densities in the range 130-440 kg/m^3 were achieved. These results prove the great potential of the proposed method to achieve high performance in insulating materials such as PUFs and not only these materials but, more in general, thermosetting materials. The aforementioned method gives also the possibility to tune the processing conditions and the choice of the BA, depending on the desired final properties of the foam.

In *chapter 5*, computerized digital imaging has been used in order to investigate the foaming mechanisms occurring in rigid PU and PIR foaming process. The air bubbles inclusion plays a key role in determining the final foam morphology. It has been revealed that the BA molecules diffuse toward the pre-existing air bubbles rather than nucleate in gas bubbles into the polymeric matrix. This behavior may be attributed to the presence of air bubbles within the reacting mixture providing the system no energy barrier to overcome with the regard to the PBA/CBA nucleation and bubble growth. Furthermore, during the early foaming stage, in the case of PU, it has been observed that coalescence in combination with OR are the mechanisms responsible for the cell coarsening, whereas it has a minor effect on cell coarsening of PIR. In the case of the late foaming stage, only the OR affected the cell coarsening and, also in this case, less predominant with reference to PIRFs.

In *chapter 6*,

7.2. Future perspectives

For future developments in the achievement of microcellular PUFs characterized by very low thermal conductivity, several additional strategies may be considered.

- As it regards the processing procedure developed to foam PU by high-pressure CO_2, the processing conditions may be refined to obtain PUFs with an even more reduced cell size (current cell diameter of 4 µm reached in the work of this thesis). For instance, higher pressure conditions may be considered in order to push more on the nucleation of the CO_2 bubbles. The processing temperature can be an additional parameter to adjust, as lower temperatures may lead to lower CO_2 pressures required to foam the polymer.

- With the reference to the same aforementioned method, it may be explored the possibility to obtain graded thermosetting foams as they have proven superior to their uniform counterparts in terms of structural and functional properties for applications such as energy efficiency and sound absorption. In fact, given the design of the high-pressure vessel in which PUFs were obtained, it is possible to design the sorption step in order to achieve non-trivial gas concentration profiles and consequently, at pressure releases, PU (but also other thermosetting) foams with graded density and morphology.

- With reference to the strategy of using incompatible compounds in PU and PIRFs in order to limit the cell coarsening, further investigations are needed in order to give a stronger elucidation on the mechanisms observed here in the work of this thesis. For instance, N_2 sorption in polyol/PMDI, with OFAs added, can be monitored in order to quantify the N_2 mass fraction in presence and absence of the additives. Moreover, as future perspectives, once clearly elucidated which are the mechanisms induced by these additives, new molecules may be designed in order obtain an even better stabilization of the cell coarsening.

- Last but not least, a further improvement can be a combination of the two aforementioned strategies. For instance, the use of the OFAs may be implemented in the PU formulation used for high-pressure CO_2 applications. Provided that these additives are suitable for this application, the use of OFAs may considerably improve CO_2 sorption (given their high affinity with N_2, O_2, CO_2 etc.) allowing to reduce the pressure required to solubilize the gas. In a more important way, this suggested methodology may lead to an important reduction of the cell size attained by an eventual combination of the high cell nucleation induced by PDR and high cell stabilization induced by OFAs.

Appendices

In this section additional data and plots are provided. Aiming at preserving the fluency, the data which are not strictly necessary to the discussion of the results presented throughout the dissertation have been collected separately. The final part reports a list of the resulting publications and the different activities carried out during the investigation.

Appendix to chapter 4

Derivation of reaction-chasing pressure drop rate

On the basis of our previous investigation [1], we assumed that the polymer-gas reacting mixture (assumed as a spatial uniform system) is in equilibrium with the external pure CO_2 phase at any instant of the process. With the imposition of the phase equilibrium condition, the two internal variables of the polymer-phase system, namely the volume, V, and $\overline{w}_{CO_2}$ can be expressed as a function of the state (p,T,X) at any time of the process. Hence, the only internal variable for the polymer phase is represented by X. In particular, the equation of State (EoS) of the polymer reacting mixture at phase equilibrium condition can be expressed as follows:

$$F\left[p,T,X,V(p,T,X),\overline{w}_{CO_2}(p,T,X)\right]=0 \tag{1}$$

According to the thermodynamics of internal state variables treated in [2], the reaction rate can be proposed as a function of the following state:

$$\dot{X}=\frac{dX}{dt}=f\left[p,T,X,V(p,T,X),\overline{w}_{CO_2}(p,T,X)\right]=g(p,T,X) \tag{2}$$

In Equation 2, the reaction rate is expressed as a function of only the two external state variables p, T and the internal state variable X. The temperature T can be removed from the state variables of the system since the temperature is kept constant during the process. Therefore, implicitly referring on RHS of Equation 2 to the corresponding partial function $g(p,T=T_0,X)=h(p,X)$ (T_0 being the constant temperature for the considered process), the state for the curing rate is expressed as:

$$\dot{X}=h(p,X) \tag{3}$$

Note that, in the process described here, the pressure p is externally controlled and, thus, our aim is to determine a possible depressurization rate $\dot{p}$ that assures a target value for X (e.g. $X=0.99$). As it will be discussed in the following, we need to establish a law for $h(p,X)$ in order to solve the described issue. To this aim, we observe that $\dot{X}$ is not dependent upon a particular evolution law of $p(t)$ and analogously it does not depend on $X(t)$ being only function of the value of p and X. Therefore, in our previous work [1], aimed to investigate the effect of CO_2 on the PU synthesis, we designed experimental isobaric tests (at the described common isothermal condition for every investigated CO_2 pressure) to determine experimental points of $\dot{X} = h(p, X)$ so that by a non linear regression of these experimental data, the proposed explicit function law based upon elementary function was determined.

As aforementioned, PUs are synthesized by reaction between polyol and isocyanate. The urethane formation was monitored by in situ FT-NIR spectroscopy and the NH associated peak, characteristic group of the urethane linkage, was detected in order to evaluate the reaction kinetics. Therefore, the integrated absorbance area under the band of the NH group was utilized to monitor the urethane formation by an Arrhenius-type model [3]:

$$A_{NH}(t) = A_{NH}^{f}\,(1 - e^{-kt}) \tag{4}$$

Where A_{NH} and A_{NH}^{f} represent the integrated absorbance areas under the NH band at time t and its final value, respectively, and k is the Arrhenius-type reaction rate constant [3]. The degree of curing can be appropriately expressed by normalizing with respect to the final A_{NH}^{f}, as follows:

$$X(t) = \frac{A_{NH}}{A_{NH}^{f}} = 1 - e^{-kt} \tag{5}$$

Equation 5 represents the PU extent of cure at a determined amount of dissolved CO_2 ($\overline{w}_{CO_2}$) within the reaction mixture (at a certain CO_2 pressure after a given sorption time). The Equation 5 is derived as a function of time and the curing rate can be then expressed as follows:

$$\frac{dX}{dt} = k\, e^{-kt} \tag{6}$$

The exponential function e^{-kt} in Equation 6 can be substituted by $(1 - X)$ from Equation 5:

$$\frac{dX}{dt} = k\,(1 - X) \tag{7}$$

The constitutive equation (Equation 3) can be then expressed in view of Equation 7 as:

$$\frac{dX}{dt} = f(p)\,(1 - X) \tag{8}$$

Here in Equation 8, the curing rate dependence from the internal state variable X is expressed by $(1 - X)$. As reported in [1], a slowing down effect of the sorbed CO2 ($\overline{w}_{CO_2}$) on the reaction rates was revealed and, therefore, for the different investigated $\overline{w}_{CO_2}$ (Figure A), k can be expressed as a function of $\overline{w}_{CO_2}$:

$$k(\overline{w}_{CO_2}) = A\, e^{-(B\,\overline{w}_{CO_2})} \tag{9}$$

Fitting the data retrieved in [1] by Equation 9 gives A = 0.72 and B = 45.82 (see inset in Figure A).

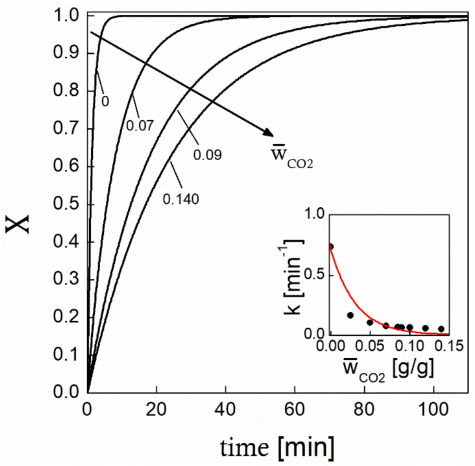

Figure A. Curing degree of PUs reacted at different $\overline{w}_{CO2}$ evaluated as a function of the reaction time. Line represents the fitting of experimental data by Equation 5. The inset shows a detailed view of the reaction rate constants at different $\overline{w}_{CO_2}$: the symbols are the experimental data and the red line represents fitting by Equation 9.

With the assumption that, during the slow pressure release (SPR), the dissolved CO_2 is always in equilibrium with the gas phase, (in turn in equilibrium at $p(t)$ and T fixed), in contact with the liquid reaction mixture, and assuming that $\overline{w}_{CO_2}$ is linearly dependent on the pressure (validity of Henry's law), the relationship between the CO_2 pressure and the liquid-phase concentration is given by [4]:

$$\overline{w}_{CO_2}(t) = H\,p(t) \tag{10}$$

Here, the Henry constant H is obtained from the CO_2 sorption previously studied in our work [1]. k can be expressed as a function of $p(t)$ by substitution of Equation 10 in Equation 9:

$$k\,(p) = A\,e^{-B\,H\,p} \tag{11}$$

The Equation 11 is then replaced in Equation 8:

$$\frac{dX}{dt} = \left(A\,e^{-B\,H\,p}\right)(1 - X) \tag{12}$$

The integration of Equation 12, performed by separation of variables method, between the initial and final points of SPR yields:

$$\int_{X'}^{X_f} \frac{dX}{(1 - x)} = \int_{0}^{t_f} \left(A\,e^{-B\,H\,p(t)}\right)\,dt \tag{13}$$

In the case of a constant depressurization rate from the initial pressure, p' (at the beginning of SPR stage, being t=0) to final pressure p_f at t_f (end of the SPR stage), the CO_2 pressure reduction takes the following form:

$$p(t) = \left(\frac{p_f - p^{'}}{t_f}\right) t + p^{'} \tag{14}$$

In this case, the constant depressurization rate is given by $\dot{p} = \left(\frac{p_f - p'}{t_f}\right)$ and the Equation 14 can be expressed as follows:

$$p(t) = \dot{p}\ t + p^{'} \tag{15}$$

With a direct integration of the LHS of Equation 13 and by integration of the RHS of Equation 13 by using the change of variables $t(p)$, the following expression is determined:

$$ln\left(\frac{1 - X'}{1 - X_f}\right) = \frac{1}{\dot{p}} \int_{p^{'}}^{p_f} \left(A\ e^{-B\ H\ p}\right)\ dp \tag{16}$$

Note that in obtaining Equation 16 the use of change of variable integration theorem according to monotonic law p(t), p(t(p))=p was applied and that $dt/dp = 1/\dot{p}$. Moreover, being the depressurization drop rate a decreasing function with the time, we can define $|\dot{p}| = -dp/dt$. Therefore, with the integration of the RHS of Equation 16, the constant depressurization rate can be expressed as follows:

$$|\dot{p}| = \frac{A}{B\ H} \frac{\left(e^{-B\ H\ p_f} - e^{-B\ H\ p'}\right)}{ln\left(\frac{1 - X'}{1 - X_f}\right)} \tag{17.a}$$

In case of $p_f = 0$[1] and being in this case $|\dot{p}| = \frac{p'}{t_f}$, the Equation 17.a collapses to:

$$|\dot{p}| = \frac{A}{B\ H} \frac{\left(1 - e^{-B\ H\ p'}\right)}{ln\left(\frac{1 - X'}{1 - X_f}\right)} \tag{17.b}$$

---

[1] *CO_2 fraction of the atmosphere is 0.04 ca. [see, for instance, Zhang YG, Pagani M, Liu Z, Bohaty SM, DeConto R., A 40-million-year history of atmospheric CO_2. Phil Trans R Soc A371 2013.0096], and, when the curing matter is exposed to the atmosphere by valve opening, the CO_2 partial pressure attains negligible value, for what concerns $\overline{w}_{CO_2}$ and the reaction (for instance, compared to the lowest p' = 0.35 MPa considered in the present study). Consistently, in [1] the CO_2 pressure at ambient pressure was reported as p=0 and corresponds to the kinetics of a neat PU reaction at ambient conditions.*

References

[1] M. R. Di Caprio, C. Brondi, E. Di Maio, T. Mosciatti, S. Cavalca, V. Parenti, S. Iannace, G. Mensitieri, P. Musto, Polyurethane synthesis under high-pressure CO_2, a FT-NIR study, Eur. Polym. J. 115 (2019) 364-374.

[2] G. Astarita, Thermodynamics An advanced Textbook for Chemical Engineers, Plenum Press, Newark, Delaware and Naples, Italy (1989).

[3] G. Ragosta, M. Abbate, P. Musto, G. Scarinzi, Spectroscopic, Mechanical and Dynamic-Mechanical Studies on the Photo-Aging of a Tetrafunctional Epoxy Resin, Macromol. Symp. 286 (2009) 34-41.

[4] R. H. Perry, D. W. Green, Perry's Chemical Engineers' Handbook, McGraw-Hill, 8th edition (2007).

Appendix to chapter 6

Publications, conferences and activities

A total of 6 scientific articles have been drafted during the development of this thesis. Several works have been published and others submitted (pending publication), all in international journals. The relative chapters of these results are also reported in Table 1.

Table 1. Publications in international journals reported in this thesis.

	RESEARCH ARTICLES	Chapter
1	M. R. Di Caprio*, **C. Brondi***, E. Di Maio, T. Mosciatti, S. Cavalca, V. Parenti, S. Iannace, G. Mensitieri, P. Musto *First authors Title: **Polyurethane synthesis under high-pressure CO_2, a FT-NIR study** European polymer journal 115 (2019) 364-374. https://doi.org/10.1016/j.eurpolymj.2019.03.047.	**3**
2	**C. Brondi**, M. R. Di Caprio, G. Scherillo, E. Di Maio, T. Mosciatti, S. Cavalca, V. Parenti, M. Corti, S. Iannace Title: **Thermosetting polyurethane foams by physical blowing agents: Chasing the synthesis reaction with the pressure** The Journal of Supercritical Fluids 154 (2019) 104630. https://doi.org/10.1016/j.supflu.2019.104630	**4**
3	**C. Brondi**, M. R. Di Caprio, E. Di Maio, T. Mosciatti, S. Cavalca, V. Parenti, S. Iannace Title: **Microcellular thermosetting polyurethane foams** International Polymer Processing (2020) (Accepted)	**4**
4	**C. Brondi**, E. Di Maio, T. Mosciatti, V. Parenti, L. Bertucelli Title: **Competing bubble formation mechanisms in rigid polyurethane foaming** (In preparation)	**5**
5	**C. Brondi**, E. Di Maio, T. Mosciatti, V. Parenti, L. Bertucelli Title: **Controlling the Ostwald Ripening in rigid polyurethane foams** (In preparation)	**6**
6	**C. Brondi**, E. Di Maio, T. Mosciatti, V. Parenti, L. Bertucelli Title: **The effect of organofluorine additives on the morphology, thermal conductivity and mechanical properties of water-pentane blown polyurethane and polyisocyanurate rigid foams** (Under review)	**6**

In addition to the previous publications, the work developed in this thesis has been presented in national and international conferences, as collected in Table 2. Moreover, the results achieved during these three years have been also awarded.

Table 2. Contributions to international and national conferences and awards received.

	CONTRIBUTIONS TO CONGRESS
1	M.R. Di Caprio, **C. Brondi**, E. Di Maio, S. Cavalca, V. Parenti, S. Iannace, P. Musto Title: **Effect of high-pressure CO_2 on polyurethane synthesis** 12th International Symposium on Supercritical Fluids, ISASF2018, Antibes (France) 2018. (Poster)
2	(Keynote) M.R. Di Caprio, **C. Brondi**, E. Di Maio, S. Cavalca, V. Parenti, S. Iannace Title: **Thermosetting polyurethane foams by physical blowing agents: chasing the synthesis reaction with the pressure** 35th INTERNATIONAL CONFERENCE of THE POLYMER PROCESSING SOCIETY, PPS-35, Izmir (Turkey) 2019. (Talk)
3	**C. Brondi**, E. Di Maio, T. Mosciatti, V. Parenti, L. Bertucelli Title: **The effect of air bubbles inclusion on polyurethane foaming - Insight into bubble nucleation and growth mechanisms** Water and water systems – Polymers and soft materials: glasses, gels and networks, Erice (Italy) 2019. (Poster)
4	**C. Brondi**, E. Di Maio, T. Mosciatti, V. Parenti, L. Bertucelli Title: **The effect of air bubbles inclusion on polyurethane foaming - Insight into bubble nucleation and growth mechanisms** ***Award: Raymond Shute Travel Award 2019*** 17th International Conference on Advances in Foam Materials & Technology, SPE FOAMS 2019, Valladolid (Spain). (Talk)
5	**C. Brondi**, E. Di Maio, T. Mosciatti, V. Parenti, L. Bertucelli Title: **The effect of air bubbles inclusion on polyurethane foaming - Insight into bubble nucleation and growth mechanisms** 17th International Conference on Advances in Foam Materials & Technology, SPE FOAMS 2019, Valladolid (Spain). (Poster)
6	**C. Brondi**, M. R. Di Caprio, G. Scherillo, E. Di Maio, T. Mosciatti, S. Cavalca, V. Parenti, M. Corti, S. Iannace Title: **Matching timescales in thermosetting polyurethane foaming: slow curing vs. fast blowing agent release** 17th International Conference on Advances in Foam Materials & Technology, SPE FOAMS 2019, Valladolid (Spain). (Talk)
7	**C. Brondi**, M. R. Di Caprio, G. Scherillo, E. Di Maio, T. Mosciatti, S. Cavalca, V. Parenti, M. Corti, S. Iannace Title: **Schiume poliuretaniche termoindurenti ottenute mediante CO_2 come agente espandente fisico: inseguendo la reazione di sintesi con la pressione** 4ª Conferenza Nazionale Poliuretano Espanso rigido (ANPE), Rome (Italy) 2019. (Talk)

The knowledge generated in the present work, at the moment in which this thesis is written, has generated one intellectual property (filed) with the company, shown in Table 3. This is a decisive indicator of the main importance of this research for important industrial sectors such as refrigeration.

Table 3. Patent in which the present work is involved.

	FILED PATENTS
1	V. Parenti, S. Cavalca, T. Mosciatti, E. Di Maio, M.R. Di Caprio, **C. Brondi**, S. Iannace Title: **Methods for Producing Polyurethane Foams** Domanda di brevetto italiano No. 102018000009122 (2018)

Table 4 summarizes the research stays in other institutions during the development of this thesis. The research stay at Dow Italia s.r.l. (Correggio, Italy), under the supervision of Dr. Luigi Bertucelli, lasted seven months. Experimental results included in *Chapter 7* and *Chapter 8* have been gathered during this time and resulted in two publications (Table 1). The other research stay in the Condensed Matter Physics Department at the University of Valladolid (Spain), under the supervision of Prof. Dr. Miguel Ángel Rodríguez-Pérez, lasted six months. This period has allowed to work in other projects related to the investigation of the competing bubble formation mechanisms taking place during the PU foaming process and will be object of other two publications, independent from this thesis (Table 4).

Table 4. Research stays in the other institutions during the investigation.

	RESEARCH STAYS
1	Dow Italia s.r.l., Correggio, Italy. From October 2018 to March 2019 (six months). From November 2019 to December 2019 (one month). Research work: **Observation of the Ostwald Ripening inhibition by liquid OFAs (Chapter 7)** Research work: **Production and characterization of PU and PIR foams obtained by liquid OFAs (Chapter 8)**.
2	CellMat group, Condensed Matter Physics Department, University of Valladolid, Spain. From May 2019 to October 2019 (six months). Research work: **Observation of the cell coarsening mechanisms validated by X-ray radioscopy** (Research article in preparation) Research work: **Observation and quantification by FTIR spectroscopy of the effect of air bubbles inclusion on the polyurethane reaction kinetics** (Research article in preparation)

Moreover, additional academic activities were performed and the Ph.D. student was involved in an European project during the three years of the thesis project (Table 5).

Table 5. Additional activities carried out during this thesis.

	ACADEMIC ACTIVITIES
1	Help teaching. From October 2017 to February 2018 (five months). Title of the course: **Matematica e Elementi di Statistica** Department of Chemical Sciences, University of Naples Federico II, Naples, Italy
2	Help teaching. From March 2018 to July 2018 (five months). Title of the course: **Fisica ed elementi di statistica** Department of Chemical Sciences, University of Naples Federico II, Naples, Italy
	RESEARCH PROJECTS
3	Title of the project: European Union's LIFE13-EN/IT/001238 project http://ec.europa.eu/environment/life/project/Projects/index.cfm?fuseaction=search.dspPage%26n_proj_id=5077

The following courses have been attended during the Ph.D. (Table 6).

Table 6. Attended courses during this thesis.

	ATTENDED COURSES
1	Prof. Young W. Kwon, Department of Mechanical & Aerospace Engineering, Naval Postgraduate School, Monterey, California, USA Title**: Research on Multiscale and Multiphysics** University of Naples Federico II, Naples, Italy. May 2017.
2	Dr. Alessandra Caggiano, Department Industrial Engineering, University of Naples Federico II, Naples, Italy Title**: An Introduction to Industry 4.0: Scientific and R&D Action Fields** University of Naples Federico II, Naples, Italy. April-May 2017.
3	Dr. Giuseppe Scherillo, Department of Chemical, Materials and Production Engineering, University of Naples Federico II, Naples, Italy Title**: Numerical methods in materials science and technology** University of Naples Federico II, Naples, Italy. June 2017.
4	Dr. Giuseppe Scherillo, Department of Chemical, Materials and Production Engineering, University of Naples Federico II, Naples, Italy Title**: Thermodynamics of constitutive equations for coupled momentum and energy transfer in materials** University of Naples Federico II, Naples, Italy. June 2017.
5	Prof. Pietro Pucci, Department of Chemical Sciences, University of Naples Federico II, Naples, Italy Title**: Advanced course of mass spectroscopy** University of Naples Federico II, Naples, Italy. June 2017.
6	Dr. Pellegrino Musto, Institute on Polymers Composites and Biomaterials, National Research Council, Pozzuoli, Italy Title**: Vibrational Spectroscopy** Institute on Polymers Composites and Biomaterials, National Research Council, Pozzuoli, Italy. February 2018.
7	Prof. Krzysztof Matyjaszewski, Natural Sciences, Carnegie Mellon University, Pittsburgh, USA Title**: Advanced materials by externally controlled ATRP** University of Naples Federico II, Naples, Italy. March 2018.
8	Prof. Pierluigi Rippa, Department Industrial Engineering, University of Naples Federico II, Naples, Italy Title: **Innovation Management and Technology transfer from universities to companies** University of Naples Federico II, Naples, Italy. April 2019.
9	Prof. Francesco Greco and Prof. Giuseppe Mensitieri, Department of Chemical, Materials and Production Engineering, University of Naples Federico II, Naples, Italy Title: **Water and water systems – Polymers and soft materials: glasses, gels and networks** Ettore Majorana Foundation and Centre for Scientific Culture, Erice, Italy. July 2019.

Acknowledgements

I would like to thank my supervisor, prof. Ernesto Di Maio, for giving me the opportunity to carry out this industrial PhD. This dynamic experience continuously stimulated my curiosity in the wide world of foams and my interest in learning how to do research.

I would like to thank Dr. Maria Rosaria Di Caprio for introducing me in the field of polyurethane foams at the beginning of this journey.

Many thanks go to the members of Dow Italia, Dr. Sara Cavalca, Thomas Mosciatti and Vanni Parenti for the fruitful collaboration and the stimulating comments on the ongoing work.

I would like to thank the members of CellMat, Merce, Edu, Paula, Santi, Josias and Alberto for making me feel like in a family since the beginning. Special thanks go to Prof. Miguel Ángel Rodríguez-Perez that helped me a lot to improve in my work. It has been an honor to have such a supervisor.

I would like to thank also the members of DICMaPI: Rosaria, Scherillo, Rosario, Antonio and Fabrizio for all the "scientific" and recreational moments we shared in these years.

I would like to thank the most important people of my life: my family. Thank you for supporting me also in these years for this new important piece of my life.

Finally, I want to thank the most important person that this experience brought me, my love, Angela.